DESIGN AND MANUFACTURING OF A HIGH SPEED
JET POWERED TARGET DRONE

A THESIS SUBMITTED TO
THE GRADUATE SCHOOL OF NATURAL AND APPLIED SCIENCES
OF
MIDDLE EAST TECHNICAL UNIVERSITY

BY

ENDER ÖZYETİŞ

IN PARTIAL FULFILLMENT OF THE REQUIREMENTS
FOR
THE DEGREE OF MASTER OF SCIENCE
IN
AEROSPACE ENGINEERING

SEPTEMBER 2013

Approval of the thesis:

**DESIGN AND MANUFACTURING OF A HIGH SPEED,
JET POWERED TARGET DRONE**

submitted by **ENDER ÖZYETİŞ** in partial fulfillment of the requirements for the degree of **Master of Science in Aerospace Engineering Department, Middle East Technical University** by**,**

Prof. Dr. Canan Özgen   _____
Dean, Graduate School of **Natural and Applied Sciences**

Prof. Dr. Ozan Tekinalp   _____
Head of Department, **Aerospace Engineering**

Prof. Dr. Nafız Alemdaroğlu   _____
Supervisor, **Aerospace Engineering Dept., METU**

Examining Committee Members:

Prof. Dr. Serkan Özgen   _____
Aerospace Engineering Dept., METU

Prof. Dr. Nafız Alemdaroğlu   _____
Aerospace Engineering Dept., METU

Prof. Dr. Altan Kayran   _____
Aerospace Engineering Dept., METU

Prof. Dr. Yusuf Özyörük   _____
Aerospace Engineering Dept., METU

Prof. Dr. Kahraman Albayrak   _____
Mechanical Engineering Dept., METU

Date: _____

I here declare that all information in this document has been obtained and presented accordance with academic rules and ethical conduct. I also declare that, as required by these rules and conduct, I have fully cited and referenced all material and results that are not original to this work.

Name, Last name :   Ender ÖZYETİŞ

Signature :

ABSTRACT

DESIGN AND MANUFACTRING OF A HIGH SPEED, JET POWERED TARGET DRONE

ÖZYETİŞ, Ender

M.S., Department of Aerospace Engineering

Supervisor : Prof. Dr. Nafız ALEMDAROĞLU

September 2013, 127 pages

This thesis presents the design and manufacturing of a high speed jet powered UAV which is capable of flying at M=0.5. Flight time of the UAV is 30 minutes at 1700 m above sea level. Aerodynamic and structural design of the UAV is conducted for 6g sustained and 9g instantaneous loads. Low aspect ratio blended wing-body design is decided due to low drag and high maneuverability. The Structure of the UAV consists of the composite parts such as frames and skin and mechanical parts such as landing gears which are from aluminum and steel, engine holders, parachute release mechanism and etc.

The purpose of the thesis is to design and build a unique aircraft to be used as a target drone or a multi mission aircraft. Initial study is conducted by developing a design tool which works in an input-output way. Input parameters are categorized as blended wing-body parameters, tail parameters, propulsion system parameters, mission profile parameters, landing gear and parachute parameters, air properties and sample structural weights. Performance calculations are conducted by introducing an iterative weight calculation method. The Optimization process is conducted around the initial design by using the initial design parameters as a starting point. Some of the design inputs are selected as variable design parameters to construct the design cases which are formed via the combination of these variables. After final design is decided, modeling of the external geometry and modeling and integration of the sub-systems are conducted. Production is conducted in a step by step process which starts with the manufacturing of the skin pieces and frames and continues with joining of the structural parts prior to surface fibering and integration.

The propulsion unit of the aircraft is selected as a mini turbojet engine which is capable of giving a 230 N thrust at sea level. The weight of the engine 2.85 kg and has a fuel consumption of 600 grams/minute at full throttle. The engine is controlled by an electronic control unit which controls the fuel flow through the engine.

Keywords : Target Drone, UAV, Preliminary Design, Detail Design.

ÖZ

YÜKSEK HIZLI JET MOTORLU HEDEF UÇAĞI TASARIMI VE ÜRETİMİ

ÖZYETİŞ, Ender

Yüksek Lisans, Havacılık ve Uzay Mühendisliği Bölümü

Tez Yöneticisi : Prof. Dr. Nafız ALEMDAROĞLU

Eylül 2013, 127 sayfa

Bu tez, 0.5 Mach hızında uçabilen yüksek hızlı jet motorlu bir insansız hava aracının tasarım ve üretim faaliyetlerini içermektedir. Hava aracının deniz seviyesinden 1700 m yukarıdaki uçuş süresi 30 dakikadır. Aerodinamik ve yapısal tasarımı 6g'lik devamlı ve 9g'lik anlık yüklere göre gerçekleştirilmiştir. Düşük sürtünme katsayısı ve de yüksek manevra kabiliyeti nedeniyle kanat tasarımı düşük açıklık oranına sahip uçan kanat olarak seçilmiştir. Hava aracının yapısal parçaları; kompozit malzemeden üretilmiş yatay kesitler ve dış yüzey, alüminyum ve çelikten üretilmiş iniş kalkış takımı, motor montaj aparatları, paraşüt mekanizması gibi birimlerden oluşmaktadır.

Projenin amacı, hedef uçağı ve de çok amaçlı uçak olarak kullanılabilecek özgün bir insansız hava aracının tasarlanıp üretilmesidir. İlk çalışma, girdi-çıktı yöntemine dayanan bir tasarım aracının geliştirilmesiyle başlamıştır. Girdi parametreleri; bütünleşik kanat-gövde parametreleri, kuyruk parametreleri, itki sistemi parametreleri, görev profili parametreleri, iniş kalkış takımı ve paraşüt parametreleri, hava özellikleri ve örnek yapısal ağırlıklar olarak kategorize edilmiştir. Performans hesapları yineleme yöntemine dayalı bir ağırlık hesabı metodu geliştirilerek yerine getirilmiştir. Optimizasyon, ilk tasarım etrafında ilk tasarım parametreleri başlangıç noktası kabul edilerek gerçekleştirilmiştir. Bazı tasarım girdileri değişken olarak seçilmiş ve bu değişken parametrelerin birbirleriyle kombinasyonları sonucu birbirinden farklı tasarım senaryoları oluşturulmuştur. Son tasarım seçildikten sonra, dış geometri ve iç sistemlerin modellemesi ve entegrasyonu yapılmıştır. Üretim, yüzey parçaları ve kesitlerin üretilmesiyle başlayıp yüzey güçlendirme ve entegrasyon öncesi yapısal parçaların birleştirilmesiyle devam eden aşama aşama bir üretim yöntemi kullanılarak gerçekleştirilmiştir.

İtki sistemi olarak deniz seviyesinde 230N itki kuvveti verebilen mini bir turbojet motoru seçilmiştir. Motorun ağırlığı 2.85 kg iken tam gazda yakıt tüketimi 600g/dk'dir. Motor, yakıt akışını kontrol eden elektronik bir kontrol ünitesi ile kontrol edilmektedir.

Anahtar Kelimeler : Hedef Uçağı, İnsansız Hava Aracı, Ön Tasarım, Detaylı Tasarım.

To aviation…

Havacılığa…

ACKNOWLEDGMENTS

I am grateful to my supervisor Prof. D. Nafız Alemdaroğlu for his support, advice and encouragements through my thesis work.

TABLE OF CONTENTS

LIST OF TABLES

TABLES

LIST OF FIGURES

FIGURES

LIST OF SYMBOLS

Symbol	Description	Unit
AR_{main_wing}	Aspect ratio of main wing	-
AR_{tail}	Aspect ratio of tail	-
b_{LEX}	LEX span	m
b	Wing span	m
$b_{fuel\ tank}$	Available span ratio for the fuel tank	-
$C_{L_{max}}$	Maximum lift coefficient of the wing	-
$C_{l_{\alpha,wing}}$	Lift curve slope of the main wing airfoil	-
c_r	Wing root chord	m
c_t	Wing tip chord also thrust specific fuel consumption or thrust coefficient	m or s^{-1}
$c_{r,LEX}$	LEX root chord	m
$c_{t,LEX}$	LEX tip chord	m
C_{l_0}	Zero angle lift coefficient of the wing airfoil.	-
C_{m_0}	Zero angle section moment coefficient.	-
$C_{l_{\alpha,LEX}}$	Lift curve slope of the LEX.	-
$c_{r,tail}$	Tail root chord	m
$c_{t,tail}$	Tail tip chord	m
$C_{l_{\alpha,tail}}$	Lift curve slope of the tail airfoil	-
$c_{fuel\ tank}$	Available wing chord ratio for the fuel tank	-
$\bar{c}$	Main wing aerodynamic chord	m

$\bar{c}_{LEX}$	LEX wing aerodynamic chord	m
C_{L_α}	Total lift curve slope	-
$C_{L_{\alpha_{WB}}}$	Wing-body lift curve slope	-
$C_{L_{\alpha_H}}$	Horizontal tail lift curve slope	-
$C_{L_{\alpha_{LEX}}}$	LEX lift curve slope	-
$C_{L_{\alpha_W}}$	Main wing lift curve slope	-
$C_{L,max}$	Maximum lift coefficient	-
$C_{D0_{subsonic}}$	Subsonic drag coefficient	-
C_L	Lift coefficient	-
C_D	Drag coefficient	-
C_F	Turbulent flow parasite drag factor	-
$d_{fuselage}$	Fuselage diameter	m
e	Span efficiency factor	-
F_{fill}	Fill ratio	-
hn_{wing}	Neutral point of the main wing.	-
hn_{LEX}	Neutral point of the front wing.	-
$h_{obs.}$	Obstacle height for takeoff	m
$h_{takeoff}$	Takeoff height	m
h_{cruise}	Cruise height	m
$h_{descent}$	The descent altitude with respect to sea level	m
h_{tail}	Vertical tail height	m
K_A	Aspect ratio downwash factor	-
K_H	Horizontal tail downwash factor	-
K_λ	Taper ratio downwash factor	-

k	Proportionality constant	-
l_{inlet}	Engine inlet length	m
l_{tail}	Distance between tail aerodynamic point and wing-body aerodynamic point	m
M	Mach Number	-
$NOFD$	Number of Designs	-
N_{engine}	Number of engines.	-
$N_{ground\,roll}$	Distance constant for rotation phase	-
n	Load factor	-
n_{max}	Maximum load factor	-
P_0	Air pressure at sea level	Pa
P_r	Power required	Watts
R_{inlet}	Equivalent radius of the engine inlet	M
Re	Reynolds Number	-
R	Turn radius	M
R/C	Rate of climb	m/s
R_{range}	Range	Km
RPM	Revolutions per minute	-
S_{LR}	Landing ground roll distance	M
S_{main_wing}	Main wing Area	m^2
S_{LEX}	LEX area	m^2
S_{tail}	Tail area	m^2
S_{sp_frame}	Span-wise frame area	m^2
$S_{mw\_lng\_frame}$	Main wing longitudinal frame area	m^2
S_{in_frame}	Inlet frame area	m^2

S_g	Takeoff ground roll distance	m
S_a	Transition distance	m
t_{climb}	Climb time	s
$t_{fuel\ tank}$	Available wing thickness ratio for the fuel tank	-
$\left(\dfrac{t}{c}\right)_{wing\ airfoil}$	Wing airfoil thickness to chord ratio.	-
$\left(\dfrac{x}{c}\right)_{m}$	Wing airfoil chord-wise location of the maximum thickness of the airfoil	-
$\left(\dfrac{x}{c}\right)_{tail\ airfoil}$	Tail airfoil chord-wise location of the maximum thickness of the airfoil	-
t_{loiter}	Loiter time	Min.
t_{cruise}	Cruise time	Min.
T_0	Air temperature at sea level	K
T_r	Thrust required	N
T_A	Available thrust	N
$V_{approach}$	Approach velocity	m/s
V_{flare}	Flare velocity	m/s
V_{cruise}	Cruise speed	m/s
$V_{v,descent\ rate}$	Vertical component of velocity duting the descent phase	m/s
V_{stall}	Stall velocity	m/s
V^*	Corner velocity	m/s
$V_{v,descent}$	Vertical component of decent velocity	m/s
W_{s_skin}	Wing-body skin composite unit weight	gr/m^2
W_{s_frame}	Frame unit weight	gr/m^2
W_{s_paint}	Paint unit weight.	gr/m^2
W_{s_tail}	Tail skin composite unit weight	gr/m^2
W_{s_tank}	Fuel tank composite unit weight	gr/m^2

W_{TOTAL}	Total aircraft weight	N or gram
$W_{aircraft}$	Aircraft structural weight	N or gram
$W_{sys\_internal}$	System weight	N or gram
$W_{payload}$	Payload weight	N or gram
W_{wing_body}	Wing-body structural weight	N or gram
W_{tail}	Tail structural weight	N or gram
$W_{blended\_wing}$	Blended wing structural weight	N or gram
W_{inlet}	Inlet structural weight	N or gram
W_{paint}	Paint weight	N or gram
W_{wing_skin}	Blended wing skin weight	N or gram
W_{frame}	Total frame weight	N or gram
W_{sp_frame}	Total span-wise frame weight	N or gram
W_{lng_frame}	Total longitudinal frame weight	N or gram
W_{in_frame}	Total inlet frame weight	N or gram
$W_{mw\_lng\_frame}$	Main wing total longitudinal frame weight	N or gram
$W_{fw\_lng\_frame}$	Front wing total longitudinal frame weight	N or gram
W_{fuel}	Fuel weight	N or gram
$W_{main\_l\_gear}$	Main gear weight	N or gram
$W_{nose\_l\_gear}$	Nose gear weight	N or gram
$W_{engines}$	Engine weight	N or gram
W_{engine_comp}	Engine component weight	N or gram
$W_{avionics}$	Avionics weight	N or gram
$W_{batteries}$	Battery weight	N or gram
$W_{parachute}$	Parachute weight	N or gram

WF	Fuel flow	Kg/s
X_{range}	Range of design input	-
Y_{inputs}	Number of variable design inputs	-

GREEKS SYMBOLS

$\alpha_{i.tail}$	Tail incidence angle	Deg.
η_H	Horizontal tail efficiency factor	-
η_{LEX}	LEX efficiency factor.	-
η_{LEX}	LEX efficiency factor	-
$\Lambda_{c/4}$	Main wing sweep angle at quarter chord	Deg.
$\Lambda_{c/2}$	Main wing sweep angle at semi chord	Deg.
Λ_{LE}	Wing leading edge sweep angle	Deg.
$\Lambda_{LE,tail}$	Tail leading edge sweep angle.	Deg.
$\Lambda_{TE,tail}$	Tail trailing edge sweep angle	Deg.
$\Lambda_{m,tail}$	Tail maximum thickness sweep	Deg.
$\mu_{r,landing}$	Friction coefficient during landing.	-
μ_r	Friction coefficient during takeoff.	-
μ	Viscosity	Pa·s
ρ_0	Air density at sea level	Kg/m^3
θ_{climb}	Climb angle	Deg.
$\theta_{descent}$	Descent angle	Deg.
$\emptyset_{max}$	Maximum bank angle	Deg.
θ_{obs}	Obstacle clearance angle	Deg.
ω	Turn rate	Deg./s

CHAPTER 1

INTRODUCTION

1. Introduction to the Aircraft Design

The aircraft design phase is an iterative process which includes the analysis of the requirements, the initial conceptual sketch, first performance analyses, sizing and optimization. This process can be divided to phases which are called as conceptual, preliminary and detailed design. Figure 1. 1 shows the aircraft design process. Although it is a progressive process, after the sizing and optimization or the analyses the initial concept can be subjected to change. This is the iterative feature of the aircraft design.
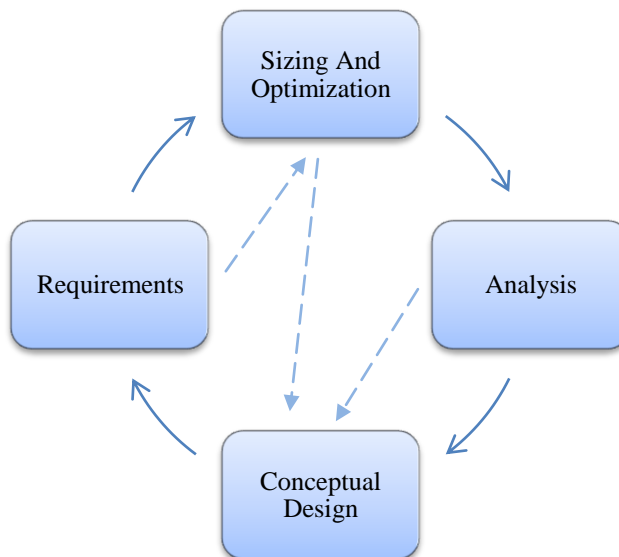
Figure 1. 1 Design Phases

Aircraft design can be divided to phases which are called as conceptual, preliminary and detailed design as shown in Figure 1. 2.

Analyzing the requirements is the first step through the design cycle. After analyzing the requirements, the initial shape of the aircraft including the wing shape, tail type, and fuselage shape is determined and the first sketch is drawn. This phase is called as conceptual design.

Preliminary design is the phase where most of the critical features of the design have been decided. Full-scale lofting of the design is started during this phase and more sophisticated aerodynamic, structural and stability and control analyses are conducted.

Requirements
- Analysis of the requirements

Conceptual Design
- First sketch
- Concept satisfies the requirements?
- Initial weight guess

Preliminary Design
- Freezing the design
- 3D modeling
- Performance calculations and flight mechanics

Detail Design
- Design of all sub-parts
- Production methodology
- Final perfomance calculations

Production
- Production phases

Figure 1. 2 Aircraft design phases.

As a progression of the preliminary design, detail design phase is conducted during the design cycle. This phase includes the design of the actual parts of the aircraft such as ribs, skin and other parts which are not considered in detail during the conceptual and preliminary design. Production methods are considered during detail design phase which can require special machining tools due to the complexity of the designed part. Cost analysis which may be a driven factor for the aircraft design is conducted in this phase.

2. Target Drones and Small Jets

Target drones are unmanned air vehicles which can be used for different type of missions, including: simulating enemy threats for gunnery and missile training, testing of new weapons such as air-to-air or surface-to-air missiles and pilot training such as air-to-air combat. Most of the target drones are specially designed for the mission while some is converted from real fighter aircraft. Critical design criteria for the target drones are maneuverability and speed. High cost sophisticated drones are made as re-usable/recoverable while some are directly hit and destroyed during the tests. Target drones are installed with electronic equipments such as active and passive radar systems, scoring systems and smoke systems. Due to the high speed necessity, turbojet engines are the most common propulsive units of this type of UAVs. Similarly, low aspect ratio small wings are general wing configurations. Catapult launch and parachute recovery are often seen for these aircraft which can be also assisted with rockets during take-off due to high wing loading and high takeoff speed.

3. Literature Survey

Similar aircraft which are used as target drones are investigated to have knowledge about the current status of this type of UAVs. CEI-Firejet [10] is described as a multi-role subsonic aerial target system with the opportunity to deploy payloads such as smoke, scalar scoring, passive and active radars and infrared. Maximum launch weight is 150 kg. The maximum speed is declared as 241 m/s. The launch is performed via a pneumatic rail. Figure 1. 3 shows the CEI-Firejet and its specifications.

Weight (kg)	MTOW 150
Wing Span (m)	2
Length (m)	3.3
Max. Speed (m/s)	241
Endurance (min.)	60
Maneuverability	6g sustained, 10g instantaneous

Figure 1. 3 CEI Firejet and Specifications [10].

AAA-Phoenix [11] is a small target drone as shown in Figure 1. 4. The launch is done via a catapult and recovery is done via parachute. The propulsion system is a single turbojet engine. The wing configuration is delta and the fuselage is nearly cylindrical. It is stated that the fuel capacity is 30.4 liters.

Weight (kg)	55
Wing Span (m)	2
Length (m)	2.4
Max. Speed (m/s)	154
Endurance (min.)	Up to 90

Figure 1. 4 AAA-Phoenix and Specifications [11].

ADCOM-Yahbon HMD [12] has a different design than the others. The wing is located at the back of the slender fuselage. Between the fuselage and the wing aerodynamic surfaces similar to leading edge extensions are located. Engine inlet is located on the upper surface unlike others. Maximum takeoff weight is stated to be 220 kg. Maximum speed is declared as 222 m/s and endurance is 60 minutes. The origin of the UAV is UAE (United Arab Emirates). Figure 1. 5 shows the specifications.

Weight (kg)	220
Wing Span (m)	3.38
Length (m)	4.32
Max. Speed (m/s)	222
Endurance (min.)	60

Figure 1. 5 ADCOM-Yahbon HMD and Specifications [12].

4. Conceptual Considerations

During the conceptual design, the UAV is decided to have a low aspect ratio and slender wing-body geometry due to the high aerodynamic and structural performance. Low aspect ratio wings are known to have low lift curve slopes than the high aspect ratio wings which require high speed flight. On the other hand, they have a higher maximum angle of attack due to the vortex lift generation at low speeds than the high aspect ratio wings.

Delta wings have thicker root sections which results in higher allowable bending stress, naturally. That is higher g loads which are common in highly maneuverable aircraft. This is structurally advantageous. Structural and aerodynamic properties make the delta wings desirable, for the highly maneuverable concept.

4. 1 Blended Wing-Body Design

Aerodynamically blended wing-body geometries have less fuselage-wing interference and as a result lower drag coefficient and higher aerodynamic efficiency. Moreover, blended wing-body geometry has a more effective lifting area than the conventional fuselage-wing

4

configurations. Additionally, blended wing body geometry is supposed to produce less side force at cross-flows which is desirable for control capability of the UAV. Figure 1. 6 shows a slender wing geometry.

Figure 1. 6 A Slender Wing.

4. 2 Leading Edge Extensions: LEX

Leading edge extensions are known as vortex generators which are beneficial to attach the flow at high angles of attack at low speeds. Most of the modern fighter jets are designed with leading edge extensions. Figure 1. 7 shows the vortices generated at the leading edge.
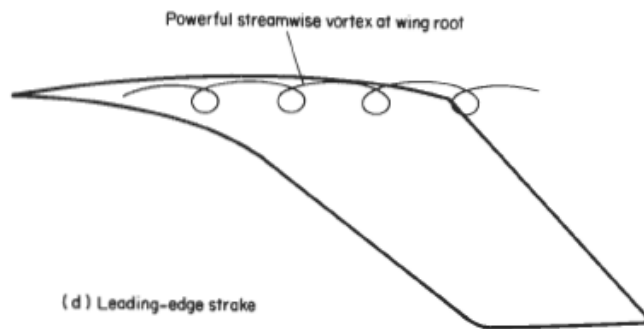
Figure 1. 7 The Leading Edge Vortices (taken from Ref. [13])

4.3 Low Aspect Ratio Wing Aerodynamics

Low aspect ratio aerodynamics quite different from the conventional high aspect ratio wings with respect to the vortex structure on the wings. The vortices developed at leading edges are very effective on the lifting characteristics. Delta wings at high angles have very strong vortices and these vortices provide additional lift which is called as vortex lift. Figure 1. 8 shows a typical lift variation with angle for a slender delta wing. At high angles the vortex lift contribution is higher due to the fact that the leading edge vortex gets stronger. Figure 1. 9 shows the vortex generation around a slender delta wing for two differentanglese of attack and Reynolds numbers (Pictures are taken from Ref. [13]).
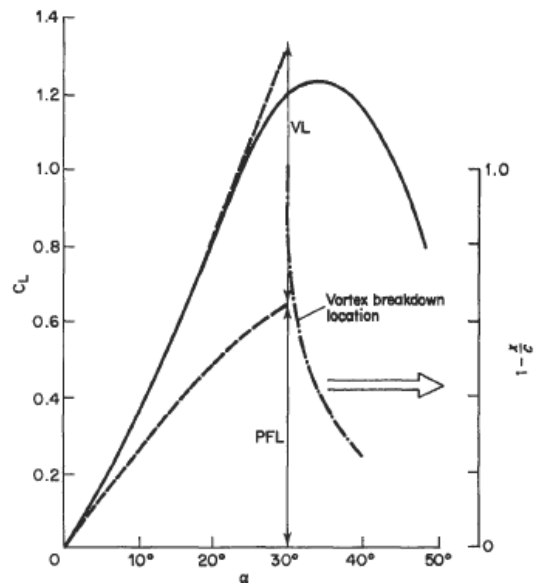
Figure 1. 8 The lift variation for a slender delta wing with angle (taken from Ref. [13] Fig. 5.43)
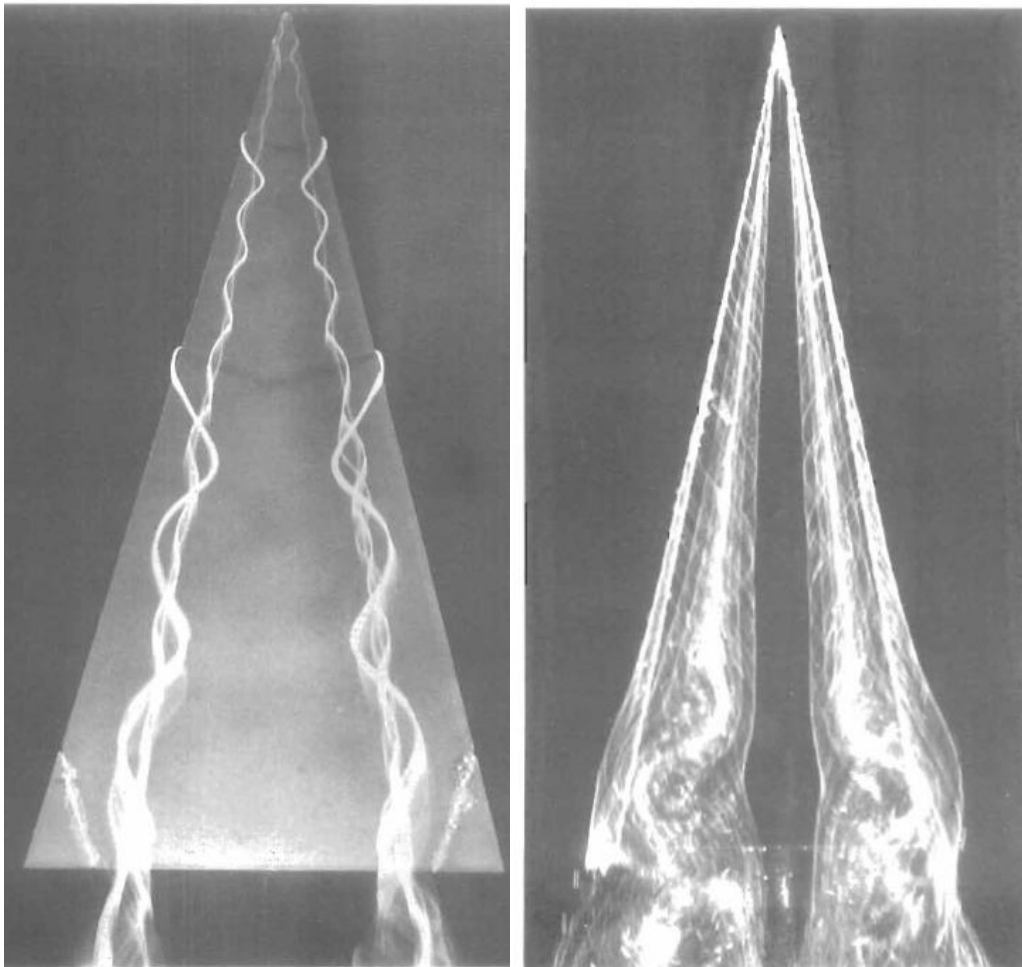
*Figure 1. 9 The Voritces Around A Symmetrical Delta Wing, For the Picture on the left: Reynolds Number is 20000 and angle of attack is **20**°; For the Picture on the right: Reynolds Number is 3000 and angle of attack is **35**° (Taken from Ref. [13] Fig. 5.41 and 5.42)*

6

CHAPTER 2

DEVELOPING THE DESIGN TOOL

1. Design Methodology

Design and analysis process is integrated by introducing an input-output analysis method. Input design parameters are categorized as geometric parameters of wing and tail surfaces, mission profile parameters including take-off height and desired cruise time, landing gear parameters such as maximum allowable normal force during landing , propulsive unit parameters such as maximum thrust available and number of engines to be used and composite structure sample weights. Necessary look-up tables are generated for analysis process which includes variation of thrust coefficient of the engine over the mission profile and variation of maximum fuselage height that is derived from airfoil coordinates. Performance calculations are conducted by presenting an iterative detailed weight calculation method which gives more appropriate results than the conventional weight estimation methods that are generally based on historical data. The weights of structural parts such as frames and aircraft skin have been generated by using the composite structure sample weights together with the necessary design inputs. Necessary fuel weight, the landing gear and parachute weights have been generated iteratively to satisfy the selected design parameters. Figure 2. 1 shows the design methodology.
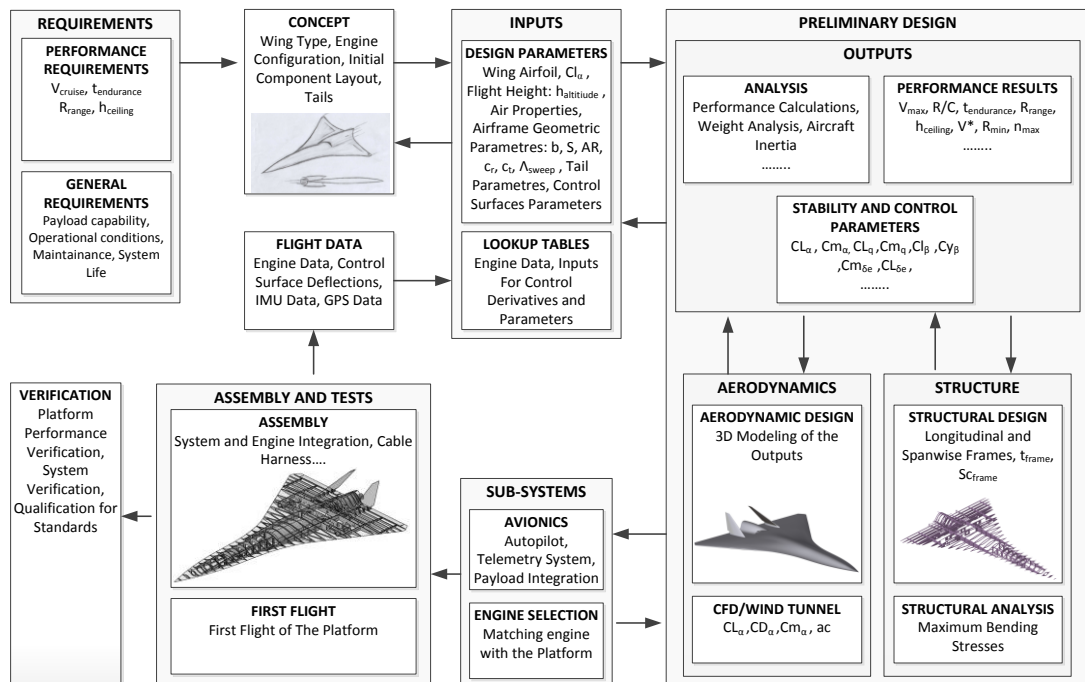
Figure 2. 1 The Design Methodology.

As a part of the analysis process the stability and control derivatives has been calculated by using analytical methods presented by Jan Roskam [1]. The stability of the aircraft has been checked during the analysis process by using these parameters.

The blended wing-body geometry is considered as a combination of the main wing and the front wing which is called as LEX. During the iterative calculations the longitudinal sections of the wing-body are assumed to be in the form of the wing airfoil and the span-wise sections are assumed to be in the form of diamond heights of which are determined by the airfoil upper and lower surface splines which are generated from the airfoil coordinates. Control surfaces are designed as elevons which are used as the elevator and ailerons at the same. The tail is considered as a passive surface which doesn't have any control surfaces but provides stability.

2. Design Tool Methodology

The design process is conducted by developing a tool which reads the input file consisting of the necessary design parameters for the analysis and gives the outputs. The input file is an Excel file in which the design parameters such as cruise speed, wing span, wing root and tip chord and etc. are stored. Sample composite material unit weights are also considered as inputs. Performance calculations are made by an iterative weight calculation method. Following sections include detailed information about the process. Figure 2. 2 shows the method, basically.
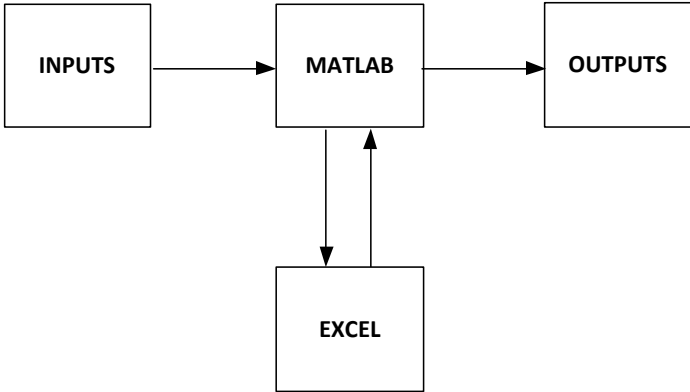
Figure 2. 2 Basic Design Tool Methodology.

Performance calculations are made on the Excel file while the read and write loops are coded into the Matlab script file. At each step the input parameters are assigned to the related cells in the Excel file and the outputs are read from the related cells. The steps are repeated for the number of designs.

8

3. Defining the Inputs: Design Parameters

The initial step for the analysis is the determination of the design parameters. Design parameters define the wing and tail shape and include the engine properties, takeoff, cruise and landing air properties and conditions, mission profile parameters and necessary parameters for the stability and control parameter calculations.

3.1 Blended Wing-Body Parameters

During the conceptual design, the aircraft body is decided to be blended wing-body due to aerodynamic considerations as mentioned in Chapter 1 and the wing is assumed to be a combination of the front wing, LEX and the main wing. Blended wing-body parameters are:

$C_{L_{max}}$: Maximum lift coefficient of the wing.

$C_{l_{\alpha,wing}}$: Lift curve slope of the main wing airfoil

$\left(\dfrac{t}{c}\right)_{wing\ airfoil}$: Wing airfoil thickness to chord ratio.

$\left(\dfrac{x}{c}\right)_{m}$: Wing chord-wise location of the maximum thickness of the airfoil.

Λ_{m} : Wing maximum thickness sweep. [Degrees]

c_{r} : Wing root chord. [m]

c_{t} : Wing tip chord. [m]

b : Wing span. [m]

Λ_{LE} : Wing leading edge sweep angle. [Degrees]

hn_{wing} : Neutral point of the main wing.

$C_{l_{0}}$: Zero angle lift coefficient of the wing airfoil.

$C_{m_{0}}$: Zero angle section moment coefficient.

$c_{r,LEX}$: LEX root chord. [m]

$c_{t,LEX}$: LEX tip chord. [m]

b_{LEX} : LEX span. [m]

$C_{l_{\alpha,LEX}}$: Lift curve slope of the LEX.

hn_{LEX} : Neutral point of the front wing.

η_{LEX} : LEX efficiency factor.
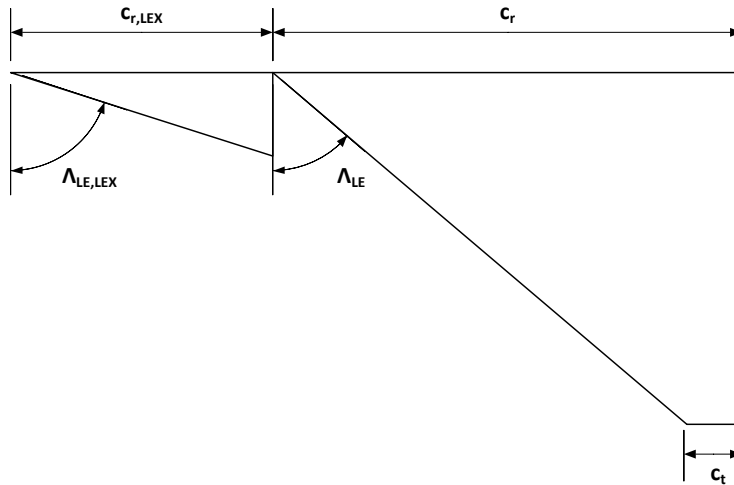
Figure 2. 3 Wing-Body Layout

3.2 Tail Parameters

Tail parameters include the geometric properties of the tail similar to the wing-body parameters. They are:

$c_{r,tail}$: Tail root chord [m]

$c_{t,tail}$: Tail tip chord [m]

$\Lambda_{LE,tail}$: Tail leading edge sweep angle. [Degrees]

$\Lambda_{TE,tail}$: Tail trailing edge sweep angle. [Degrees]

$C_{l_{\alpha,tail}}$: Lift curve slope of the tail airfoil

$\alpha_{i.tail}$: Tail dihedral angle (Figure 2. 4). [Degrees]

l_{tail} : Distance between tail aerodynamic point and wing-body aerodynamic point. [m]

$\left(\frac{t}{c}\right)_{tail\ airfoil}$: Tail airfoil thickness to chord ratio.

$\left(\frac{x}{c}\right)_{m,tail}$: Tail chord-wise location of the maximum thickness of the airfoil

$\Lambda_{m,tail}$: Tail maximum thickness sweep. [Degrees]

10
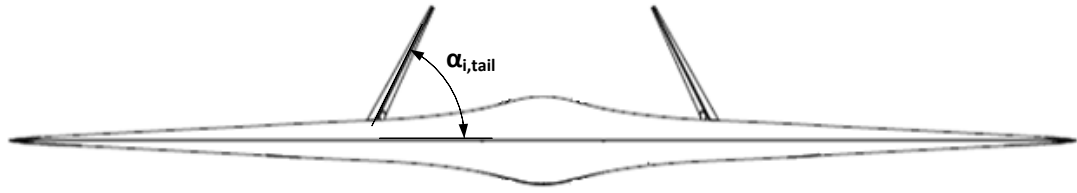
Figure 2. 4 Tail Dihedral Angle.

3.3 Propulsion System Parameters

Propulsion system parameters include variables such as the number of engines to be used and the fuel volume parameters to calculate the available fuel tank volume for each design.

N_{engine} : Number of engines.

R_{inlet} : Equivalent radius of the engine inlet. (Equivalent radius used if the inlet shape is not circular) [m]

$b_{fuel\ tank}$: Available span ratio for the fuel tank. (Between 0.0-1.0)

$t_{fuel\ tank}$: Available wing thickness ratio for the fuel tank. (Between 0.0-1.0)

$c_{fuel\ tank}$: Available wing chord ratio for the fuel tank. (Between 0.0-1.0)

l_{inlet} : Engine inlet length. [m]

3.4 Mission Profile Parameters

Mission profile parameters include one of the most critical design parameters which is the cruise time. In this analysis method cruise time is one of the design inputs. The total weight is dramatically addicted to the cruise time input due to the fact that the amount of fuel burned during the mission is determined by this parameter and added to the weight summation iteratively.

$N_{ground\ roll}$: Distance constant for rotation phase (N=1 for small aircraft, N=3 for large aircraft, see [2])

$V_{v,descent\ rate}$: Vertical component of velocity during the descent phase. [m/s]

11

$\mu_{r,landing}$: Friction coefficient during landing.

μ_r : Friction coefficient during takeoff.

$h_{obs.}$: Obstacle height for takeoff. [m]

t_{loiter} : Loiter time. [s]

t_{cruise} : Cruise time. [min.]

V_{cruise} : Cruise speed. [m/s]

3.5 Landing Gear and Parachute Parameters

During the iterative calculations the weight of the landing gears and the parachute is calculated from the related parameters. So, for each design at each step the weight of the landing gears and parachute are generated uniquely. The weight constants can be acquired from the existing similar aircraft.

$W_{m.gear}\big/W_{TOTAL}$ = The ratio of the weight of the main landing gear to the total aircraft

weight.

$W_{nose\,gear}\big/W_{TOTAL}$ = The ratio of the weight of the nose landing gear to the total aircraft

weight.

$W_{parachute}\big/W_{TOTAL}$ = The ratio of the weight of the parachute to the total aircraft weight.

3.6 Air Properties

This section includes the takeoff, cruise and heights and the air properties for the standard sea level such as air density, temperature and pressure.

$h_{takeoff}$: Takeoff height. [m]

h_{cruise} : Cruise height. [m]

$h_{descent}$: The descent altitude with respect to sea level. [m]

$h_{cruise2}$: Second cruise altitude. [m]

$h_{cruise3}$: Third cruise altitude. [m]

12

T_0 : Air temperature at sea level. [K]

P_0 : Air pressure at sea level. [Pa]

ρ_0 : Air density at sea level. [gr/m^3]

3.7 Sample Structural Weights

Sample structural weights are used for the structural weight calculation of aircraft. The sample composite laminate weights for the frames and skin are considered as a structural design input. The sample weights are taken for the laminates which have thickness. So, the units are given gr/m^2.

W_{s_skin} : Wing-body skin composite unit weight. (gr/m^2.)

W_{s_frame} : Frame unit weight. (gr/m^2.)

W_{s_paint} : Paint unit weight. (gr/m^2.)

W_{s_tail} : Tail skin composite unit weight. (gr/m^2.)

W_{s_tank} : Fuel tank composite unit weight. (gr/m^2.)

4. Geometric Model

The geometry of the aircraft is determined by using the wing-body design parameters. Wing planform is assumed to be in the form of a delta wing combined with a front wing. The selection of the wing-body design parameters may cause positive sweep angles at the leading edge as in Figure 2. 3 and positive or negative sweep angles at trailing edge, together. Total wing area is the sum the front wing area and the main wing area.

The tail is considered as a passive control surface and deflected according the deflection parameter mentioned in section 3.2.
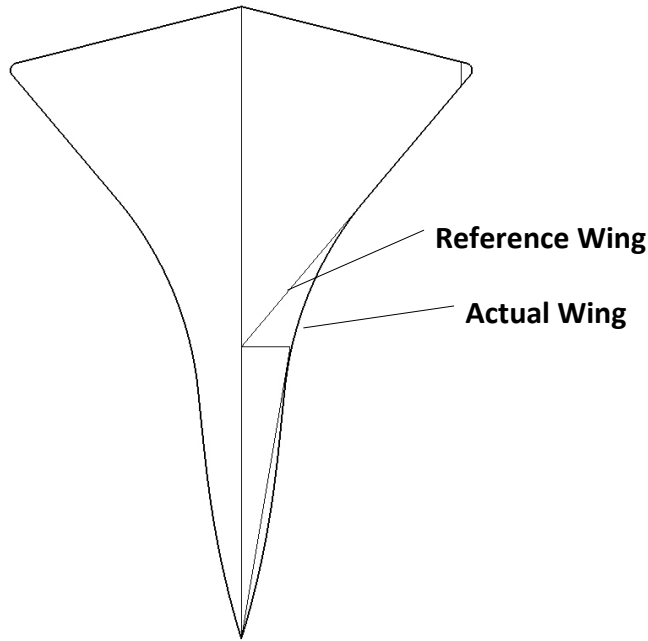
Figure 2. 5 Reference and the Actual Wing

4.1 Parameterization of the Wing-Body Geometry

The structure of the aircraft is assumed such that it consists of internal frames which are located according to the given parameters and the aircraft skin. The parameterization is made for the frames which are generated automatically during the analysis for each design case. The aim of this process is to relate the change of aircraft geometry with the weight calculation. As a result, a better weight calculation can be obtained.

The longitudinal sections are assumed to be in the shape of the wing airfoil due to the fact that the aircraft is a blended wing- body design. The airfoil coordinates are read from the airfoil text file. The upper and lower airfoil splines are generated by the curve fitting method by using the coordinates of the airfoil. Figure 2. 6 shows the actual airfoil and the 9th degree curve fitting spline on NACA 66006 symmetric airfoil.
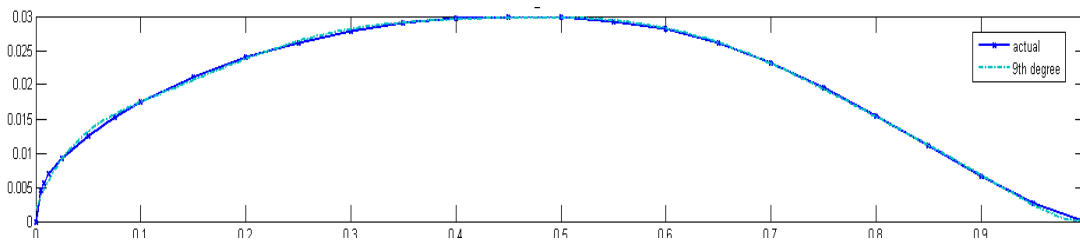
Figure 2. 6 Actual Airfoil Upper Spline and the 9th Degree Curve Fitting.

The points on the upper surface are determined by the following function;

$$y\left(\frac{x}{c}\right) = p1 \cdot \left(\frac{x}{c}\right)^8 + p2 \cdot \left(\frac{x}{c}\right)^7 + p3 \cdot \left(\frac{x}{c}\right)^6 + p4 \cdot \left(\frac{x}{c}\right)^5 + p5 \cdot \left(\frac{x}{c}\right)^4 + p6 \cdot \left(\frac{x}{c}\right)^3 + p7$$
$$\cdot \left(\frac{x}{c}\right)^2 + p8 \cdot \left(\frac{x}{c}\right) + p9$$

$\frac{x}{c}$ is the ratio of x position to the chord and p is the coefficients of curve fitting function.

The span-wise sections are assumed to be in the shape of diamonds for the ease of formulation. The heights of the diamonds are determined from the $y\left(\frac{x}{c}\right)$ function for the related x positions and the widths of the diamonds are determined from the span-wise length of the geometry at the x positions.
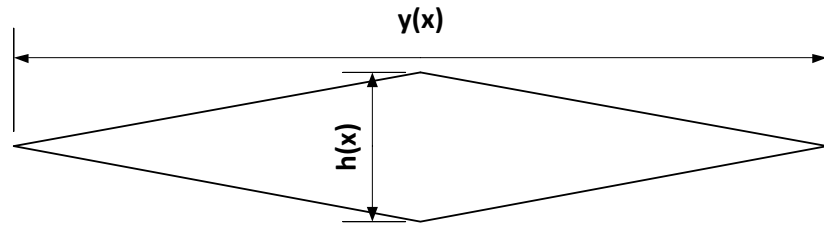
Figure 2. 7 The Diamond Properties.
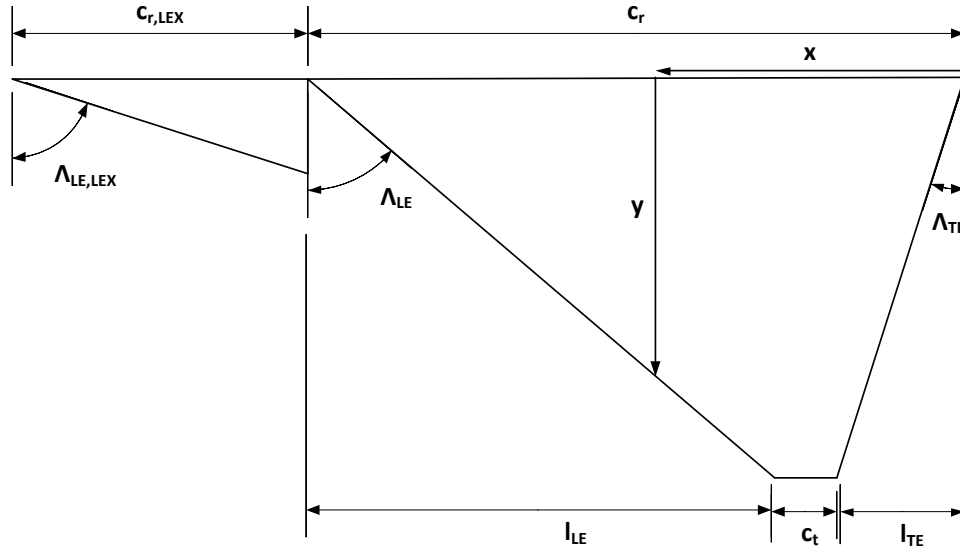
Figure 2. 8 The Longitudinal and Spanwise Section Parameters

From Figure 2. 7;

$\boldsymbol{h(x)} = \boldsymbol{y}\left(\frac{x}{c}\right)\Big|_{upper} - \boldsymbol{y}\left(\frac{x}{c}\right)\Big|_{lower}$ and the $y(x)$ are determined as follows;

For the $x < l_{TE}$, where $l_{TE} = \left(\frac{b}{2}\right) \cdot \tan\left(\varLambda_{TE}\right)$;

$$y = \frac{\tan\left(\varLambda_{TE}\right)}{x}$$

15

For the $l_{TE} < x < l_{TE} + c_t$,

$$y = b$$

For the $l_{TE} + c_t < x < c_r$,

$$y = \frac{c_r - x}{\tan(\Lambda_{LE})}$$

For the $c_r < x < c_r + c_{r,LEX}$,

$$y = \frac{c_r + c_{r,LEX} - x}{\tan(\Lambda_{LE,LEX})}$$
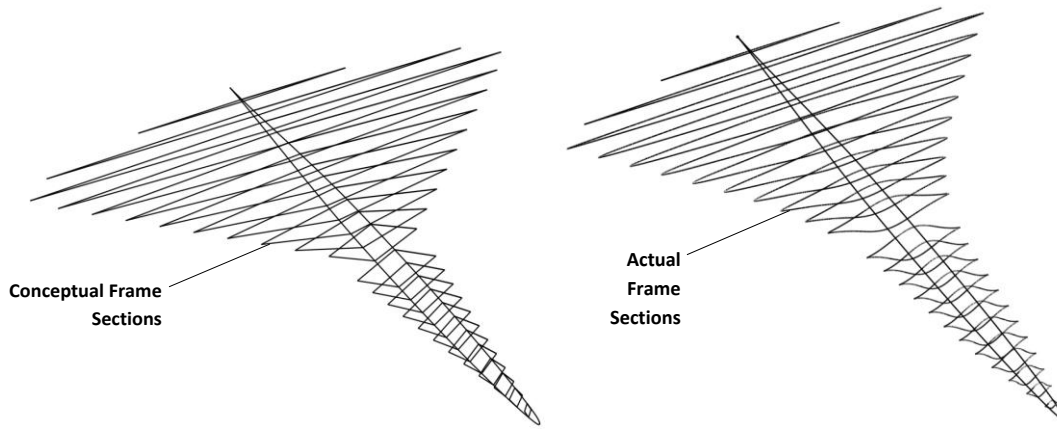
Figure 2. 9 Initial Conceptual and Actual Frame Sections

Figure 2. 9 shows the initial conceptual and the actual frame sections. Conceptual frame sections are generated by the method described previously. Span-wise sections are in the diamond shape and the longitudinal ones in the form of the airfoil. Conceptual frame sections will be used to calculate frame section area. Although the actual wing shape is different from the conceptual one, this model is adequate to generate the weight distribution for the internal structure during the calculations. Actual frames will get detail during the detailed design phase. Figure 2. 9 just shows the outer boundaries of the actual frames.

The calculations of other properties are shown below. The main wing area;

$$S_{main\_wing} = \frac{(c_r + c_t) \cdot b}{2}$$

The aspect ratio of the main wing;

$$AR_{main\_wing} = \frac{b^2}{S_{main\_wing}}$$

Taper ratio;

$$\lambda = \frac{c_t}{c_r}$$

16

Sweep angle at quarter chord;

$$\Lambda_{c/4} = atan\left(\frac{b}{2} \cdot \tan(\Lambda_{LE}) + \frac{c_t - c_r}{2b}\right)$$

Sweep angle at semi chord;

$$\Lambda_{c/2} = atan\left(\frac{b}{2} \cdot \tan(\Lambda_{LE}) + \frac{c_t - c_r}{b}\right)$$

Mean aerodynamic chord [2];

$$\bar{c} = \frac{2}{3} c_r \frac{1 + \lambda + \lambda^2}{1 + \lambda}$$

The position of the mean aerodynamic chord in span-wise direction [2];

$$\bar{y} = \frac{b}{6} \frac{1 + 2\lambda}{1 + \lambda}$$

Similarly for the virtual front wing, LEX;

The LEX area;

$$S_{LEX} = \frac{(c_{r,LEX} + c_{t,LEX}) \cdot b_{LEX}}{2}$$

The aspect ratio of the LEX;

$$AR_{LEX} = \frac{b_{LEX}^2}{S_{LEX}}$$

Taper ratio;

$$\lambda_{LEX} = \frac{c_{t,LEX}}{c_{r,LEX}}$$

Sweep angle at quarter chord;

$$\Lambda_{c/4,LEX} = atan\left(\frac{b_{LEX}}{2} \cdot \tan(\Lambda_{LE,LEX}) + \frac{c_{t,LEX} - c_{r,LEX}}{2b_{LEX}}\right)$$

Sweep angle at semi chord;

$$\Lambda_{c/2,LEX} = atan\left(\frac{b_{LEX}}{2} \cdot \tan(\Lambda_{LE,LEX}) + \frac{c_{t,LEX} - c_{r,LEX}}{b_{LEX}}\right)$$

Mean aerodynamic chord;

$$\bar{c}_{LEX} = \frac{2}{3} c_{r,LEX} \frac{1 + \lambda_{LEX} + \lambda_{LEX}^2}{1 + \lambda_{LEX}}$$

The position of the mean aerodynamic chord in spanwise direction;

$$\bar{y}_{LEX} = \frac{b_{LEX}}{6} \frac{1 + 2\lambda_{LEX}}{1 + \lambda_{LEX}}$$

The total wing-body area;

$$S_{TOTAL} = S = S_{main\_wing} + S_{LEX}$$

4.2 Tail Geometry

Tail geometry is defined as follows. The internal structure is neglected.
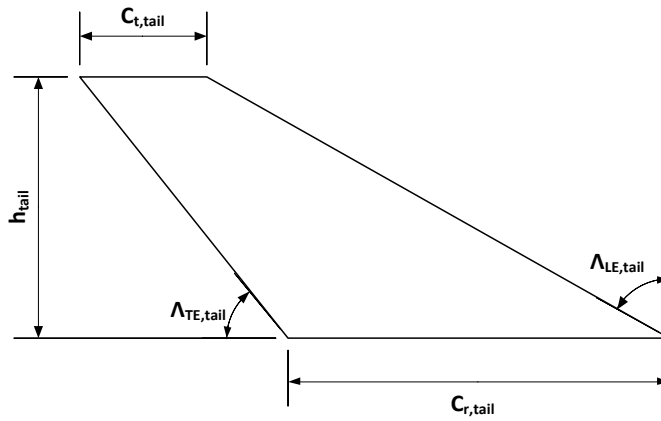
Figure 2. 10 Tail Geometry

Geometric properties are calculated as follows;

The vertical tail height;

$$h_{tail} = \frac{c_{r,tail} - c_{t,tail}}{tan\,(\Lambda_{LE,tail}) - \dfrac{1}{tan\,(\Lambda_{TE,tail})}}$$

The tail area;

$$S_{tail} = h_{tail} \cdot \left(\frac{c_{r,tail} + c_{t,tail}}{2}\right)$$

Aspect ratio of the tail;

$$AR_{tail} = \frac{(2h_{tail})^2}{S_{tail}}$$

Taper ratio of the tail;

$$\lambda_{tail} = \frac{c_{t,tail}}{c_{r,tail}}$$

18

Sweep angle at quarter chord;

$$\Lambda_{c/4,tail} = atan\left(\frac{3}{4} \cdot \frac{c_{r,tail} - c_{t,tail}}{h_{tail}}\right)$$

Sweep angle at semi chord;

$$\Lambda_{c/2,tail} = atan\left(\frac{1}{2} \cdot \frac{c_{r,tail} - c_{t,tail}}{h_{tail}}\right)$$

Mean aerodynamic chord of the tail [2];

$$\bar{c}_{tail} = \frac{2}{3}c_{r,tail}\frac{1 + \lambda_{tail} + \lambda_{tail}^2}{1 + \lambda_{tail}}$$

The position of the mean aerodynamic chord in span-wise direction;

$$\bar{y}_{tail} = \frac{h_{tail}}{3}\frac{1 + 2\lambda_{tail}}{1 + \lambda_{tail}}$$

5. Weight Model

During the conceptual design phase the weight estimation is the first step through the performance calculations. The conventional weight calculation method is based on the historical data which are obtained from the previously built commercial or military aircraft. Several constants are taken for each mission profile segment and the total weight is estimated. Instead of conventional method which can be inadequate for small unmanned aircraft, a detailed weight build-up method is used for the weight calculation. The weight of each component of the aircraft is calculated by using the design weight inputs. The frame and skin weight is calculated by using the sample unit weights for the frame and skin and the values generated from the geometric model calculations. The avionic weights are considered as an input. The fuel weight, landing gear weight, the parachute weight and the fuel tank weight are calculated iteratively. The fuel weight is calculated by running the mission profile for the initial weight guess which also includes the fuel weight. When the values are converged, the total weight is generated. This process is done on the Excel file for the design inputs sent from the Matlab code.
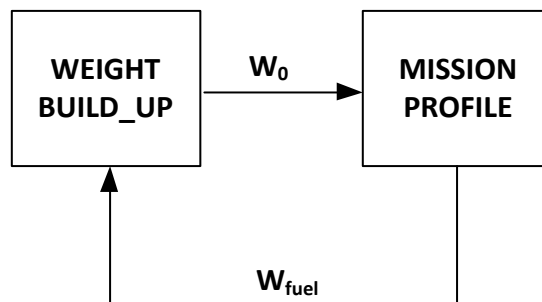
Figure 2. 11 Iterative Calculation of Total Weight

19

Figure 2. 11basically shows the iterative calculation of total weight, W_0.

Total weight is calculated by summing up the structural weights and the internal component weights such as engine and fuel system, fuel, avionics, etc. The total weight is calculated as follows;

$$W_0 = W_{TOTAL} = W_{empty} + W_{fuel} + W_{payload}$$

$\boldsymbol{W_{fuel}}$ is the output of the mission profile and calculated iteratively.

Aircraft total weight is considered as the dry weight which includes the weight of structural parts such as the frames and the skin. It is calculated as follows;

$$W_{empty} = W_{wing\_body} + W_{tail} + W_{sys\_internal}$$

The weight of the wing-body is calculated as follows;

$$W_{wing\_body} = W_{blended\_wing} + W_{inlet} + W_{paint}$$

The weight of blended wing-body;

$$W_{blended\_wing} = W_{wing\_skin} + W_{frame}$$

The weight of skin is calculated by assuming the wetted area is 2.3 times the planform area;

$$W_{wing\_skin} = 2.3 \cdot S_{TOTAL} \cdot W_{s\_skin}$$

Frame weights are calculated according to the conceptual frame section surface areas as described in section 4.2. The conceptual frames are multiplied with a fill ratio parameter which accounts for the gaps on the frame sections. The sample laminate weight is used to calculate the local frame weight.

The total frame weight is the sum of span-wise frames, longitudinal frames and inlet frames.

$$W_{frame} = W_{sp\_frame} + W_{lng\_frame} + W_{in\_frame}$$

For $\boldsymbol{N_{sp\_f}}$ number of span-wise frames, the total span-wise frame weight;

$$W_{sp\_frame} = \sum_{i=1}^{N_{sp\_f}} W_{sp\_frame}(i)$$

The local frame weight;

$$W_{sp\_frame}(i) = S_{sp\_frame}(i) \cdot W_{s_{frame}} \cdot F_{fill}(i)$$

$F_{fill}(i)$ is the fill ratio constant for the frames.

Local frame areas are calculated by using the method described in section 4.1. Figure 2. 12 shows the location of the diamonds. The calculation of the diamond areas is as follows;

For the $x(i) < l_{TE}$, where $l_{TE} = \left(\frac{b}{2}\right) \cdot \tan(\Lambda_{TE})$;

$$S_{sp\_frame}(i) = \frac{\tan(\Lambda_{TE})}{x(i)} \cdot \frac{h(i)}{2}$$

For the $l_{TE} < x(i) < l_{TE} + c_t$,

$$S_{sp\_frame}(i) = b \cdot \frac{h(i)}{2}$$

For the $l_{TE} + c_t < x(i) < c_r$,

$$S_{sp\_frame}(i) = \frac{c_r - x(i)}{\tan(\Lambda_{LE})} \cdot \frac{h(i)}{2}$$

For the $c_r < x(i) < c_r + c_{r,LEX}$,

$$S_{sp\_frame}(i) = \frac{c_r + c_{r,LEX} - x(i)}{\tan(\Lambda_{LE,LEX})} \cdot \frac{h(i)}{2}$$

The local positions are generated by the following function;

$$x(i) = \frac{c_r + c_{r,LEX}}{N_f + 1} \cdot (i)$$

The height of each frame from the equation in section 4.2;

$$h(i) = y\left(\frac{x(i)}{c}\right)\bigg|_{upper} - y\left(\frac{x(i)}{c}\right)\bigg|_{lower}$$

$$= p1 \cdot \left(\frac{x(i)}{c}\right)^8 + p2 \cdot \left(\frac{x(i)}{c}\right)^7 + p3 \cdot \left(\frac{x(i)}{c}\right)^6 + p4 \cdot \left(\frac{x(i)}{c}\right)^5 + p5 \cdot \left(\frac{x(i)}{c}\right)^4$$

$$+ p6 \cdot \left(\frac{x(i)}{c}\right)^3 + p7 \cdot \left(\frac{x(i)}{c}\right)^2 + p8 \cdot \left(\frac{x(i)}{c}\right) + p9$$

c is the chord length which is equal to $c_r + c_{r,LEX}$ and the constants are the subtractions of the upper and lower surface function constants in this case.
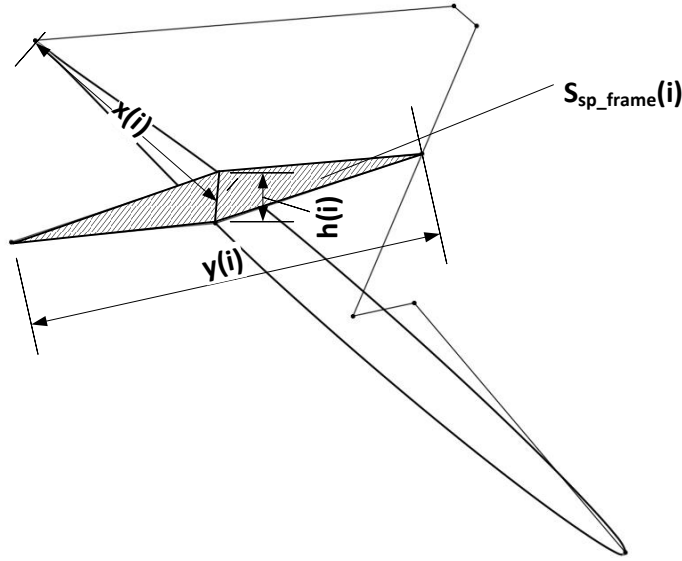
Figure 2. 12 The Location of the Local Frame

The areas of the longitudinal frames are calculated by taking the integral of $y\left(\frac{x}{c}\right)$ for upper and lower surfaces of the airfoil for different span-wise positions. The calculations are made for the main wing and the front wing separately.

$$W_{lng\_frame} = W_{mw\_lng\_frame} + W_{fw\_lng\_frame}$$

For the main wing;

For $N_{mw\_lng\_f}$ number of longitudinal frames in main wing, the total frame weight;

$$W_{mw\_lng\_frame} = 2 \cdot \sum_{i=1}^{N_{mw\_lng\_f}} W_{mw\_lng\_frame}(i)$$

The reason of multiplying by two is the fact that longitudinal frames are symmetrical.

The local frame weight;

$$W_{mw\_lng\_frame}(i) = S_{mw\_lng\_frame}(i) \cdot W_{S_{frame}} \cdot F_{fill}(i)$$

$F_{fill}(i)$ is again fill ratio constant for the longitudinal frames.

The area of the longitudinal frames;

$$S_{mw\_lng\_frame}(i) = [c(i)]^2 \cdot \left(\int_0^{\frac{x}{c}} h(i) \Bigg|_{upper} - \int_0^{\frac{x}{c}} h(i) \Bigg|_{lower} \right)$$

The chord length of the local longitudinal frame;

$$c(i) = c_r - y(i) \cdot tan(\Lambda_{TE}) - y(i) \cdot tan(\Lambda_{LE})$$

22

For the front wing;

For $N_{fw\_lng\_f}$ number of longitudinal frames in front wing, the total frame weight;

$$W_{fw\_lng\_frame} = 2 \cdot \sum_{i=1}^{N_{fw\_lng\_f}} W_{fw\_lng\_frame}(i)$$

The chord length of the local longitudinal frame;

$$c(i) = c_{r,LEX} - y(i) \cdot \tan(\Lambda_{LE,LEX})$$

$y(i)$ is the spanwise position of each longitudinal frame.

The weight of inlet frame is calculated by assuming the inlet section circular. The circular frames are multiplied by local fill ratio value and the weight is calculated.

For N_{in_f} number of frames, the total frame weight;

$$W_{in\_frame} = \sum_{i=1}^{N_{in\_f}} W_{in\_frame}(i)$$

The local frame weight;

$$W_{in\_frame}(i) = S_{in\_frame}(i) \cdot W_{S_{frame}} \cdot F_{fill}(i)$$

The area of the inlet frame;

$$S_{in\_frame}(i) = \pi \cdot (R_{inlet})^2$$

The weight of inlet skin;

$$W_{inlet} = 2 \cdot 2\pi \cdot R_{inlet} \cdot l_{inlet} \cdot W_{s\_skin}$$

The weight of paint;

$$W_{paint} = 2.3 \cdot S_{TOTAL} \cdot W_{s\_paint}$$

The weight of the tail is considered as the weight of the skin only; it is calculated as follows;

$$W_{tail} = 2 \cdot S_{tail} \cdot W_{s\_tail}$$

The internal system weight includes the weight of the fuel, engine/engines, avionics such as autopilot, servos, telemetry system, fuel system, batteries and etc. The total internal system weight calculation requires an iterative process since some of the unit weights are directly related to the total weight such as fuel weight which is derived from the mission profile and landing gear weights which are calculated from the total weight.

$$W_{sys\_internal} = W_{main\_l\_gear} + W_{nose\_l\_gear} + W_{engines} + W_{engine\_comp} + W_{avionics} \\ + W_{batteries} + W_{parachute}$$

The main and nose landing weights are calculated as follows;

$$W_{main\_l\_gear} = \left(W_{m.gear} \middle/ W_{TOTAL} \right) \cdot W_{TOTAL}$$

$$W_{nose\_l\_gear} = \left(W_{nose\ gear} \middle/ W_{TOTAL} \right) \cdot W_{TOTAL}$$

$W_{engines}$ is an input parameter for the engines.

W_{engine_comp} is an input parameter and includes the weights engine controller, fuel pumps, solenoid valves, gas tank, fuel pipes and etc.

$W_{avionics}$ is weight of the electronic equipments such as autopilot, data and video modems, antennas, sensors, cables and servos. It is an input parameter.

$W_{batteries}$ is the weight of batteries which are used to power the electronic equipments. It is an input parameter.

The parachute weight is directly related to the total weight;

$$W_{parachute} = 0.05 \cdot W_{TOTAL}$$

$W_{payload}$ accounts for the payload weight. Payloads can be gimbals for surveillance missions, radars or similar systems.

6. Aerodynamics

This includes the calculation of aerodynamic coefficients like lift curve slope of the blended wing-body, drag coefficients and etc.

6.1 Air Properties

Air properties are formulated according to Ref. [3] as follows;

The density of air;

$$\rho = ((1 - 6.875 \cdot 10^{-6} \cdot 3.2808 \cdot h)^{4.2561}) \cdot \rho_0$$

The temperature of air;

$$T = (1 - 6.875 \cdot 10^{-6} \cdot 3.2808 \cdot h) \cdot T_0$$

6.2 Lift Curve Slopes

Lift curve slope describes the change of lift coefficient with respect to angle of attack. Lift curve slopes are calculated for each unit which are main wing, LEX and tail. At the end the total aircraft lift curve slope is calculated.

The aircraft's total lift curve slope [4] is calculated by assuming the LEX behaves like a canard. So,

$$C_{L_\alpha} = C_{L_{\alpha WB}} + C_{L_{\alpha H}} \cdot \eta_H \cdot \frac{S_H}{S}\left(1 - \left(\frac{d\epsilon}{d\alpha}\right)_{downwash}\right) + C_{L_{\alpha LEX}} \cdot \eta_{LEX} \cdot \frac{S_{LEX}}{S}(1 - \left(\frac{d\epsilon}{d\alpha}\right)_{upwash})$$

The lift curve slope of the wing body [4];

$$C_{L_{\alpha WB}} = C_{L_{\alpha W}} \cdot \left(1 - 0.25\left(\frac{d_{fuselage}}{b}\right)^2 + 0.025\left(\frac{d_{fuselage}}{b}\right)\right)$$

The virtual fuselage diameter is calculated from the inputs;

$$d_{fuselage} = \sqrt{4\pi \cdot w_{fuselage} \cdot h_{fuselage}}$$

The lift curve slope of the wing [4];

$$C_{L_{\alpha W}}\Big|_M = \frac{2\pi AR_{main\_wing}}{2 + \sqrt{\frac{(AR_{main\_wing})^2 \beta^2}{\kappa^2} \cdot \left(1 + \frac{tan^2 \Lambda_{c/2}}{\beta^2}\right) + 4}} \quad (rad^{-1})$$

$$\beta = \sqrt{1 - M_{cruise}^2}$$

$$\kappa = \frac{\beta \cdot C_{l_{\alpha,wing}}}{2\pi}$$

Mach number;

$$M_{cruise} = \frac{V_{cruise}}{\sqrt{1.4 \cdot 287 \cdot \rho_{cruise}}}$$

The tail lift curve slope is calculated by introducing the virtual horizontal and vertical tails due to the fact that the inclined tail is similar to the V-tail configuration.

The aspect ratio of the virtual horizontal wing;

$$AR_{tail\_HT} = \frac{\left(2 \cdot h_{tail} \cdot cos(90 - \alpha_{i.tail})\right)^2}{S_{tail\_HT}}$$

The area of the virtual horizontal tail;

$$S_{tail\_HT} = S_{tail} \cdot cos(90 - \alpha_{i.tail})$$

The sweep angle at the semi chord;

$$\Lambda_{c/2,tail\_HT} = atan\left(\frac{1}{2} \frac{c_{r,tail} - c_{t,tail}}{\frac{b_{HT}}{2}}\right)$$

The span of the virtual horizontal tail;

$$b_{HT} = \sqrt{AR_{tail\_HT} \cdot S_{tail\_HT}}$$

$$C_{L_{\alpha_H}}\bigg|_M = \frac{2\pi AR_{tail\_HT}}{2 + \sqrt{\frac{\left(AR_{tail\_HT}\right)^2 \beta^2}{\kappa_{tail}^2} \cdot \left(1 + \frac{tan^2\Lambda_{c/2,tail\_HT}}{\beta^2}\right) + 4}} \quad (rad^{-1})$$

$$\kappa_{tail} = \frac{\beta \cdot C_{l_{\alpha,tail}}}{2\pi}$$

The downwash factor [4] is found from,

$$\left(\frac{d\epsilon}{d\alpha}\bigg|_M\right)_{downwash} = \frac{d\epsilon}{d\alpha}\bigg|_{M=0} \cdot \frac{C_{L_{\alpha_W}|_M}}{C_{L_{\alpha_W}|_{M=0}}}$$

$$\frac{d\epsilon}{d\alpha}\bigg|_{M=0} = 4.44\left[K_A \cdot K_\lambda \cdot K_H \sqrt{cos\Lambda_{c/4}}\right]^{1.19}$$

$$K_A = \frac{1}{AR_{main\_wing}} - \frac{1}{1 + \left(AR_{main\_wing}\right)^{1.7}}$$

$$K_\lambda = \frac{10 - 3\lambda}{7}$$

$$K_H = \frac{1 - \frac{h_{tail}}{b}}{\left(\frac{2l_{tail}}{b}\right)^{\frac{1}{3}}}$$

26

The lift curve slope of the LEX is calculated by assuming the front wing is similar to a canard.

$$C_{L_{\alpha_{LEX}}}\Big|_M = \frac{2\pi AR_{LEX}}{2 + \sqrt{\frac{(AR_{LEX})^2 \beta^2}{\kappa_{LEX}^2} \cdot \left(1 + \frac{tan^2 \Lambda_{c/2,LEX}}{\beta^2}\right) + 4}} \quad (rad^{-1})$$

$$\kappa_{LEX} = \frac{\beta \cdot C_{l_{\alpha,LEX}}}{2\pi}$$

The upwash parameter, $\left(\frac{d\epsilon}{d\alpha}\right)_{upwash}$, is input for the this formulation and can be obtained from Figure 2. 13 (Ref. [5], Figure 8.67).

DISTANCE FORWARD OF ROOT QUARTER-CHORD POINT IN ROOT CHORDS
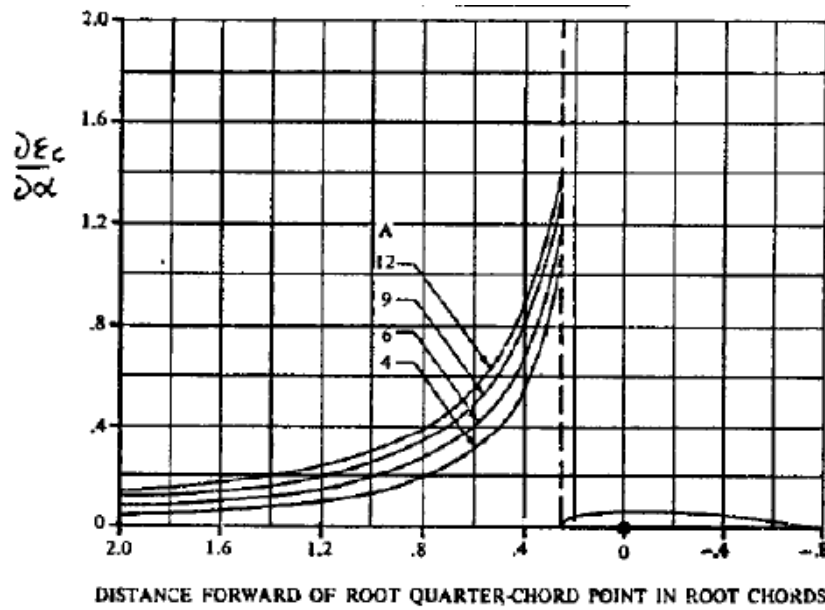
Figure 2. 13 Wing Upwash Gradient. (Copied From Ref. [5], Figure 8.67)

6.3 Maximum lift Coefficient

The maximum lift coefficient is estimated as follows;

$$C_{L,max} = 0.9 \cdot C_{l,max} \cdot \Lambda_{c/4}$$

6.4 Parasite Drag Coefficient

The aircraft parasite drag coefficient is calculated by summing up the each unit drag coefficients as defined below. (Formulation is taken from Ref. [6]).

The total parasite drag coefficient;

$$C_{D0_{subsonic}} = \frac{\Sigma(C_{F_c} \cdot FF_c \cdot Q_c \cdot S_{wet_c})}{S_{ref}} + C_{d_{misc}} + C_{d_{L\&P}}$$

For turbulent flow;

$$C_F = \frac{0.455}{(log_{10}Re)^{2.58}(1 + 0.144M^2)^{0.65}}$$

For wing and tail surfaces;

$$FF = \left[1 + \frac{0.6}{\left(\frac{x}{c}\right)_m}\left(\frac{t}{c}\right) + 100\left(\frac{t}{c}\right)^4\right] \cdot [1.34M^{0.18}(cos\lambda_m)^{0.28}]$$

Reynolds Number is calculated as follows;

The viscosity of air;

$$\mu = 1.458 \cdot 10^{-6} \cdot T^{\frac{3}{2}} \cdot \left(\frac{1}{T + 110.4}\right)$$

The temperature of air;

$$T = (1 - 6.875 \cdot 10^{-6} \cdot 3.2808 \cdot h) \cdot T_0$$

Where T_0 is the air temperature at the sea level.

The Reynolds Number;

$$Re = \rho \cdot V_{cruise} \cdot \frac{\bar{c}}{\mu}$$

The lift to drag ratio at cruise conditions are found as;

$$\left(\frac{C_L}{C_D}\right)_{cruise} = \frac{C_{L,cruise}}{C_{D0_{TOTAL}} + kC_{L,cruise}^2}$$

The cruise lift and drag coefficients are found from below equations;

$$C_{L,cruise} = \frac{2 \cdot W_{TOTAL}/S}{\rho_{cruise} \cdot V_{cruise}^2}$$

$$C_{D0,TOTAL} = C_{D0,wing\_body} + C_{D0,tail}$$

$$k = \frac{1}{\pi \cdot e \cdot AR_{main\_wing}}$$

The span efficiency factor [6] for $\Lambda_{LE} > 30\ deg.$;

$$e = 4.61 \cdot \left(1 - 0.045(AR_{main\_wing})^{0.68}\right) \cdot (\cos(\Lambda_{LE}))^{0.15} - 3.1$$

7. Performance

Performance calculations include the calculation of thrust and power required during cruise, the rate of climb performance, turn rates, turn radius, maximum sustained and instantaneous loads, corner velocity, pull up and pull down performances.

7.1 Stall Velocity

Stall velocity is calculated as follows;

$$V_{stall} = \sqrt{\frac{2\frac{W}{S}}{\rho C_{L,max}}}$$

7.2 Thrust and Power Required

The thrust and power required calculations are shown below;

$$T_r = DV = \frac{1}{2}\rho_{cruise}V_{cruise}^2 S(C_{D0,TOTAL} + kC_{L,cruise}{}^2)$$

$$P_r = T_r V = DV = \frac{1}{2}\rho_{cruise}V_{cruise}^3 S(C_{D0,TOTAL} + kC_{L,cruise}{}^2)$$

7.3 Rate of Climb

Rate of climb is defined as follows;

$$R/_C = \frac{Excess\ Power}{Weight} = \frac{P_{available} - P_r}{W} = \frac{V \cdot (T_A - T_R)}{W}$$

7.3 Maximum Velocity

The maximum velocity is calculated where the rate of climb is zero. This situation is due to the fact that all excess power is consumed at that velocity so; it is at the maximum value.

$$R/_C = \frac{V \cdot (T_A - T_R)}{W} = 0$$

$$T_A = T_R = \frac{1}{2}\rho_{cruise}V_{max}^2 S(C_{D0,TOTAL} + kC_L{}^2)$$

$$C_L = \frac{2 \cdot W_{TOTAL}/S}{\rho_{cruise} \cdot V_{max}^2}$$

In above equation, $C_{D0,TOTAL}$ and C_L are calculated for the speed $V = V_{max}$. So the drag and lift coefficients are different than the ones at cruise condition. The above equation is calculated iteratively at Excel file.

7.4 Maximum Load Factor

The load factor is defined as the ratio of lift to weight. During maneuvers this ratio changes as the lift must increase. The maximum load factor is constrained with both $C_{,,max}$ and $T_{A,max}$.

The load factor constraint with $C_{L,max}$,

$$n = \frac{L}{W} = \frac{1}{2}\rho_\infty V_\infty^2 C_L \frac{S}{W}$$

When $C_L = C_{L\,max}$;

$$n_{max} = \frac{1}{2}\rho V^2 \frac{C_{L\,max}}{(W_{TOTAL}/S)}$$

The load factor constraint with $T_{A,max}$,

$$T = D = \frac{1}{2}\rho_\infty V_\infty^2 S(C_{D0} + KC_L{}^2)$$

$$C_L = \frac{2nW}{\rho_\infty V_\infty^2 S}$$

$$T = \frac{1}{2}\rho_\infty V_\infty^2 S\left[C_{D0} + K\left(\frac{2nW}{\rho_\infty V_\infty^2 S}\right)^2\right]$$

$$n = \left[\frac{\frac{1}{2}\rho_\infty V_\infty^2}{K(W/S)}\left(\frac{T}{W} - \frac{1}{2}\rho_\infty V_\infty^2 \frac{C_{D0}}{W/S}\right)\right]^{1/2}$$

When $T_A = T_{A,max}$;

$$n_{max} = \left[\frac{\frac{1}{2}\rho_\infty V_\infty^2}{K(W/S)}\left(\left\{\frac{T}{W}\right\}_{max} - \frac{1}{2}\rho_\infty V_\infty^2 \frac{C_{D0}}{W/S}\right)\right]^{1/2}$$

$$= \left[\frac{\frac{1}{2}\rho_\infty V_\infty^2}{K(W/S)}\left(\frac{1}{V_\infty}\left\{\frac{P}{W}\right\}_{max} - \frac{1}{2}\rho_\infty V_\infty^2 \frac{C_{D0}}{W/S}\right)\right]^{1/2}$$
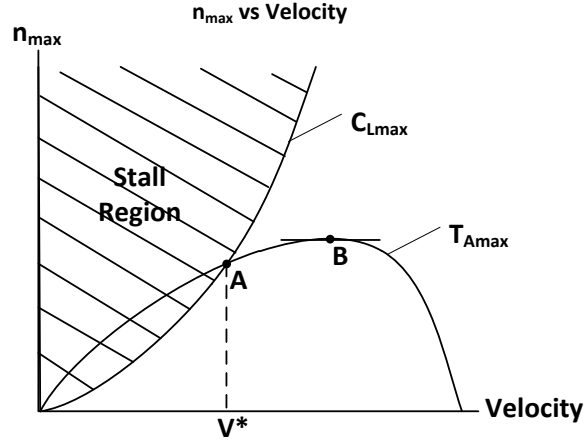
Figure 2. 14 Constraints on the Maximum Load Factor

The crossed region in Figure 2. 14 represents the region where the necessary C_L value is greater than the $C_{L_{max}}$. Point A is the n_{max} value which satisfies both $C_{L_{max}}$ and $T_{A,max}$ constraint. Point B is the maximum value of n_{max} .

The calculation is conducted by generating n_{max} values from both $C_{L_{max}}$ and $T_{A,max}$ equations and finding the speed where n_{max} values are the same.

7.5 Turn Performance

Turn performance demonstrates the limits of the aircraft during maneuvering. These maneuvers include level turn, pull up and pull down maneuvers.

One of the important parameters of turn performance is the corner velocity which is shown at point A in Figure 2. 14. At this point, maximum turn rate and minimum turn radius are obtained. It is defined as [2];

$$V^* = \sqrt{\frac{2n_{max}}{\rho C_{L_{max}}} \frac{W}{S}}$$

Turn rate is defined as [2];

$$\omega = \frac{V}{R}$$

R is the turn radius and defined as [2];

$$R = \frac{V^2}{g\sqrt{n^2 - 1}}$$

31

The maximum turn rate is found as [2];

$$\omega_{max} = \frac{g\sqrt{n_{\omega_{max}}^2 - 1}}{V^*}$$

Minimum turn radius [2];

$$R_{min} = \frac{(V^*)^2}{g\sqrt{n_{max}^2 - 1}}$$

Maximum bank angle;

$$\emptyset_{max} = acos\left(\frac{1}{n_{max}}\right)$$

The pull up and pull down maneuver performance conducted by considering instantaneous turn unlike the level turn maneuver.

For the pull up maneuver;

The turn radius;

$$R = \frac{V^2}{g(n-1)}$$

The turn rate;

$$\omega = \frac{g(n-1)}{V}$$

For the pull down maneuver;

The turn radius;

$$R = \frac{V^2}{g(n+1)}$$

The turn rate;

$$\omega = \frac{g(n+1)}{V}$$

8. Mission Profile

Mission profile consists of the sub segments that are takeoff ground roll, transition, climb, cruise, descent, loiter, approach and landing ground roll.

8.1 Takeoff Ground Roll: Segment 0-1

Figure 2. 15 shows the Ground roll distance, S_g , the initial velocity, $V_{i,01}$ and the final velocity, $V_{f,01}$.
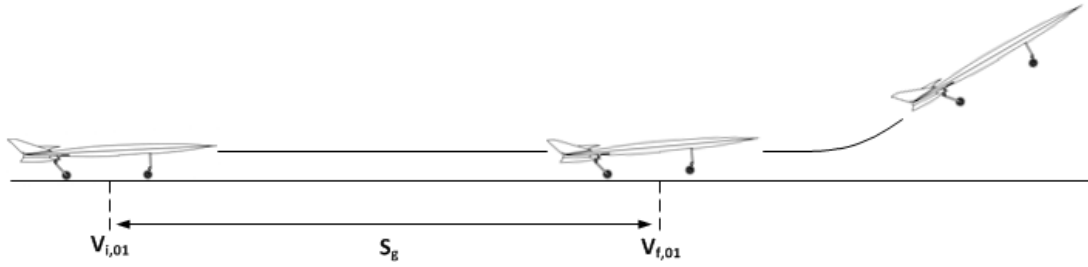
Figure 2. 15 Takeoff Ground Roll

The takeoff distance is found by [2];

$$S_g = \frac{1}{2gK_A} ln \left(\frac{K_T + K_A \cdot V_{f,01}^2}{K_T + K_A \cdot V_{i,01}^2} \right) + N \cdot V_{f,01}$$

Where;

$$K_A = \frac{\rho}{2(W/S)} \cdot [\mu_r C_{L0} - C_{D0} - k \cdot C_{L0}^2]$$

$$K_T = \left(\frac{T_A}{W} \right)_{takeoff} - \mu_r$$

The final velocity on the takeoff leg is calculated as;

$$V_{f,01}^2 = 1.3 \cdot V_{stall}$$

The time, t_{01}, to accelerate to $V_{f,01}$ from $V_{i,01}$;

$$t_{01} = \frac{2S_g}{V_{f,01}}$$

Total weight after the takeoff;

$$W_1 = W_0 - \left(c_{t,ground\_roll} \right) \cdot T_{A,takeoff} \cdot t_{01}$$

$c_{t,ground\_roll}$ is the thrust specific fuel consumption during takeoff ground roll.

8.2 Transition: Segment 1-2

Figure 2. 16 shows the transition section. S_a represents the distance to clear an obstacle with a height of h_{obs}.
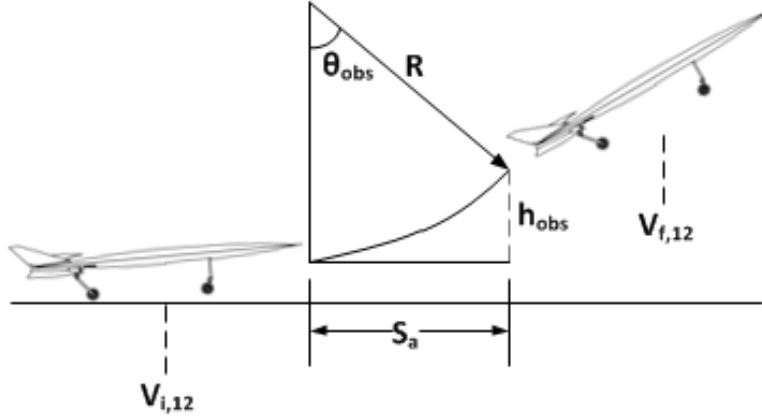
Figure 2. 16 The Transition

The transition distance is calculated from;

$$S_a = R \cdot sin(\theta_{obs})$$

The climb radius;

$$R = \frac{\left(\dfrac{V_{i,12} + V_{f,12}}{2}\right)^2}{g \cdot (n-1)}$$

Where;

$$n = \frac{\dfrac{1}{2}\rho \cdot S \cdot C_{Lmax} \cdot \left(\dfrac{V_{i,12} + V_{f,12}}{2}\right)^2}{W}$$

$V_{i,12}$ is the initial speed at the start of the section and $V_{f,12}$ is the final speed at the end of the section.

The climb angle;

$$\theta_{obs} = acos\left(1 - \frac{h_{obs}}{R}\right)$$

The time, t_{01}, to accelerate to $V_{f,12}$ from $V_{i,12}$;

$$t_{12} = \frac{2S_a}{V_{f,01} + V_{i,01}}$$

34

Total weight after the transition;

$$W_2 = W_1 - \left(c_{t,transition}\right) \cdot T_{A,takeoff} \cdot t_{12}$$

$c_{t,transition}$ is the thrust specific fuel consumption during transition.

8.3 Climb: Segment 2-3

During the climb section aircraft is considered to perform a full throttle, constant angle climb to until the cruise altitude and cruise speed. The aircraft starts the climb with the transition final speed, $V_{f,12}$ and climb angle, θ_{obs}. So, $V_{i,23} = V_{f,12}$ and $\theta_{climb} = \theta_{obs}$. The aircraft accelerates to cruise speed during the climb and continues to climb with constant speed until the cruise altitude. Figure 2. 17 shows the climb segment details.
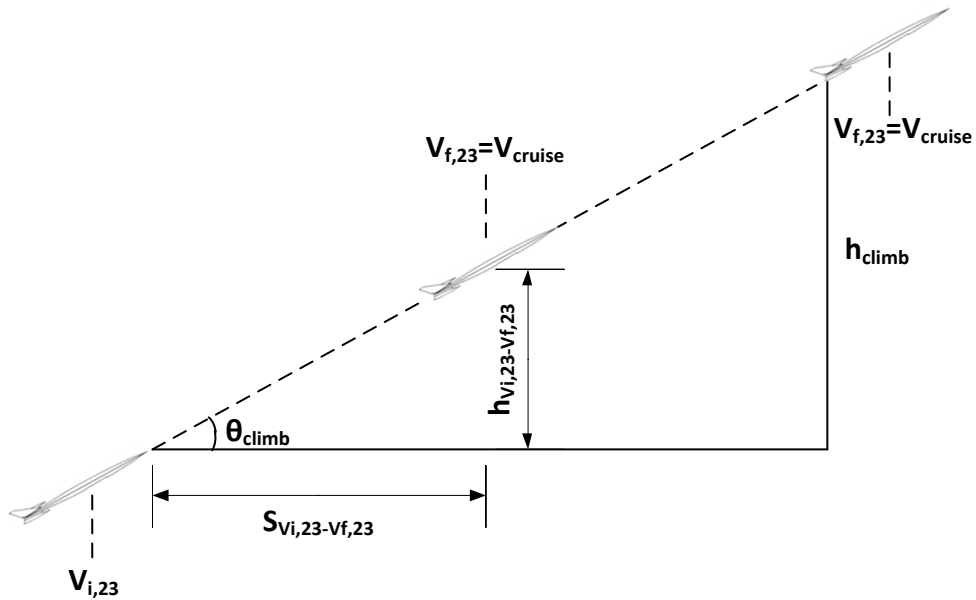
Figure 2. 17 Climb Segment

The initial speed at the start of the climb segment;

$$V_{i,23} = V_{f,12}$$

The final speed at the end of the climb segment;

$$V_{f,23} = V_{cruise}$$

The constant climb angle during the climb segment;

$$\theta_{climb} = \theta_{obs}$$

The climb time to cruise speed during the climb;

$$t_{Vi,23-Vf,23} = \frac{V_{f,23} - V_{i,23}}{g\left(\frac{T_A}{W} - \sin(\theta_{climb})\right)}$$

The height achieved during $t_{Vi,23-Vf,23}$,

$$h_{Vi,23-Vf,23} = \left[V_{i,23} \cdot (t_{Vi,23-Vf,23}) + \frac{1}{2}\left(\rho \cdot \left(\frac{T_A}{W} - \sin(\theta_{climb})\right)\right) \cdot (t_{Vi,23-Vf,23})\right] \cdot \sin(\theta_{climb})$$

The time elapsed during constant speed climb;

$$t_{climb} = \frac{h_{cruise} - \left(h_{Vi,23-Vf,23}\right) - h_{obs}}{\left(\frac{(R/C)_{takeoff} + (R/C)_{cruise}}{2}\right)}$$

Where;

$(R/C)_{takeoff}$ is the rate of climb at the takeoff altitude and $(R/C)_{cruise}$ is the rate of climb at cruise altitude.

The total time during the climb segment;

$$t_{climb,TOTAL} = t_{23} = \left(t_{Vi,23-Vf,23}\right) + t_{climb}$$

Total weight after the climb segment;

$$W_3 = W_2 - \left(c_{t,climb}\right) \cdot \left(\frac{T_{A,takeoff} + T_{A,cruise}}{2}\right) \cdot t_{23}$$

$c_{t,climb}$ is the thrust specific fuel consumption during climb. $T_{A,takeoff}$ is the available thrust at takeoff altitude and $T_{A,cruise}$ is the available thrust at the cruise attitude.

8.4 Cruise: Segment 3-4

Cruise segment is considered as a constant speed- constant altitude flight leg. The cruise time is used as an input and the necessary fuel is calculated as an output together with the total weight after the cruise segment.

The total weight after the cruise [2] is;

$$W_4 = \frac{W_3}{e^{\left(\frac{t_{cruise} \cdot c_{t,cruise}}{(C_L/C_D)_{cruise}}\right)}}$$

36

Where;

t_{cruise} is the flight time which is an input and $c_{t,cruise}$ is the thrust specific fuel consumption during cruise segment.

The range achieved during the cruise [2] is;

$$R_{range} = \frac{2}{c_{t,cruise}} \cdot \left(\sqrt{\frac{2}{\rho \cdot S}} \right) \cdot \frac{\sqrt{C_L}}{C_D} \cdot \left(\sqrt{W_3} - W_4 \right)$$

8.5 Descent: Segment 4-5

During the descent segment, the aircraft loses altitude until the loiter altitude with a constant descent rate which is a component of the vertical velocity. The velocity component which is parallel to the flight path is considered as the cruise speed. Figure 2. 18 shows the descent flight leg.
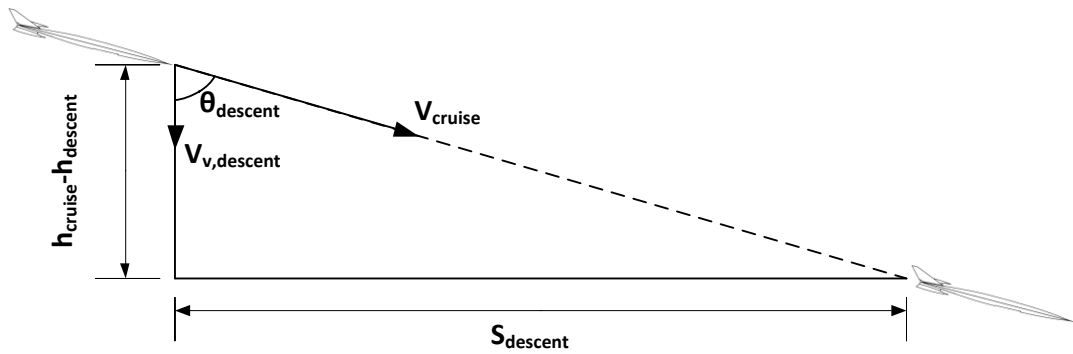
Figure 2. 18 The Descent Segment

The descent time during the altitude loss of $h_{cruise} - h_{descent}$;

$$t_{45} = \frac{h_{cruise} - h_{descent}}{V_{v,descent}}$$

Where;

$V_{v,descent}$ is the vertical component of the constant descent velocity.

The descent angle;

$$\theta_{descent} = asin \left(\frac{V_{v,descent}}{V_{descent}} \right)$$

37

Where;

$$V_{descent} = V_{cruise}$$

The horizontal distance covered during the descent;

$$S_{descent} = \frac{h_{cruise} - h_{descent}}{tan(\theta_{descent})}$$

The total weight after the descent segment;

$$W_5 = W_4 - \left(c_{t,descent}\right) \cdot \left(T_{R,descent}\right) \cdot t_{45}$$

Where;

$c_{t,descent}$ is the thrust specific fuel consumption during descent segment and $T_{R,descent}$ is the necessary thrust to achieve the constant speed descent; it is calculated as follows;

$$T_{R,descent} = \frac{1}{2} \cdot \left(\frac{\rho_{cruise} + \rho_{descent}}{2}\right) \cdot S \cdot (V_{descent})^2 \cdot \left(C_{D0,TOTAL} + k \cdot \left(C_{L,descent}\right)^2\right) - W_4 \cdot sin(\theta_{descent})$$

The lift coefficient during the descent;

$$C_{L,descent} = \frac{2 \cdot W_4 \cdot cos(\theta_{descent})}{\left(\frac{\rho_{cruise} + \rho_{descent}}{2}\right) \cdot S \cdot (V_{descent})^2}$$

During descent the lift coefficient changes due to the change of weight and flight angle.

8.6 Loiter: Segment 5-6

During the loiter segment, the aircraft is considered to achieve a constant speed loiter. The speed is considered as the same as the cruise speed. The loiter time, t_{56} is the input.

The total weight after the loiter segment [2];

$$W_6 = \frac{W_5}{e^{\left(\frac{t_{loiter} \cdot c_{t,loiter}}{(C_L/C_D)_{loiter}}\right)}}$$

Where;

$$t_{loiter} = t_{56}$$

$c_{t,loiter}$ is the thrust specific fuel consumption during the loiter and $(C_L/C_D)_{loiter} = (C_L/C_D)_{cruise}$.

8.7 Approach: Segment 6-7

Figure 2. 19 shows the approach and flare segment. The aircraft starts to approach with a speed of $V_{approach}$. The vertical component of the velocity is the descent rate for the approach, $V_{v,approach}$.

The flare path is considered as circular. The velocity at the start of the flare segment is V_{flare} and the velocity at the end is V_{TD}.
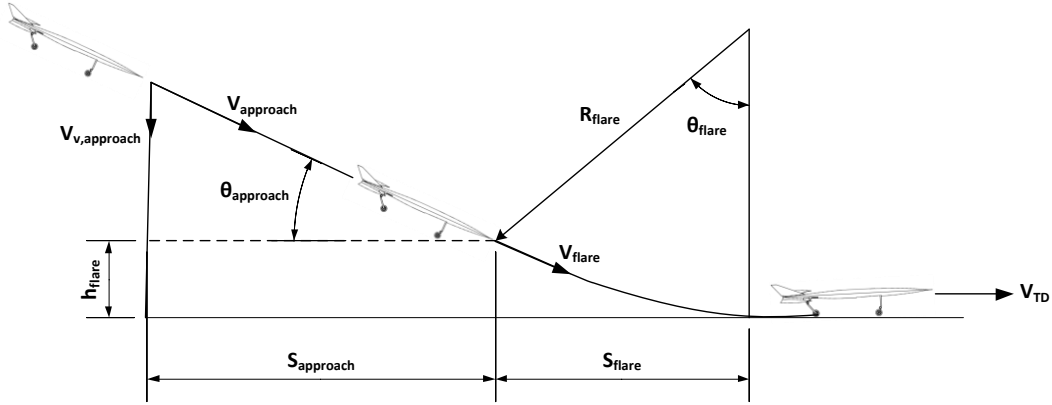
Figure 2. 19 The Approach and Flare Geometry

The approach velocity is taken as;

$$V_{approach} = 1.3 \cdot V_{stall}$$

The flare velocity is taken as;

$$V_{flare} = 0.95 \cdot V_{approach}$$

The approach angle;

$$\theta_{appraoch} = asin\left(\frac{V_{v,approach}}{\frac{V_{v,approach} + V_{flare}}{2}}\right)$$

The Flare radius is calculated from Ref. [3];

$$R_{flare} = \frac{V_{flare}^2}{C_L/\Delta C_L}$$

Where;

ΔC_L is the lift coefficient change during flare and found as (Ref. [3]);

$$\Delta C_L = C_{L,flare} - C_{L,TD}$$

Where $C_{L,flare}$ is the lift coefficient at the start of the flare segment and $C_{L,TD}$ is the lift coefficient at the end of the flare segment.

$$C_{L,flare} = \frac{2 \cdot W_6 \cdot cos(\theta_{appraoch})}{\left(\frac{\rho_{landing} + \rho_{descent}}{2}\right) \cdot S \cdot \left(V_{flare}\right)^2}$$

$$C_{L,TD} = \frac{2 \cdot W_6}{\left(\frac{\rho_{landing} + \rho_{descent}}{2}\right) \cdot S \cdot (V_{TD})^2}$$

The vertical distance covered during the flare,

$$h_{flare} = R_{flare} \cdot \left(1 - cos(\theta_{appraoch})\right)$$

The horizontal distance covered during the flare;

$$S_{flare} = \frac{R_{flare}}{sin(\theta_{appraoch})}$$

The horizontal distance covered during approach;

$$S_{approach} = \frac{h_{descent} - h_{flare}}{tan(\theta_{appraoch})}$$

The time elapsed during the approach;

$$t_{approach} = \frac{h_{descent} - h_{flare}}{V_{v,approach}}$$

The time elapsed during the flare;

$$t_{flare} = \frac{2 \cdot R_{flare} \cdot \theta_{appraoch}}{V_{flare} + V_{TD}}$$

The total weight after the approach segment;

$$W_7 = W_6 - \left(c_{t,approach}\right) \cdot \left(T_{R,approach}\right) \cdot t_{approach} - \left(c_{t,flare}\right) \cdot \left(T_{R,flare}\right) \cdot t_{flare}$$

The thrust required during the approach;

$$T_{R,approach} = \frac{1}{2} \cdot \left(\frac{\rho_{landing} + \rho_{descent}}{2}\right) \cdot S \cdot \left(\frac{V_{approach} + V_{flare}}{2}\right)^2$$
$$\cdot \left(C_{D0,TOTAL} + k\left(C_{L,approach}\right)^2\right) - W_6 \cdot sin(\theta_{appraoch})$$

The lift coefficient during the approach;

$$C_{L,flare} = \frac{2 \cdot W_6 \cdot cos(\theta_{appraoch})}{\left(\frac{\rho_{landing} + \rho_{descent}}{2}\right) \cdot S \cdot \left(\frac{V_{approach} + V_{flare}}{2}\right)^2}$$

The thrust required during the flare;

$$T_{R,flare} = \frac{1}{2} \cdot \left(\frac{\rho_{landing} + \rho_{descent}}{2}\right) \cdot S \cdot \left(\frac{V_{TD} + V_{flare}}{2}\right)^2 \cdot \left(C_{D0,TOTAL} + k\left(C_{L,TD}\right)^2\right) - W_6 \\ \cdot sin(\theta_{appraoch})$$

The necessary fuel for the cruise segment;

$$W_{fuel} = W_0 - W_7$$

In terms of liters;

$$V_{fuel} = \frac{(W_0 - W_7)}{g \cdot d_{fuel}}$$

d_{fuel} is the density of the fuel.

8.8 Landing Ground Roll: Segment 7-8

Figure 2. 20 shows the landing segment. The landing starts with the velocity V_{TD} and continues with the same velocity a few seconds meanwhile the nose gear is off the ground. This part is called the free roll. After the free roll, the aircraft stops in the distance, S_L. During this period, the brakes are applied.
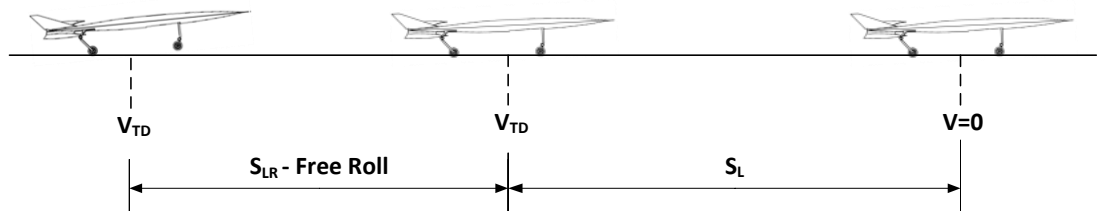
Figure 2. 20 The Landing Segment

41

The free roll distance is calculated from;

$$S_{LR} = N_L \cdot V_{TD}$$

N_L is the landing rotation time.

The total landing distance;

$$S_{L,TOTAL} = S_{LR} + \frac{1}{2gJ_A} \cdot ln\left(1 + \frac{J_A}{J_T}\right) \cdot (V_{TD})^2$$

Where;

$$J_A = \frac{\rho_{landing}}{2\left(\frac{W}{S}\right)} \cdot \left(C_{D0,landing} + k\left(C_{L,landing}\right)^2\right) - \left(\mu_{r,landing}\right) \cdot C_{L,landing}$$

$$J_T = \frac{T_{rev}}{W} + \mu_{r,landing}$$

$C_{D0,landing}$ is the parasite drag coefficient during landing. The lift coefficient during landing;

$$C_{L,landing} = \frac{2W_6}{\rho_{landing} \cdot S \cdot (V_{TD})^2}$$

T_{rev} is the thrust with thrust reverse.

The landing ground roll time;

$$t_{land\_grd\_roll} = \frac{2 \cdot S_{L,TOTAL}}{V_{TD}}$$

The total mission time;

$$t_{mission} = t_{01} + t_{12} + t_{23} + t_{34} + t_{45} + t_{56} + t_{67} + t_{78}$$

t_{34} and t_{56} are inputs which are the cruise time and loiter time, respectively.

9. Engine Model

The propulsion system performance is parameterized by using the graphs provided by the manufacturer of the propulsion system. The change of fuel flow and thrust with the RPM is converted into a function by using the engine data. The thrust specific fuel consumption values for each mission profile segment are calculated from the generated function for the thrust values for each segment.

For each mission profile segment;

$$c_t = \frac{WF}{\left(\frac{T}{g}\right)}$$

Where;

WF is the fuel flow in kg/s and it is a function of T and T is the thrust required value for the mission segment and it is a function of RPM and RPM is a function of the equivalent thrust value at ground level where the engine data is valid.

The equivalent thrust value is estimated as;

$$T_0 = T \cdot \left(\frac{\rho_0}{\rho}\right)$$

Where;

T_0 is the equivalent thrust value for the density value, ρ_0 which is valid for the ground level where the engine performance functions are valid.

The fuel flow, WF is calculated from the curve fitting function of RPM and RPM is the curve fitting function of T_0.

A typical fitting function for variation of thrust with RPM;

$$RPM = p_1 \cdot (T_0)^7 + p_2 \cdot (T_0)^6 + p_3 \cdot (T_0)^5 + p_4 \cdot (T_0)^4 + p_5 \cdot (T_0)^3 + p_6 \cdot (T_0)^2 + p_7 \cdot (T_0) + p_8$$

Similarly fuel flow can be defined as;

$$WF = p_1 \cdot (RPM)^6 + p_2 \cdot (RPM)^5 + p_3 \cdot (RPM)^4 + p_4 \cdot (RPM)^3 + p_5 \cdot (RPM)^2 + p_6 \cdot (RPM) + p_7$$

10. Design Cases

During the conceptual design the first design is determined. To find a better design, the calculations defined in previous sections are repeated for the number of designs. The important design input values are varied according to the specific limits which are selected around the first design values and matched with each other. So, for each match a different design is generated. The ones which do not satisfy the requirements are eliminated and the best design is selected.

The number of designs, $NOFD$, is determined as ;

$$NOFD = \prod_{i=1}^{Y_{inputs}} \left(X_{range}\right)_i$$

Where;

Y_{inputs} is the number of variable design inputs.

X_{range} is the range of each design input.

CHAPTER 3

THE INITIAL DESIGN

1. First Concept

The main aim of this Chapter is to introduce the initial design which is considered as the start point of the design process and to illustrate how the calculations are made. In Appendix A, each calculation step is performed to understand the method clearly although all process is performed automatically by the tool developed on Excel and Matlab software.

High maneuverability and high speed are the main design considerations during the conceptual design. The fuselage is designed as a blended wing-body geometry which is expected to be more efficient than the conventional types with respect to aerodynamics and control. Blended wing-body geometry has more wing area than the conventional fuselage-wing configurations together the fact that it has less drag due to the absence of the fuselage-wing interference. Moreover, a conventional cylindrical fuselage may encounter cross-flow separation while the blended body will have attached flow which results in low side force and less necessity for vertical stability surfaces. Figure 3. 1 shows the attached cross-flow.

Figure 3. 1 Blended Wing-Body in Cross-flow.

The longitudinal section profile is decided to be symmetrical which is very common for highly maneuverable aircraft. The lifting characteristics of symmetrical sections in inverted flight are the same as those in normal flight which provides better performance in maneuvers and satisfies the high maneuverability.

Vertical tail is decided to be a stability surface which does not provide control but provides directional stability. Low side cross section of the aircraft eliminates the necessity for a large vertical tail. Figure 3. 2 shows the tail incidence.
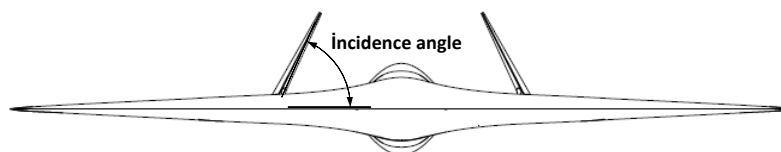
Figure 3. 2 The Tail Incidence.

The control surface is selected as elevon which behaves like aileron and elevator at the same time. Figure 3. 3 shows the surface movements for roll and pitch up. Pitching up and down is satisfied by moving the surfaces in the same direction while rolling is satisfied by moving the surface in the opposite direction. The combination of these movements satisfies rolling and pitching at the same.
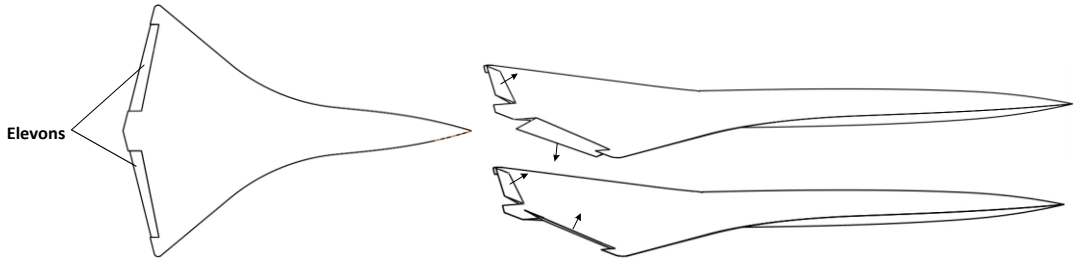
Figure 3. 3 Elevon Control Surfaces. The Roll Motion and The Nose Up Movements.

The engine is decided to be a mini turbojet engine and located at the end of the wing body. The engine nozzle is directly open to the outside atmosphere which is expected to have higher IR signature.

Takeoff is decided to be performed by the use landing gears while recovery can be made with parachute or conventional landing. The main landing gears are located in the wing-body and open in the span-wise direction while the nose gear is located in the nose section as shown in Figure 3. 5.
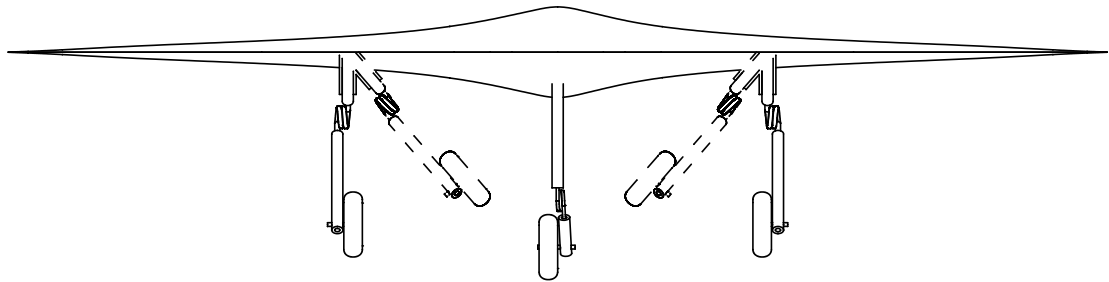
Figure 3. 4 The Nose and Main Gears (front View).
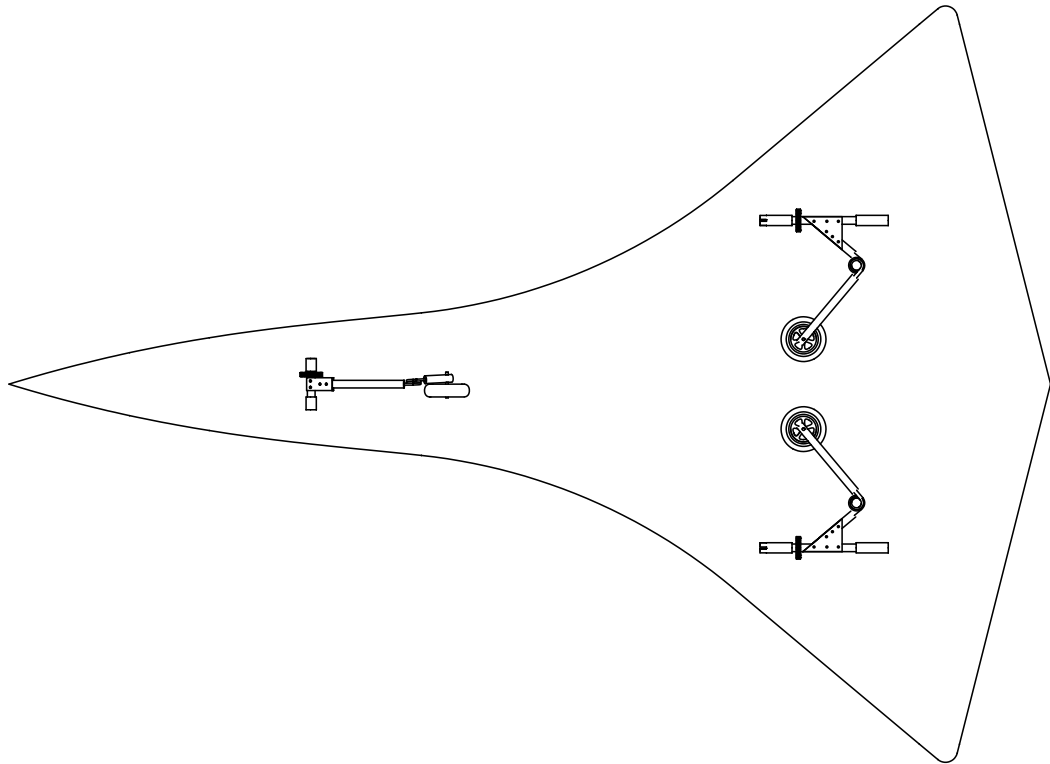
Figure 3. 5 The Location of Main and Nose Landing Gears.

The wing planform is considered as a combination of a front wing which is called as LEX in this thesis and a main wing which is in double delta form. The main and front wing together forms the blended wing-body.
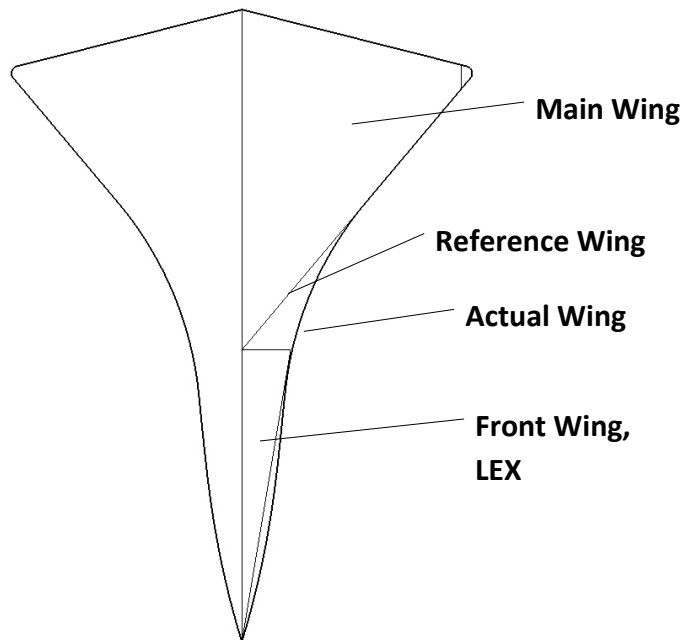
Figure 3. 6 The Front, Main Wing and Actual Wing Geometries.

47

2. Airfoil Selection

The wing-body section profile is expected to have a low drag coefficient and low pitching moment for a high speed and highly maneuverable aircraft. These properties are the main criteria for the airfoil selection. Due to the low drag consideration thin airfoils are focused.

Table 3. 1 The Comparison of Various Airfoils. (Data taken from Ref. [7])

Airfoil	Thickness (%)	$C_{l,max}$	Design C_l	C_{m0}	C_{d0} at Design C_l	$C_{d0,min}$	Re (10^6)
NACA 0009	9	1.25	-	0	-	0.0052	3
NACA 0012	12	1.5	-	0	-	0.0057	3
NACA 0012 64	12	1.35	-	0	-	0.005	3
NACA 0012 64Mod	12	1.5	-	-0.05	-	0.0042	3
NACA 1408	8	1.35	-	-0.025	-	0.005	3
NACA 1410	10	1.5	-	-0.0015	-	0.0055	3
NACA 1412	12	1.6	-	-0.0025	-	0.006	3
NACA 23012	12	1.6	0.3	-0.00125	0.0068	0.0065	3
NACA 63 006	6	0.8	-	0	-	0.0042	3
NACA 63 009	9	1.1		0		0.0042	3
NACA 63 206	6	0.95	0.2	-0.00375	0.004	0.004	3
NACA 63 209	9	1.3	0.2	-0.00313	0.0045	0.0045	3
NACA 63 210	10	1.4	0.2	-0.00375	0.00475	0.00475	3
NACA 63A210	10	1.3	0.2	-0.00375	0.0045	0.0045	3
NACA 64 108	8	0.85	0.1	-0.00125	0.0041	0.0041	3
NACA 64 110	10	1.3	0.1	-0.002	0.0048	0.0048	3
NACA 64 206	6	1	0.2	-0.00375	0.004	0.004	3
NACA 64 208	8	1.1	0.2	-0.00375	0.0045	0.0045	3
NACA 64 209	9	1.3	0.2	-0.00375	0.0045	0.0045	3
NACA 65 206	6	0.98	0.2	-0.00313	0.0037	0.0037	3
NACA 65 209	9	1.25	0.2	-0.00333	0.0042	0.0042	3
NACA 65 210	10	1.3	0.2	-0.00375	0.0041	0.0041	3
NACA 66 206	6	0.95	0.2	-0.00375	0.003	0.003	3
NACA 66 209	9	1.1	0.2	-0.00333	0.0035	0.0035	3
NACA 66 006	6	0.82	-	0	-	0.003	3

Table 3. 1 shows various NACA airfoils [7]. Symmetrical airfoils have zero pitching moment at zero angle while cambered airfoils have nose down pitching moment and it is not desirable for an acrobatic aircraft. So, the selection is focused on the symmetrical airfoils. Thin airfoils have low drag coefficient than thicker airfoils, but they have low maximum lift coefficient value as well. Due to the fact that maximum speed is a requirement for the design, thin airfoils are considered rather than the thick airfoils although they have low maximum lift coefficient. According to Table 3. 1 NACA 66 006 has the lowest minimum

drag coefficient and reasonable thickness and maximum lift coefficient value. As a result, the wing-body profile is selected as NACA 66 006.
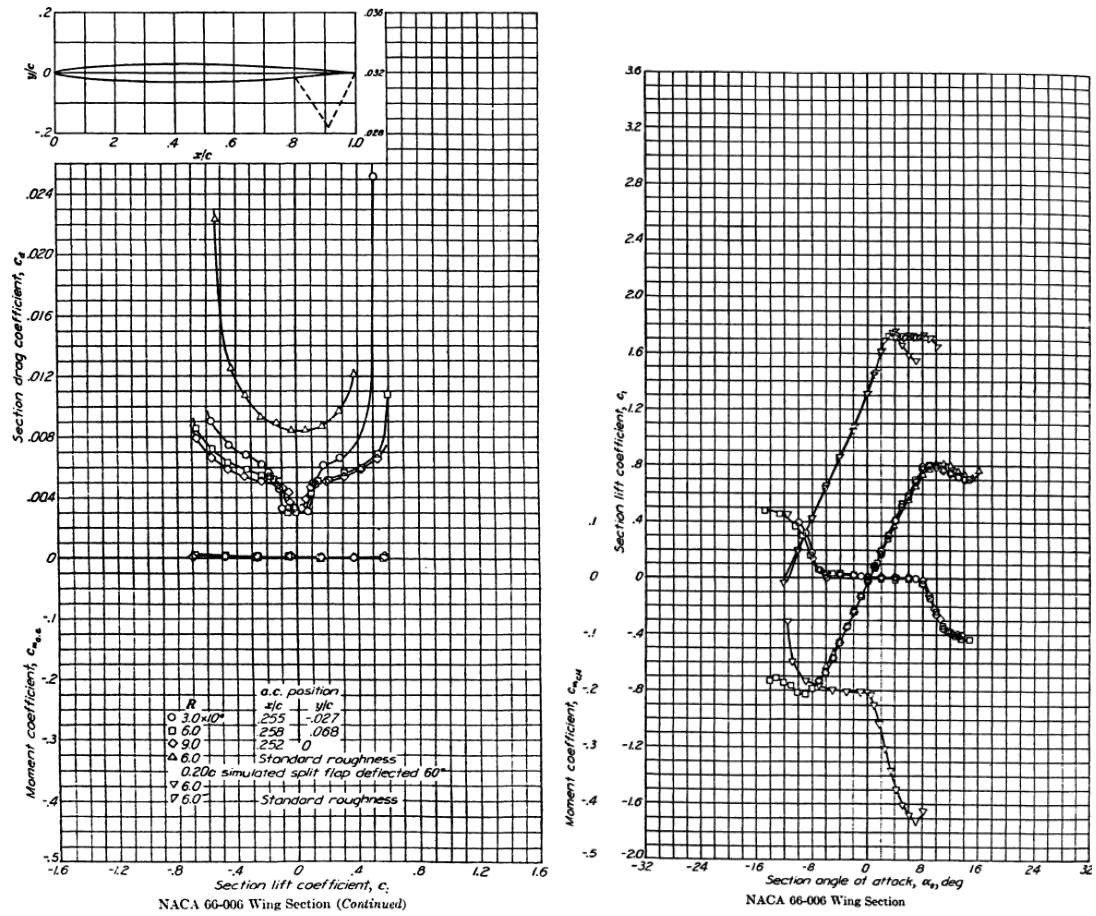
Figure 3. 7 The Performance Graphs for NACA 66 006 Airfoil.(Copied from Ref. [7])

Figure 3. 7 shows the performance graphs of NACA 66 006 airfoil different Reynolds Numbers. For Re= 3.10^6, the maximum lift coefficient value, 0.82 is obtained at an angle of 10 degrees, approximately. The moment coefficient is zero. The minimum drag coefficient is about 0.003.

3. Engine Selection

Unlike the conventional design philosophy which requires the selection of the engine according to the requirements, the engine is pre-selected in this thesis. The aim is to satisfy the requirements by using the pre-selected engine. The engine is a mini turbojet produced by the AMT company [8]. The specification of the engine is shown in Figure 3. 8.

OLYMPUS HP	
Diameter	131 mm
Length	383 mm
Turbine weight	2850 gram
Whole System Weight	3795 gram
Thrust at Max. RPM	230 N
Maximum RPM	108500
Pressure Ratio at Max. RPM	3.8:1
Mass Flow at Max. RPM	450 gr/s
Maximum EGT	750 C
Fuel Consumption at Max. RPM	640 gr/min

Figure 3. 8 The Engine Specifications. All Data at Standard Temperature and Pressure (All data taken from Ref. [8].)
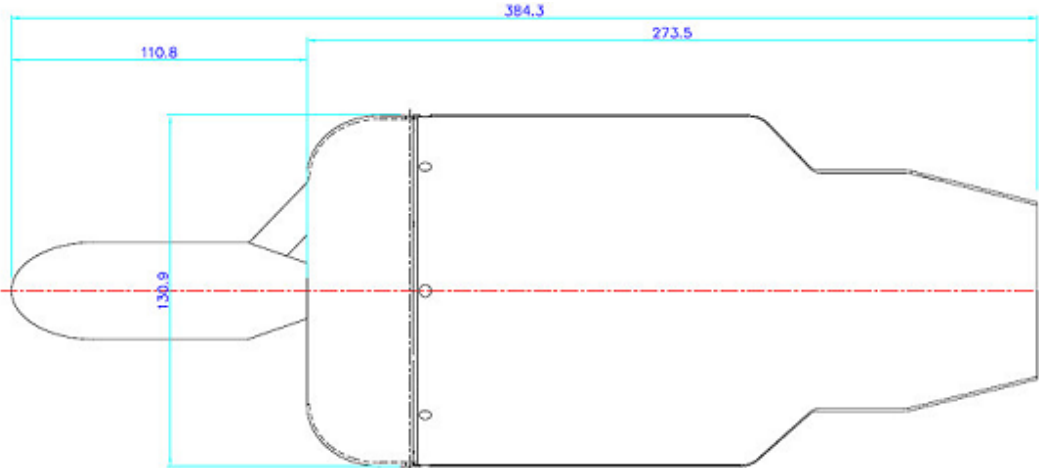
Figure 3. 9 The Dimensions of the Olympus Hp Turbojet Engine (Taken from Ref [8].)

3.1 Parameterization of Engine Data

The engine data are parameterized by using the engine data provided by the manufacturer. The fuel flow is calculated from the related RPM value and the RPM value is calculated from the related thrust value. So, in this calculation method the necessary thrust amount is found first and the fuel flow is calculated by using the curve fitting functions. The reason for doing so is the fact that during the mission profile the necessary thrust amount is different for the each mission segment and different thrust values will result in different fuel flow value. The thrust specific fuel consumption value for mission segment is calculated by this method.

Figure 3. 10 shows curve fitting function for variation of thrust with RPM for Olympus HP Engine.
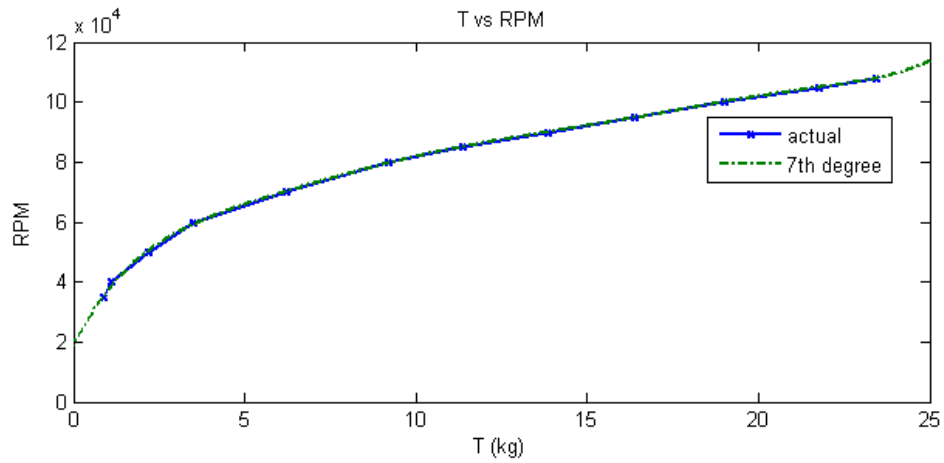
Figure 3. 10 The Curve Fitting Function and The Actual Data For T and RPM for Olympus HP Engine.

$$RPM = 0.0010673 \cdot (T_0)^7 - 0.099774 \cdot (T_0)^6 + 3.7964 \cdot (T_0)^5 - 75.755 \cdot (T_0)^4 + 855.69 \cdot (T_0)^3 - 5597.3 \cdot (T_0)^2 + 23412 \cdot (T_0) + 18776$$

T_0 is again the equivalent thrust value which is described in Chapter 2.

Similarly fuel flow can be defined as;
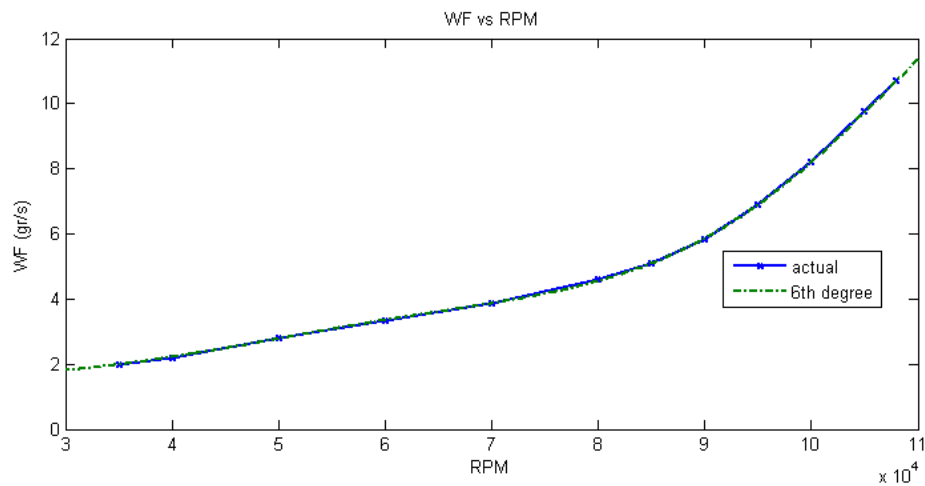
Figure 3. 11 The Curve Fitting Function and The Actual Data For WF and RPM for Olympus HP Engine.

$$WF = -3.5E^{-28} \cdot (RPM)^6 + 1.33E^{-22} \cdot (RPM)^5 - 1.96E^{-17} \cdot (RPM)^4 + 1.43E^{-12} \cdot (RPM)^3 - 5.48E^{-8} \cdot (RPM)^2 + 0.0010834 \cdot (RPM) - 7.147$$

4. Defining the Initial Inputs

The aim of defining the initial inputs is to find the closest point to the design point. Then the optimization is conducted around the initial inputs. The most important design parameters are the cruise speed and the cruise time. In this calculation method the cruise time is selected as a design input which means all the designs which are generated automatically satisfy the cruise time requirement. Similarly, the cruise speed is selected as an input as well. The maximum speed and turn rate requirements are satisfied as a result of analyzing the design cases.

4.1 The Wing-body Parameters

The wing-body parameters define the shape of the lifting geometry of the aircraft. During the conceptual design the main wing planform is decided to be in double delta form while front wing is assumed to be a very low aspect ratio delta wing. Table 3. 2 shows the wing-body design inputs.

Table 3. 2 Wing-Body Parameters

C_{Lmax}	0.738	b [m]	1.6	b_{LEX} [m]	0.4
$C_{l\alpha,wing}$	5.7	Λ_{LE} [Deg.]	60	$C_{l\alpha,LEX}$	5.7
$\left(\dfrac{t}{c}\right)_{wing\ airfoil}$	0.06	hn_{wing}	0.33	hn_{LEX}	0.36
$\left(\dfrac{x}{c}\right)_m$	0.459	C_{l0}	0	η_{LEX}	1
Λ_m	42.08	C_{m0}	0		
c_r [m]	1.55	$c_{r,LEX}$ [m]	0.96		
c_t [m]	0.2	$c_{t,LEX}$ [m]	0		

The main wing leading edge angle is selected as 60 degrees. The span of main wing is $1.6m$ while the span of virtual front wing is $0.4m$. Figure 3. 12 shows the geometric properties of the initial wing-body geometry.
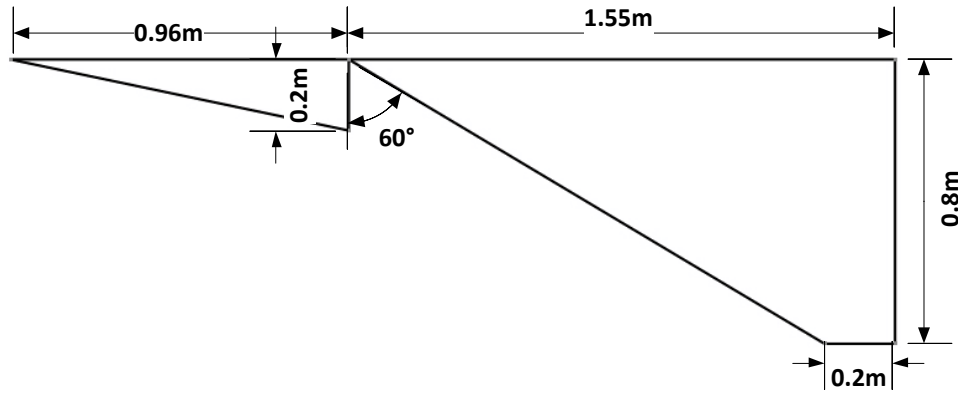
Figure 3. 12 The Initial Concept Wing-Body Geometry.

The maximum lift coefficient is calculated by using Figure 3. 7 for $Re = 3 \cdot 10^6$;

$$C_{L_{max}} = (0.82) \cdot 0.9$$

The section lift curve slope of the wing is derived from the Figure 3. 7 as $5.7 \ rad^{-1}$. Figure 3. 13 shows the chord-wise location of the maximum thickness line of the airfoil which is found as $0.459c$ and the sweep of the maximum thickness line of the main wing.
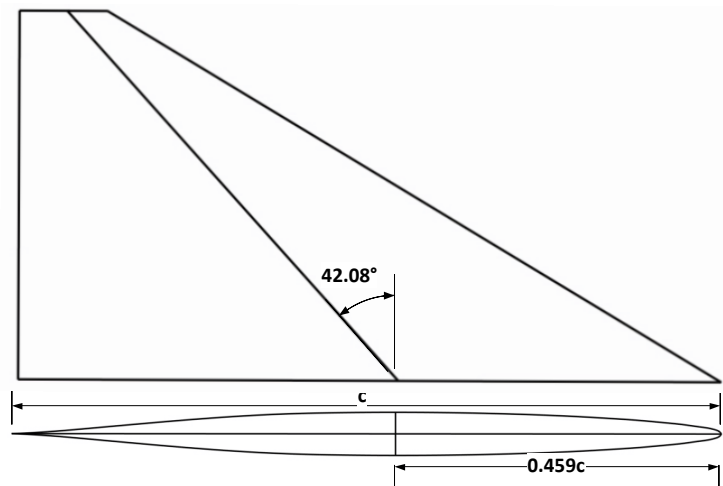
Figure 3. 13 The Chordwise Location of Maximum Thickness Line for NACA 66 006 Airfoil.

The neutral points of the main wing and the front wing, hn_{wing}, hn_{LEX} , are estimated from the Ref. [9] Figure 3.38.

4.2 Tail Parameters

The tail is considered as a passive surface which provides stability. As an initial design following parameters are selected.

Table 3. 3 Tail Initial Design Parameters

$c_{r,tail}$ [m]	0.45	$\alpha_{i.tail}$ [Deg.]	27
$c_{t,tail}$ [m]	0.96	l_{tail} [m]	0.65
$\Lambda_{LE,tail}$ [Deg.]	66	$\left(\dfrac{t}{c}\right)_{tail\ airfoil}$	0.06
$\Lambda_{TE,tail}$ [Deg.]	50	$\left(\dfrac{x}{c}\right)_{m,tail}$	0.459
$C_{l_{\alpha,tail}}$	5.7	$\Lambda_{m,tail}$ [Deg.]	57.9

The tail airfoil section is kept the same as the whole wing-body section profile, so it is NACA 66 006. Both leading and trailing edge sweeps exist as, 66 and 50 degrees, respectively. Figure 3. 14 shows the geometry.
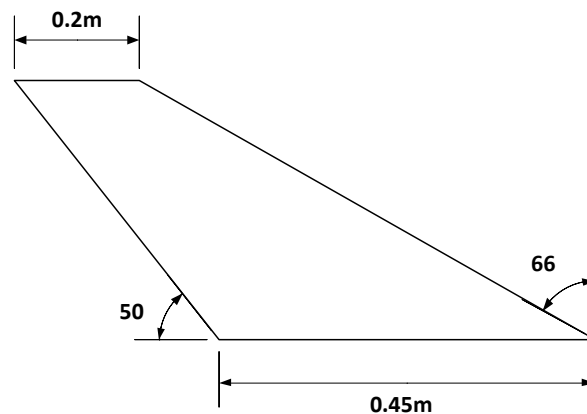
Figure 3. 14 The Tail Geometry.

4.3 Propulsion System Parameters

Propulsion system parameters define the number engines to be used, the estimated inlet diameter and length and fuel tank sizing inputs. The design is decided to have single engine. The inlet inputs are used to calculate the inlet area approximately for the weight calculation. Fuel tank sizing parameters are related to the wing geometry and used to calculate the fuel tank volume for each design. Fuel tank volume changes for each design due to the change of wing geometry. Table 3. 4 shows the propulsion system inputs for the initial design.

Table 3. 4 Propulsion System Parameters

N_{engine}	1	$t_{fuel\ tank}$	0.5
R_{inlet} [m]	0.11	$c_{fuel\ tank}$	0.5
$b_{fuel\ tank}$	0.5	l_{inlet} [m]	0.5

4.4 Mission Profile Parameters

Mission profile parameters include the most critical design parameters which are the cruise time and cruise speed. In this analysis method cruise time and cruise speed are design inputs. The total weight is dramatically addicted to the cruise time input due to the fact that the amount of fuel burned during the mission is determined by this parameter and added to the weight summation iteratively. Similarly, the total design is quite dependent on the design cruise speed since all the calculations are made for this parameter. The cruise time is decided to be 30 minutes. It means that all of the design cases satisfy the cruise time requirement. The cruise speed is selected as 87 m/s as a design input. The reason for selecting this speed is the fact that the maximum rate of climb of the aircraft is around this value. Detailed calculations are presented in Appendix A.

Table 3. 5 Mission Profile Parameters

$N_{ground\ roll}$	1	$h_{obs.}$ [m]	5
$V_{v,descent\ rate}$ [m/s]	20	t_{loiter} [s]	2
$\mu_{r,landing}$	0.3	t_{cruise} [min.]	30
μ_r	0.03	V_{cruise} [m/s]	87

Loiter time is selected as 2 minutes. The friction coefficients; μ_r represents the friction coefficient during takeoff and $\mu_{r,landing}$ represents the friction coefficient during landing with brakes on. The obstacle clearance height is selected as 5m. The friction coefficient can be figured out at reference [2] in Table 6.1.

4.5 Landing Gear and Parachute Parameters

The landing weight estimation parameters are used to calculate the weight landing gears during iterations. The values in Table 3. 6 are estimated by using the similar aircraft landing gear weights. Similarly, parachute weight parameter is also estimated from the parachute weight of the similar aircraft.

$W_{m.gear} / W_{TOTAL}$	0.075
$W_{nose\ gear} / W_{TOTAL}$	0.025
$W_{parachute} / W_{TOTAL}$	0.05

4.6 Air Properties

Air properties include the takeoff, cruise, descent heights and the sea level air properties. Takeoff height is determined as 1000m above sea level due to the fact that Ankara city where the aircraft is supposed to be tested is about at that height above the sea level. The cruise altitude is selected as 700m above the takeoff height which is a reasonable distance to perform the possible missions. The performance of the aircraft is tested at two different altitudes, too. The descent altitude is used for descent mission segment calculations and selected as 1100m above the sea level.

Table 3. 7 Air Properties

$h_{takeoff}$ [m]	1000	$h_{cruise3}$ [m]	3800
h_{cruise} [m]	1700	T_0 [K]	288.16
$h_{descent}$ [m]	1100	P_0 [Pa]	101325
$h_{cruise2}$ [m]	2300	ρ_0 [kg/m³]	1.225

4.7 Sample Structural Weights

Sample structural weights are used to calculate the weight of aircraft skin and internal structure. The sample weights are obtained from the sample laminates which are produced prior to the prototype production for calculations. The units are given gr/m^2.

Table 3. 8 Sample Structural Weights

W_{s_skin} [gr]	1000	W_{s_tail} [gr]	1000
W_{s_frame} [gr]	2000	W_{s_tank} [gr]	500
W_{s_paint} [gr]	300		

5. Weight Analysis

The weight analysis is one of the key steps in the calculation method described in the thesis. As mentioned before the weight calculation is conducted in an iterative process. The fuel weight is the output of the mission profile analysis, but the mission profile analysis starts with the total weight value. So, it needs an iterative calculation. The reason of doing this is the fact the conventional weight estimation methods which relies on the historical data is not satisfactory for the small scale UAVs. So, more accurate iterative weight estimation is presented in this thesis. Below the summary of the weight analysis is given in Table 3. 9. Detailed calculations are presented in Appendix A1.

Table 3. 9 The Weight Build-up Summary

#	Unit	Weight(gr)	#	Unit	Weight(gr)
1	W_{wing_skin}	3661.6	12	W_{fuel}	7117.4
2	W_{sp_frame} (span-wise frames)	1585.9	13	$W_{engines}$	2850
3	W_{lng_frame} (longitudinal frames)	539.8	14	W_{engine_comp}	1218.2
4	W_{in_frame} (inlet frames)	152.05	15	$W_{main\_l\_gear}$	1941.05
5	W_{frame} (3+4+5)	2277.8	16	$W_{nose\_l\_gear}$	647.01
6	$W_{blended\_wing}$ (1+5)	5939.4	17	$W_{avionics}$	438
7	W_{inlet}	378.4	18	$W_{batteries}$	600
8	W_{paint}	1098.5	19	$W_{parachute}$	1294
9	W_{wing_body} (6+7+8)	7416.3	20	$W_{sys\_internal}$ (13+14+15+16+17+18+19)	9071.3
10	W_{tail}	275.6	21	$W_{payload}$	2000
11	W_{empty} (9+10+20)	16763.2	22	W_{TOTAL} (11+12+21)	**25880.7**

6. Aerodynamic Analysis

The aerodynamic properties of the initial design are represented in this section. It includes the aerodynamic coefficients like lift curve slope of the blended wing-body, drag coefficients and etc. Detailed, step by step calculations are shown in Appendix A.

6.1 Initial Design Geometric Calculations

The geometric properties of the wing-body and LEX are presented here. Table 3. 10 shows the summary of the geometric properties.

Table 3. 10 Initial Design Geometric Properties

Main wing area, S_{main_wing} [m^2]	1.4	LEX sweep angle at semi chord, $\Lambda_{c/2,LEX}$ [deg.]	67.3
Aspect ratio of the main wing, AR_{main_wing}	1.828	LEX mean aerodynamic chord, $\bar{c}_{LEX}$ [m]	0.64
Taper ratio of main wing, λ	0.129	Total wing-body area, S_{TOTAL} [m^2]	1.592
Sweep angle at quarter chord, $\Lambda_{c/4}$ [deg.]	52.6	Vertical tail height, h_{tail} [m]	0.252
Sweep angle at semi chord, $\Lambda_{c/2}$ [deg]	41.6	Tail area, S_{tail} [m^2]	0.137
Mean aerodynamic chord, $\bar{c}$ [m]	1.04	Aspect ratio of tail, AR_{tail}	1.84
LEX area, S_{LEX} [m^2]	0.192	Taper ratio of tail, λ_{tail}	0.213
Aspect ratio of the LEX, AR_{LEX}	0.83	Tail sweep angle at quarter chord, $\Lambda_{c/4,tail}$ [deg.]	64.6
Taper ratio of LEX, λ_{LEX}	0	Tail sweep angle at semi chord, $\Lambda_{c/4,tail}$ [deg.]	54.5
LEX sweep angle at quarter chord, $\Lambda_{c/4,LEX}$ [deg.]	74.4	Tail mean aerodynamic chord, $\bar{c}_{tail}$ [m]	0.31

6.2 Lift Curve Slopes

The lift curve slopes are calculated for the so called front wing, main wing and the tail. The total lift curve slope is calculated by assuming tail is in downwash while front wing is in up-wash. By remembering the formula given in chapter 2;

$$C_{L_\alpha} = C_{L_{\alpha_{WB}}} + C_{L_{\alpha_H}} \cdot \eta_H \cdot \frac{S_H}{S}\left(1 - \left(\frac{d\epsilon}{d\alpha}\right)_{downwash}\right) + C_{L_{\alpha_{LEX}}} \cdot \eta_{LEX} \cdot \frac{S_{LEX}}{S}(1 - \left(\frac{d\epsilon}{d\alpha}\right)_{upwash})$$

The initial design lift curve slopes and other lifting parameters are summarized in Table 3. 11.

Table 3. 11 The Lifting Properties of The Wing-Body

Lift curve slope of the wing-body, $C_{L_{\alpha_{WB}}}$ [rad^{-1}]	2.132	LEX lift curve slope, $C_{L_{\alpha_{LEX}}}$ [rad^{-1}]	1.01
Lift curve slope of the wing, $C_{L_{\alpha_W}}$ [rad^{-1}]	2.13	Down-wash factor, $\left(\frac{d\epsilon}{d\alpha}\right)_{downwash}$	0.965
Cruise Mach Number	0.26	Up-wash factor, $\left(\frac{d\epsilon}{d\alpha}\right)_{upwash}$	0.1
Virtual horizontal tail lift curve slope, $C_{L_{\alpha_H}}$ [rad^{-1}]	1.13		

The tail lift curve slope is calculated by introducing the virtual horizontal and vertical tails due to the fact that the inclined tail is similar to the V-tail configuration.

6.3 Aerodynamic Coefficients

The aircraft parasite drag coefficient is calculated for the main wing, the virtual fuselage and the tail. Table 3. 12 shows the drag and lift coefficients of the aircraft.

Table 3. 12 Aerodynamic Coefficients

Main wing parasite drag coefficient, $C_{D0_{wing}}$	0.00723	Span efficiency factor, e	0.772
Tail parasite drag coefficient, $C_{D0_{tail}}$	0.000703	Cruise drag coefficient, $C_{D,cruise}$	0.009817
Total parasite drag coefficient, $C_{D0,TOTAL}$	0.009439	Cruise lift to drag ratio, $\left(\frac{C_L}{C_D}\right)_{cruise}$	4.175
Cruise lift coefficient, $C_{L,cruise}$	0.0409		

7. Performance

In this section the performance properties including the stall velocity, rate of climb, maximum velocity, turn rate and turn radius and load factor are presented. Detailed calculations are shown in Appendix A.

7.1 Thrust and Power Required, Rate of Climb and Maximum Velocity

The available thrust at the cruise altitude is calculated from;

$$T_{A,cruise} = T_{A,0} \cdot \left(\frac{\rho_{cruise}}{\rho_0}\right) = 230 \cdot \left(\frac{1.037207}{1.225}\right) = 194.7372 \text{ N}$$

The maximum thrust available for the engine is given as 230N art sea level.

Figure 3. 15 shows the change of thrust required with respect velocity. The thrust available is constant with velocity due to the turbojet engine. The maximum speed is achieved when the thrust required is equal to the thrust available. From Figure 3. 15 the maximum speed is found as $V_{max} = 159.45$ m/s at the cruise altitude.
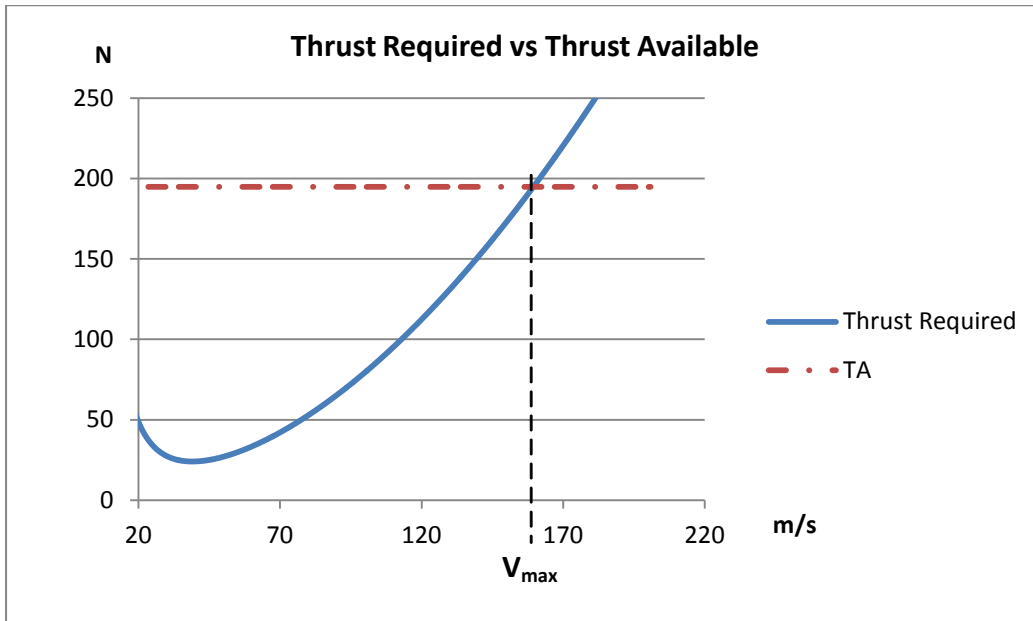
Figure 3. 15 Thrust Required and Thrust Available Curves

Rate of climb is calculated from;

$$R/_C = \frac{Excess\ Power}{Weight} = \frac{P_{available} - P_r}{W} = \frac{V \cdot (T_A - T_R)}{W}$$
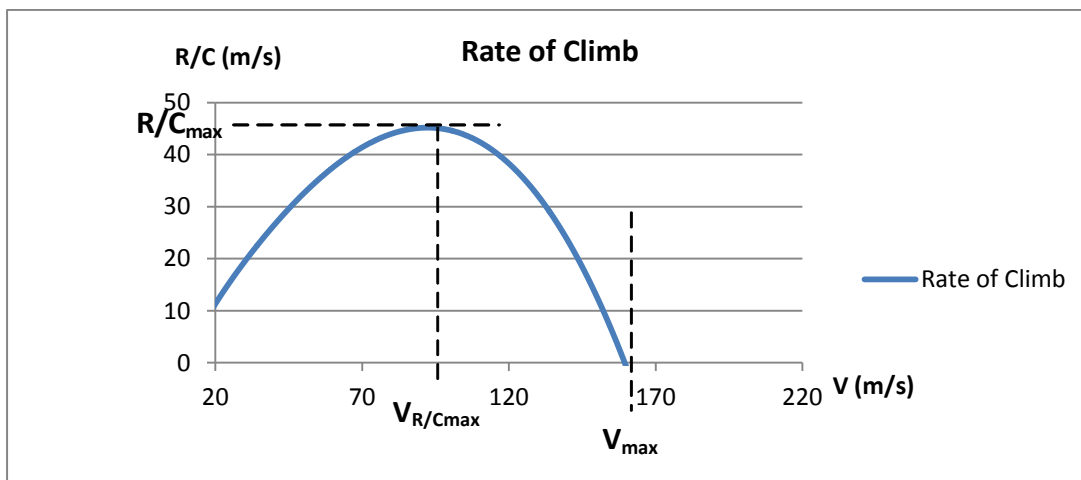
Figure 3. 16 The Change of Rate of Climb with Velocity.

60

Maximum rate of climb is found from the Figure 3. 16 as $\left(R/C\right)_{max} = 45.5261$ m/s at the cruise altitude.

Maximum velocity is calculated where the rate of climb is zero. This situation is due to the fact that all excess power is consumed at that velocity so; it is at the maximum value.

$$R/C = \frac{V_{max} \cdot (T_A - T_R)}{W} = 0$$

From Figure 3. 16, the maximum velocity is found as $V_{max} = 159.45$ m/s which is in compliance with the value found from Figure 3. 15.

7.3 Maximum Load Factor

The load factor is defined as the ratio of lift to weight. During maneuvers this ratio changes as the lift must increase. The maximum load factor is constraint with both $C_{L,max}$ and $T_{A,max}$.
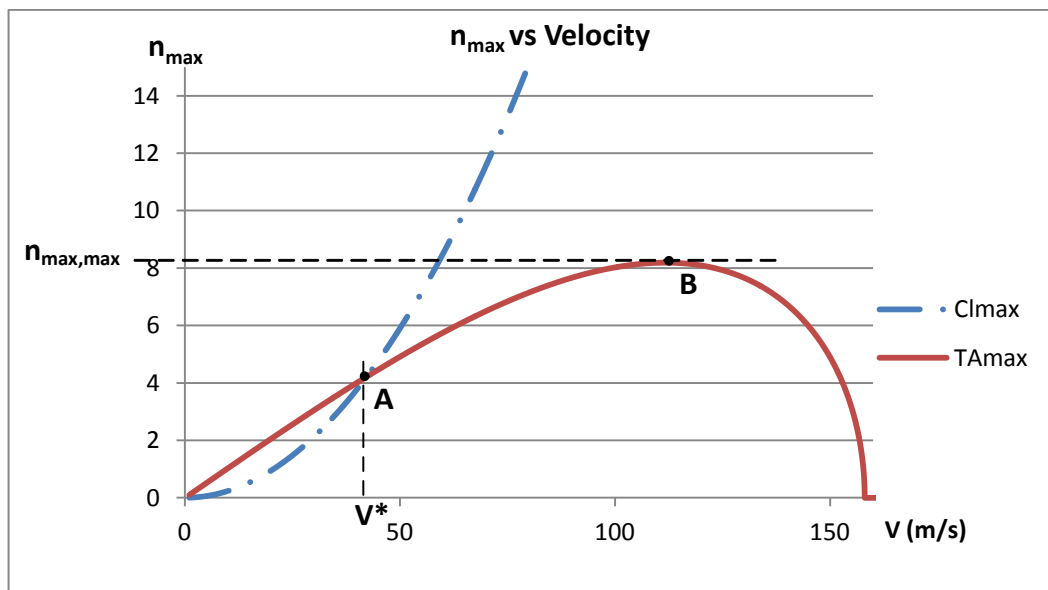
Figure 3. 17 The Maximum Load Factor Curves.

Figure 3. 17 point A is the n_{max} value which is satisfied both $C_{L_{max}}$ and $T_{A,max}$ constraint. The value at this point is the maximum sustained load factor which is found as $n_{max,sutained} = 4.245$ Point B is the maximum value of n_{max} and found as $n_{max,max} = 8.241$

The velocity at point A is the corner velocity at which the turn rate is at maximum value and the turn radius is at minimum value. The corner velocity is found as $V^* = 42.24$m/s.

7.5 Turn Performance

Corner velocity is found as $V^* = 42.24\text{m/s}$ in previous section. For maneuvering this speed is used.

Table 3. 13 shows the some of the turn performance properties. Detailed calculations are shown in Appendix A.

Table 3. 13 The Turn Performance Properties

Maximum turn rate, $\omega_{\max}$ [deg/s]	54.8
Minimum turn radius [m]	44
Maximum bank angle [deg.]	83

For the pull up maneuver the turn radius is found from;

$$R = \frac{V^2}{g(n-1)}$$
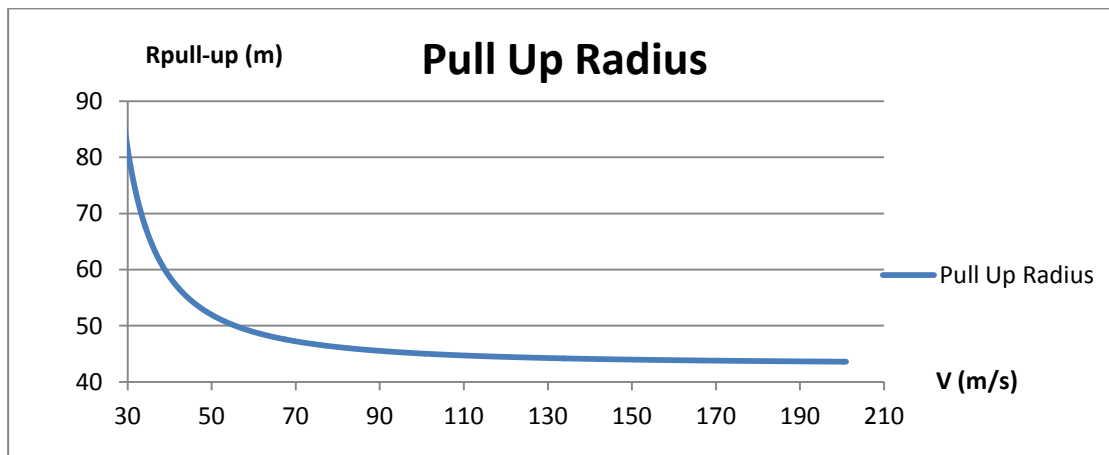
Figure 3. 18 The Change of Pull-op Radius with The Velocity.

Figure 3. 18 shows the change of pull-up turn radius with respect to velocity. The pull-up radius nearly becomes constant while the velocity increases. The minimum pull-up radius is approximately found as $R_{\min,\text{pull}-\text{up}} = 44\text{m}$.

For the pull down maneuver the turn radius;

$$R = \frac{V^2}{g(n+1)}$$
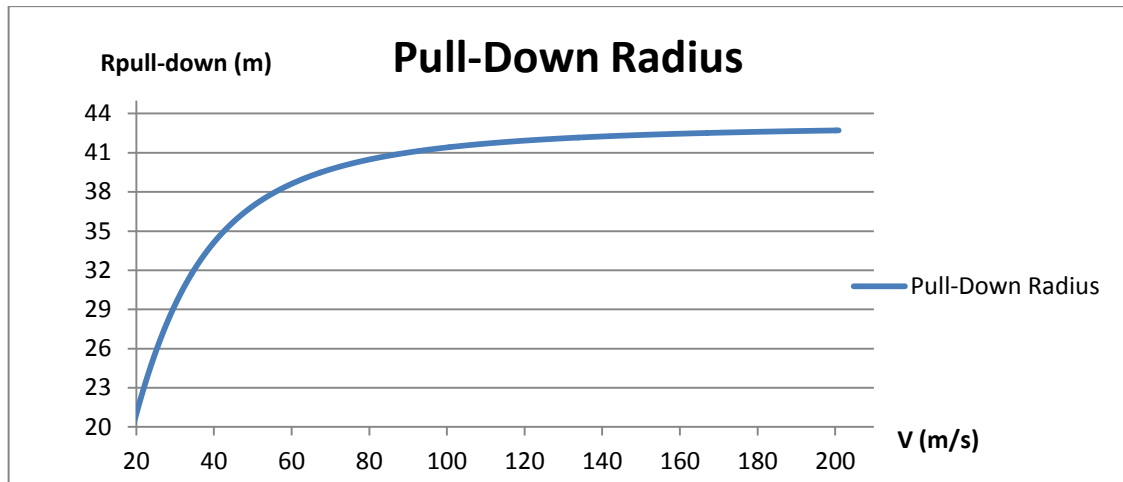
Figure 3. 19 The Change of Pull-Down Radius with The Velocity.

Figure 3. 19 shows the variation of the pull-down radius with respect to velocity. The pull-down radius is approximately found as $R_{min,pull-down} = 42m$.

8. Mission Profile

Mission profile analysis is conducted for the sub segments that are takeoff ground roll, transition, climb, cruise, descent, loiter, approach and landing ground roll. Detailed, step by step calculations are demonstrated in Appendix A. Following sections just show the most important parameters.

8.1 Takeoff Ground Roll: Segment 0-1

Table 3. 14 shows the results obtained from the takeoff ground roll calculations. Takeoff rotation time is taken as $N = 1$.

Table 3. 14 Segment 0-1 Parameters

Initial weight, W_0 [N]	256.2
Lift-off Velocity, $V_{f,01}$ [m/s]	25.7
Takeoff available thrust, $T_{A,takeoff}$ [N]	208.7
Thrust to weight ratio during takeoff, $\left(\frac{T_A}{W}\right)_{takeoff}$	0.814
Ground roll distance, S_g [m]	69.4
Weight after takeoff, W_1 [N]	255.64
Thrust specific fuel consumption during takeoff, $c_{t,ground\_roll}$ [1/s]	0.0004971

8.2 Transition: Segment 1-2

Table 3. 15 shows the transition segment parameters. The obstacle height is selected as 5 m as described in the mission profile inputs.

Table 3. 15 Segment 1-2 Parameters

Obstacle distance, h_{obs} [m]	5
Load factor during transition, n	1.82
Transition distance, S_a [m]	29.2
Weight after transition, W_2 [N]	255.52
Thrust specific fuel consumption during transition, $c_{t,transition}$ [1/s]	0.0004971

8.3 Climb: Segment 2-3

As described in previous sections climb angle is assumed to be constant during the climb. The climb speed is the cruise speed, but at the first stages of the climb segment the speed is lower than the cruise speed. So, the aircraft accelerates until it reaches the desired speed. Table 3. 16 shows the climb segment parameters.

Table 3. 16 Segment 2-3 Parameters

Climb angle, θ_{climb} [deg.]	31.7
Thrust to weight ratio during climb, $\left(\frac{T_A}{W}\right)_{climb}$	0.792
Total climb time, $t_{climb,TOTAL}$ [s]	23.2
Thrust specific fuel consumption during climb, $c_{t,climb}$ [1/s]	0.0004971
Weight after transition, W_3 [N]	253.1

8.4 Cruise: Segment 3-4

During cruise aircraft performs a constant speed and constant altitude flight. The cruise speed is one of the main design inputs as well as the cruise time. Table 3. 17 shows cruise segment parameters.

Table 3. 17 Segment 3-4 Parameters

Cruise speed, V_{cruise} [m/s]	87
Weight after cruise, W_4 [N]	190.85
Cruise time, t_{cruise} [min.]	30
Thrust specific fuel consumption during climb, $c_{t,cruise}$ [1/s]	0.0006557
Range achieved during cruise, R_{range} [km]	145.1

8.5 Descent: Segment 4-5

Descent segment is performed with constant angle and constant speed. Table 3. 18 shows the descent segment parameters.

Table 3. 18 Segment 4-5 Parameters

Descent rate, $V_{v,descent}$ [m/s]	20
Descent angle, $\theta_{descent}$ [deg.]	13.6
Weight after descent, W_5 [N]	190.1
Thrust specific fuel consumption during descent, $c_{t,descent}$ [1/s]	0.001727

8.6 Loiter: Segment 5-6

Loiter is assumed to performed with constant speed and constant altitude. The speed is the cruise speed. Loiter time is one of the design inputs. Table 3. 19 shows some of the loiter segment parameters.

Table 3. 19 Segment 5-6 Parameters

Weight after loiter, W_6 [N]	186.9
Loiter time, t_{loiter} [min.]	2
Thrust specific fuel consumption during loiter, $c_{t,loiter}$ [1/s]	0.0006257

8.7 Approach: Segment 6-7

Approach segment is divided into two sub segments. One of them is the constant speed and constant angle descent which is performed with a constant descent rate until the flare altitude and another is the flare which is assumed to be performed in a circular path until the main gears touch to the ground. Table 3. 20 shows the approach segment important parameters.

Table 3. 20 Segment 6-7 Parameters

Approach speed, $V_{approach}$ [m/s]	23.7
Approach angle, $\theta_{approach}$ [deg.]	2.4
Approach descent rate, $V_{v,approach}$ [m/s]	1
Flare speed, V_{flare} [m/s]	22.5
Approach distance, $S_{approach}$ [m]	2285
Approach time, $t_{approach}$ [s]	99
Flare distance, S_{flare} [m]	44
Weight after approach, W_7 [N]	184.6
Thrust specific fuel consumption during approach, $c_{t,approach}$ [1/s]	0.001799

8.8 Landing Ground Roll: Segment 7-8

Landing ground roll is the last mission segment which starts at the moment when the main gears touch to the ground and ends when the aircraft stops. Table 3. 21 shows the landing ground roll parameters and the total important mission profile parameters. Total fuel burned during the mission profile is found as 73.3 N and the total mission time is 34.9 min which includes the 30 min. cruise time which is a design input.

Table 3. 21 Segment 7-8 Parameters

Free roll distance, S_{LR} [m]	22
Total Landing distance, $S_{L,TOTAL}$ [m]	147.7
Fuel burned during mission, W_{fuel} [N]	73.3
Total mission time, $t_{mission}$ [min.]	34.9

CHAPTER 4

OPTIMIZATION

1. Optimization Method

The optimization is conducted by using the initial design parameters as a starting point. Some of the design inputs are selected as variables and matched each other to form the different design cases. As stated in Chapter 2 the number of designs is defined as;

The number of designs, NOFD;

$$NOFD = \prod_{i=1}^{Y_{inputs}} (X_{range})_i$$

Where; Y_{inputs} is the number of variable design inputs and X_{range} is the range of each design input.

2. Defining the Design Variables

The design variables the selected design inputs to construct the design cases. Each design case is formed via the combination of these design variables. Each design variable has a length which determined the size of the number of design parameter, NOFD.

The design parameters are selected as the main geometric parameters of the wing-body which is stated to be a combination of the main wing and the front wing which is called as LEX in this thesis. The design variables are selected as;

c_r : Wing root chord

c_t : Wing tip chord

b : Wing span

Λ_{LE} : Wing leading edge sweep angle.

$c_{r,LEX}$: LEX root chord

b_{LEX} : LEX span
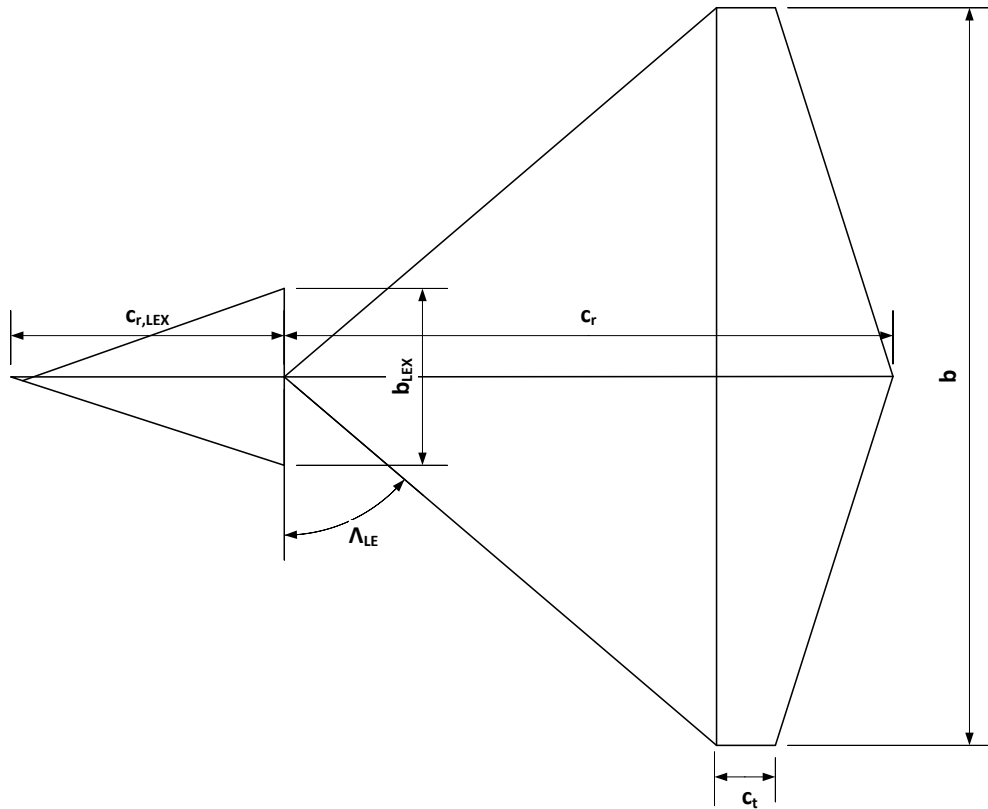
Figure 4. 1 The Design Variables On The Wing-Body Conceptual Geometry.

The design variables which are shown in Figure 4. 1 determine the basic geometry of the main wing and the front wing. Instead of selected the wing loading or aspect ratio as design variables, the basic geometric parameters are considered as variables. So, in this method the wing loading and aspect ratio are generated according to the design variables.

The length of each design variable is determined by taking the initial design parameters as reference. So, the design variables are varied around the initial design parameters. The design parameters with length;

$c_r = [1.4\ 1.55\ 1.7]$

$c_t = [0.1\ 0.15\ 0.2]$

$b = [1.4\ 1.6\ 1.8]$

$\Lambda_{LE} = [50\ 60\ 70]$

$c_{r,LEX} = [0.8\ 0.96\ 1.2]$

$b_{LEX} = [0.3\ 0.4\ 0.5]$

68

Six variables have three different values. So, the number of designs;

$$\text{NOFD} = \prod_{i=1}^{Y_{\text{inputs}}} \left(X_{\text{range}}\right)_i = \prod_{i=1}^{6} \left(X_{\text{range}}\right)_i = 3 \cdot 3 \cdot 3 \cdot 3 \cdot 3 \cdot 3 = 3^6 = 729$$

3. Setting The Requirements

The operational requirements are determined prior to the initial design. Table 4. 1 shows the operational requirements. The requirements are basically based on the maneuverability and high speed which are important design considerations for the high speed target drones. 2000 gram payload capacity is reserved to be used for avionics such as radar, smoke systems or additional avionics.

Table 4. 1 Operational Requirements

Endurance	30 min.
Maximum Speed	0.5 Mach
Maximum Sustained Load	6g
Payload Capacity	2000 gram
Operational Altitude	1700m Above Sea Level

The design requirements are set to determine the limiting cases for the optimization analysis. Table 4. 2 shows the design requirements. The maximum speed is selected as 167 m/s at 1700m above the sea level which is selected as an input. The cruise time is a constant design input. All the design cases are generated for $t_{\text{cruise}} = 30$ min. The maximum sustained load factor is selected to be equal or greater than 6g's.

Table 4. 2 Design Requirements

$V_{max} \geq 167\ m/s$	Maximum speed at the operational altitude.
$t_{cruise} = 30\ min$	Cruise time.
$n_{max,sustained} \geq 6$	Maximum Sustained Load Factor.
$\Lambda_{TE} > 0°$	Main Wing Trailing Edge Sweep Angle.
$V_{FUEL\ TANK} > V_{FUEL}$	Fuel Tank Volume.

Some design requirements are set to check the geometry of the aircraft. The fuel tank volume constrain is necessarily is set to be bigger than the fuel volume calculated from the mission profile for a feasible design. The trailing edge sweep angle is selected to be a positive value which is required for a delta wing design.

4. Defining the Inputs

The inputs are divided into two parts as constant inputs which does not change for each design case and variable inputs which change for each design case. Table 4. 3 shows the constant design inputs.

Table 4. 3 Constant Design Inputs

Wing-Body Parameters					
$C_{L_{max}}$	0.738	b	1.6	b_{LEX}	0.4
$C_{l_{\alpha,wing}}$	5.7	Λ_{LE}	60	$C_{l_{\alpha,LEX}}$	5.7
$\left(\dfrac{t}{c}\right)_{wing\ airfoil}$	0.06	hn_{wing}	0.33	hn_{LEX}	0.36
$\left(\dfrac{t}{c}\right)_{m}$	0.459	C_{l_0}	0	η_{LEX}	1
Λ_m	42.08	C_{m_0}	0		
c_r	1.55	$c_{r,LEX}$	0.96		
c_t	0.2	$c_{t,LEX}$	0		
Tail Parameters					
$c_{r,tail}$	0.45	$\alpha_{i.tail}$	27	$\Lambda_{TE,tail}$	50
$c_{t,tail}$	0.96	l_{tail}	0.65	$C_{l_{\alpha,tail}}$	5.7
$\Lambda_{LE,tail}$	66	$\left(\dfrac{t}{c}\right)_{tail\ airfoil}$	0.06	$\left(\dfrac{t}{c}\right)_{m,tail}$	0.459
$\Lambda_{m,tail}$	57.9				
Propulsion System Parameters					
N_{engine}	1	$t_{fuel\ tank}$	0.5	$b_{fuel\ tank}$	0.5
R_{inlet}	0.11	$c_{fuel\ tank}$	0.5	l_{inlet}	0.5
Mission Profile Parameters					
$N_{ground\ roll}$	1	$h_{obs.}$	5	μ_r	0.03
$V_{v,descent\ rate}$	20	t_{loiter}	2	V_{cruise}	87
$\mu_{r,landing}$	0.3	t_{cruise}	30		
Landing Gear And Parachute Parameters					
$W_{m.gear}\big/W_{TOTAL}$	0.075	$W_{nose\ gear}\big/W_{TOTAL}$	0.025	$W_{parachute}\big/W_{TOTAL}$	0.05
Air Properties					
$h_{takeoff}$	1000	$h_{cruise3}$	3800	$h_{cruise2}$	2300
h_{cruise}	1700	T_0	288.16	ρ_0	1.225
$h_{descent}$	1100	P_0	101325		
Sample Structural Weights					
W_{s_skin}	1000	W_{s_tail}	1000	W_{s_paint}	300
W_{s_frame}	2000	W_{s_tank}	500		

Table 4. 4 Variable Design Inputs

c_r	[1.4 1.55 1.7]	b	[1.4 1.6 1.8]	$c_{r,LEX}$	[0.8 0.96 1.2]
c_t	[0.1 0.15 0.2]	Λ_{LE}	[50 60 70]	b_{LEX}	[0.3 0.4 0.5]

Table 4. 4 shows the six variable design inputs which are combined with each other to generate 729 different design cases.

5. Results

After defining the constant and variable inputs for the analysis the optimization analysis is conducted. 729 designs are generated and elected according to the design requirements shown in Table 4. 2.

Table 4. 5 The Satisfactory Number of Designs According to the Design Requirements

Design Constraint	Number of Satisfactory Designs
$V_{FUEL\ TANK} > V_{FUEL}$	729
$V_{max} \geq 167$ m/s	526
$\Lambda_{TE} > 0°$	369
$n_{max,sustained} \geq 6$	21
ALL	21

Table 4. 5 shows the satisfactory number of designs which are determined according to the design requirements. The available fuel tank constraint is satisfied by all the designs which is a result of the fuel tank design inputs which allows the usage of half of the wing span, thickness and mean chord for the fuel tank and the slender delta wing configuration which enables high internal wing volume. The most challenging constraint is the maximum sustained load factor. 21 designs are satisfactory for this constraint and all of the design constraints by the same time.

Table 4. 6 shows some of the properties of the satisfactory designs which satisfy all the design constraints given in Table 4. 2. Lowest weight and maximum velocity is achieved by the design #30 as a result of the smallest total wing-body area. All the satisfactory designs have a leading edge sweep angle of 50 degrees. Highest maximum load factor is achieved by the design #57.

Table 4. 6 The Satisfactory Designs

ID	c_t	c_r	b	Λ_{LE}	$c_{r,LEX}$	b_{LEX}	W_{TOTAL}	V_{fuel}	$V_{FUEL\ TANK}$	V_{max}	Λ_{TE}	$n_{max,su}$
30	0.1	1.4	1.6	50	0.8	0.3	23811.4	8.84	13.87	185.3	23.4	6.158
31	0.1	1.4	1.6	50	0.8	0.4	24060.9	8.91	13.87	182.8	23.4	6.1
32	0.1	1.4	1.6	50	0.8	0.5	24310.1	8.97	13.87	180.4	23.4	6.039
33	0.1	1.4	1.6	50	0.96	0.3	24007.5	8.90	13.87	183.3	23.4	6.11
34	0.1	1.4	1.6	50	0.96	0.4	24306.1	8.98	13.87	180.4	23.4	6.038
36	0.1	1.4	1.6	50	1.2	0.3	24290.2	8.98	13.87	180.4	23.4	6.037
57	0.1	1.4	1.8	50	0.8	0.3	24767.7	9.08	15.6	176.4	14.1	6.419
58	0.1	1.4	1.8	50	0.8	0.4	25016.8	9.14	15.6	174.3	14.1	6.356
59	0.1	1.4	1.8	50	0.8	0.5	25266.3	9.21	15.6	172.2	14.1	6.297
60	0.1	1.4	1.8	50	0.96	0.3	24958.6	9.13	15.6	174.7	14.1	6.366
61	0.1	1.4	1.8	50	0.96	0.4	25257.4	9.21	15.6	172.2	14.1	6.294
63	0.1	1.4	1.8	50	1.2	0.3	25233.1	9.21	15.6	172.2	14.1	6.297
300	0.15	1.4	1.8	50	0.8	0.3	25051.6	9.15	15.97	174.1	11.1	6.211
301	0.15	1.4	1.8	50	0.8	0.4	25301.1	9.22	15.97	172.0	11.1	6.152
302	0.15	1.4	1.8	50	0.8	0.5	25550.7	9.28	15.97	170.0	11.1	6.091
303	0.15	1.4	1.8	50	0.96	0.3	25241.4	9.21	15.97	172.4	11.1	6.163
304	0.15	1.4	1.8	50	0.96	0.4	25540.6	9.29	15.97	170.0	11.1	6.095
305	0.15	1.4	1.8	50	0.96	0.5	25840.3	9.37	15.97	167.7	11.1	6.024
306	0.15	1.4	1.8	50	1.2	0.3	25516.3	9.29	15.97	170.0	11.1	6.094
307	0.15	1.4	1.8	50	1.2	0.4	25887.2	9.39	15.97	167.2	11.1	6.011
543	0.2	1.4	1.8	50	0.8	0.3	25335.4	9.23	16.34	171.8	8.0	6.016

As an initial election from the satisfactory designs, the design #30 due to the lowest weight and highest maximum velocity, the design #36, #63, #306 and #307 which have one of the highest total root wing-body chord which the summation of the main wing root chord and the LEX root chord and as a result thicker root section and design #57 for the highest load factor are selected. Figure 4. 2 shows the selected wing-body geometries.

#30	#36	#57	#63	#306	#307
AR_{wing} = 2.13	AR_{wing} = 2.13	AR_{wing} = 2.4	AR_{wing} = 2.4	AR_{wing} = 2.32	AR_{wing} = 2.32
S_{TOTAL}=1.32m^2	S_{TOTAL}=1.38m^2	S_{TOTAL}=1.47m^2	S_{TOTAL}=1.53m^2	S_{TOTAL}=1.575m^2	S_{TOTAL}=1.635m^2
W/S=18.03kg/m^2	W/S=17.6kg/m^2	W/S=16.84kg/m^2	W/S=16.49kg/m^2	W/S=16.2kg/m^2	W/S=15.8kg/m^2
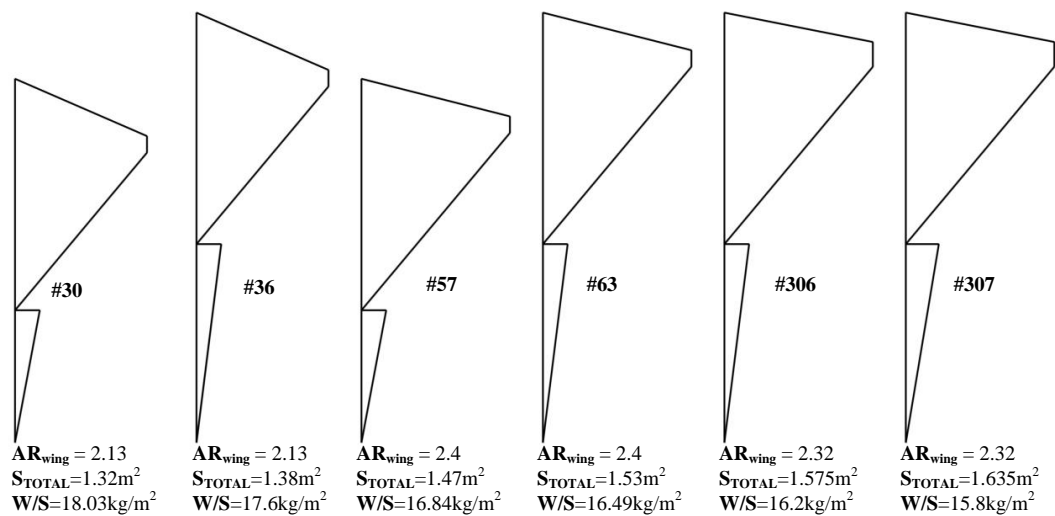
Figure 4. 2 Selected Design Wing-Body Configurations.

Second selection is conducted geometrically rather than performance. Longer wing-body root chord results in thicker wing-body root and more internal volume which is a desired property for such a slender, thin profile wing-body configuration. Although all of the designs have sufficient internal volume for the fuel, the designs which have longer root wing-body chord are selected over the others. As a result, design #30 and #57 which have the highest maximum velocity and load factor, respectively are eliminated.

Final selection is conducted according to maneuver performance. Maximum load factor is considered as a selection criteria. The highest load factor is obtained by the design #63 among others. So, the final decision is made in favor of design #63.

Figure 4. 3 The Initial Design (on the left) and The Final Design (on the right) Wing-Body Configurations.

6. Summary of the Final Design Properties

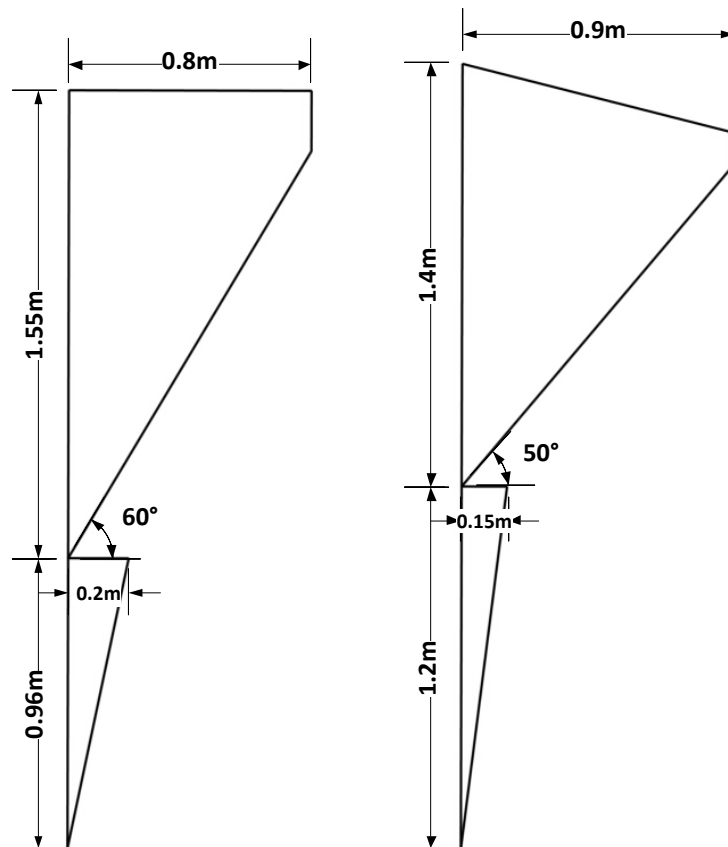The final design is selected as a result of the optimization process described in the previous section. The maximum velocity and maximum load factor are satisfied with the final design. Table 4. 7 shows the comparison of the initial and final design according to some of the important design and performance parameters.

Table 4. 7 Comparison of The Initial and Final Design

Parameters	INITIAL DESIGN	FINAL DESIGN
c_t [m]	0.2	0.1
c_r [m]	1.55	1.4
b [m]	1.6	1.8
Λ_{LE} [Deg.]	60	50
$c_{r,LEX}$ [m]	0.96	1.2
b_{LEX} [m]	0.4	0.3
W_{TOTAL} [gr]	26304.3	25233.1
V_{fuel} [Litres]	9.97	9.21
$V_{FUEL\,TANK}$ [Litres]	17.64	15.6
V_{max} [m/s]	159.45	172.25
Λ_{TE} [Deg.]	0	14.18
$n_{max,sus.}$	4.21	6.29
S_{TOTAL} [m^2]	1.592	1.53
AR_{main_wing}	1.82	2.4
C_{L_α}	2.26	2.79
W/S	16.52	16.49
V_{stall} [m/s]	20.57	20.56
R/C [m/s]	44.95	50.17
$(R/C)_{max}$ [m/s]	45.18	51.33
V^* [m/s]	42.24	51.59
$R_{min,turn}$ [m]	44.4	43.64
$\omega_{max,turn}$ [Deg./s]	54.4	67.72
(T/W)	0.808	0.843
V_{cruise} [m/s]	87	87
$V_{R/C,max}$ [m/s]	92.25	99.4
$S_{g,ground\,roll}$ [m]	70.16	68.09
$S_{a,transition}$ [m]	29.38	29.42

As shown in Table 4. 7, the maximum velocity and load factor design constraints are unsatisfactory for the initial design. The maximum velocity is 159.45 m/s and maximum load factor is 4.21. The total weight is 26304.3 grams for the initial design while the final design has a weight of 25233.1 grams which is less than the initial design. It means that design requirements are satisfied with a lighter design. The maneuvering capability is higher for the final design. The turn rate is increased from 54.4 deg/s to 67.72 deg/s and rate climb is risen from 44.95 m/s to 50.17 m/s.

7. The Final Design Geometry

In this section the modeling of the external geometry of the aircraft and modeling and integration of the sub-systems are dealt with. CATIA software is used for designing and assembling.

7.1 Modeling of The Wing Body Surface

The wing body geometry, in chord-wise direction, is in the form of NACA 66 006 airfoil while in span-wise direction it is symmetrical diamond like shape.
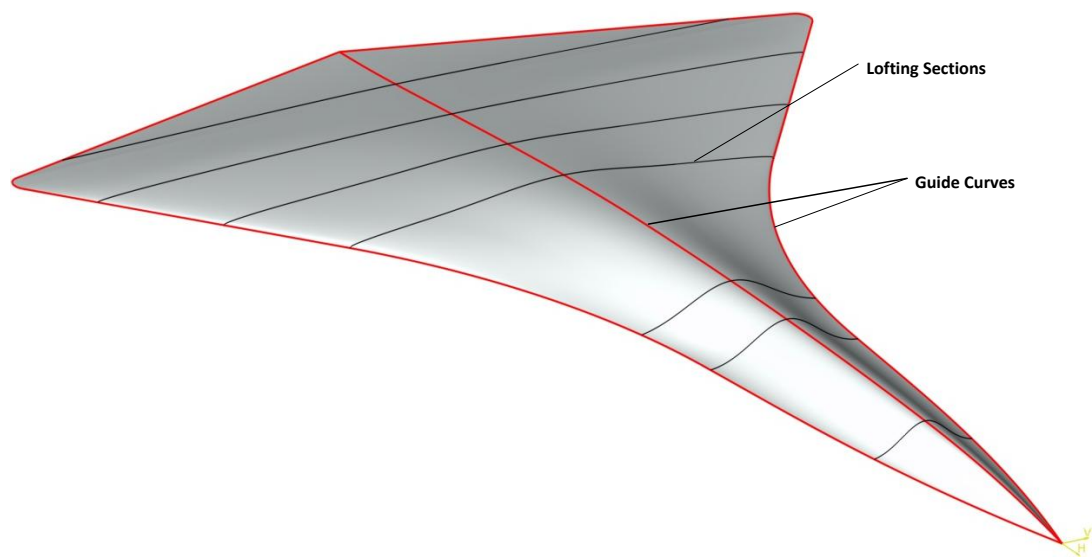
Figure 4. 4 The Lofting of the Wing-Body Geometry.

Figure 4. 4 shows the horizontal and vertical guide curves and the span-wise sections. Span-wise sections are guided with the guise curves to give the desired shape to the geometry.
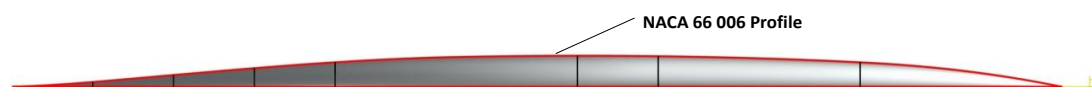
Figure 4. 5 The Side View of The upper Wing-Body Geometry.

Figure 4. 5 shows the NACA 66 006 profile on the upper guide curve. The chord-wise sections are in the form of NACA 66 006 profile. Figure 4. 6 shows the joined upper and lower lofted surfaces.

Figure 4. 6 From Up to Bottom; The Isometric, Right and Front View of The Lofted and Joined Upper and Lower Surfaces.

The inlet is modeled by considering the engine properties. The inlet is sized according to the engine lip dimensions to provide sufficient air flow to the engine. Figure 4. 7 shows the engine Inlet modeling.

Figure 4. 7 The Inlet.

Figure 4. 8 The Side View of The Inlet Part of The Geometry.

The engine is located at the end of the aircraft due to the fact that the nozzle section of the engine contains high temperature mass flow and it means high heat signature for the infrared sensors. The infrared visibility of the aircraft is increased with this configura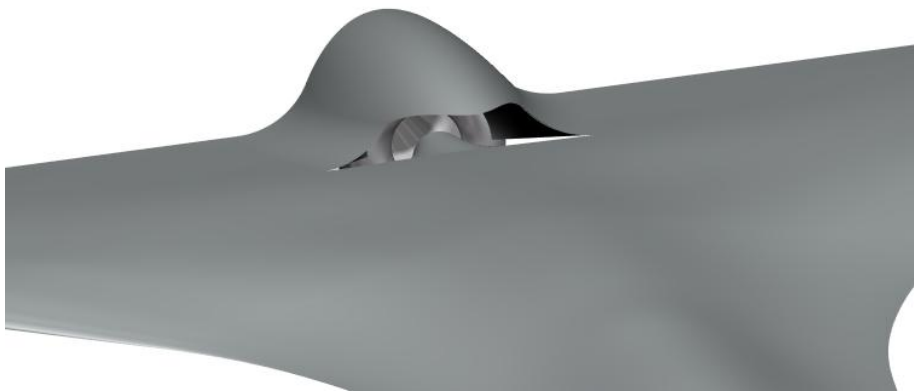tion. Another reason of locating engine to the back side is to protect structural parts of the aircraft against excessive heat.
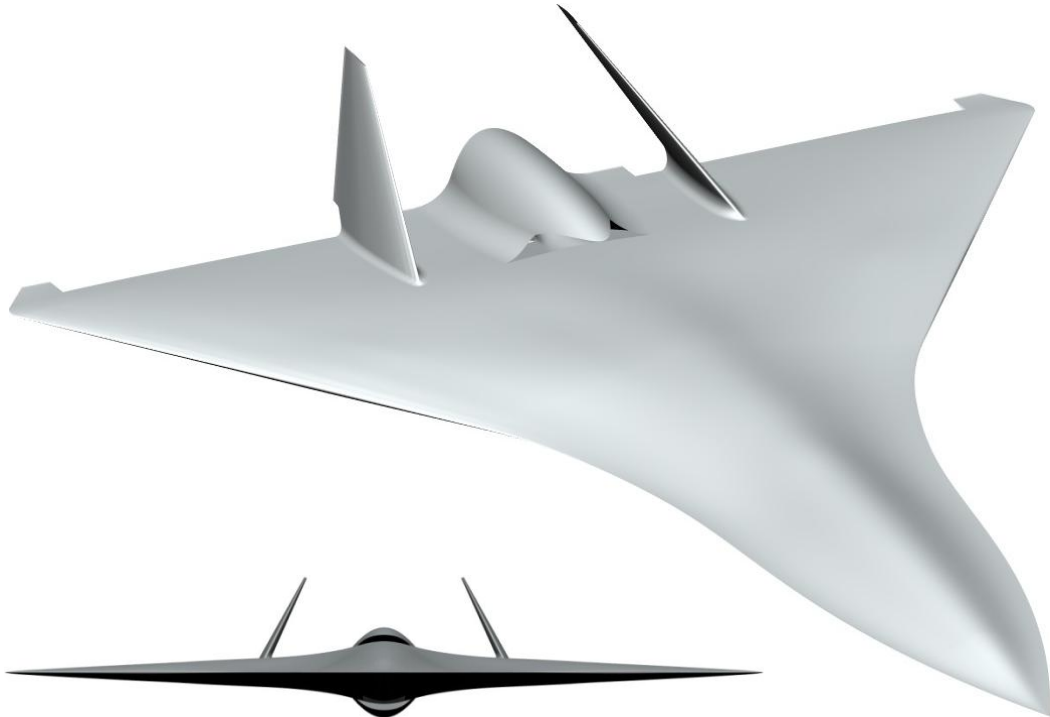
Figure 4. 9 The Tails with Wing-Body Geometry.

The tail design is considered as an inclined tail configuration to provide both longitudinal and directional stability. The tails are inclined **27** *degrees* inwards as given in the design inputs. The tails profiles are NACA 66 006 as the whole wing-body chord-wise sections.

Figure 4. 10 The Side View of The Aircraft With The Tails.

The side view is shown in Figure 4. 10. The engine nozzle is outside of the structure of the aircraft. The control surfaces are decided to be elevons as shown in Figure 4. 11.
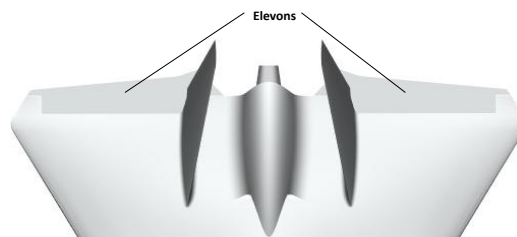
Figure 4. 11 The Elevons.

7.2 Structure

The structure of the aircraft consists of the internal frames and the outer skin. Frames are made of Beech wood while the outer skin is made of balsa wood and fiber-glass and epoxy-resin combination. The internal frames are modeled according to the conceptual frames generated during the optimization process. The locations of the conceptual frames are taken as reference. Minor changes for the positions are made during the detailed design phase. Figure 4. 12 shows the internal structure which consists of the span-wise and chord-wise frames and Figure 4. 13 shows the inside of the UAV.

Figure 4. 12 The Internal Structure.

1. Turbojet Engine
2. Elevon Pushrods
3. Elevon Servo
4. Main Gear
5. Main Gear Servo
6. Header Fuel Tank
7. Main Fuel Tank
8. Nose Gear
9. Nose Gear Servo
10. Avionics

Figure 4. 13 The Inside of The UAV.

8. Static Margin Analysis

The static margin analysis which is required for the longitudinal stability is conducted in this section. The positions of the units are shown in Table 4. 8.

Table 4. 8 The Weight Distribution.

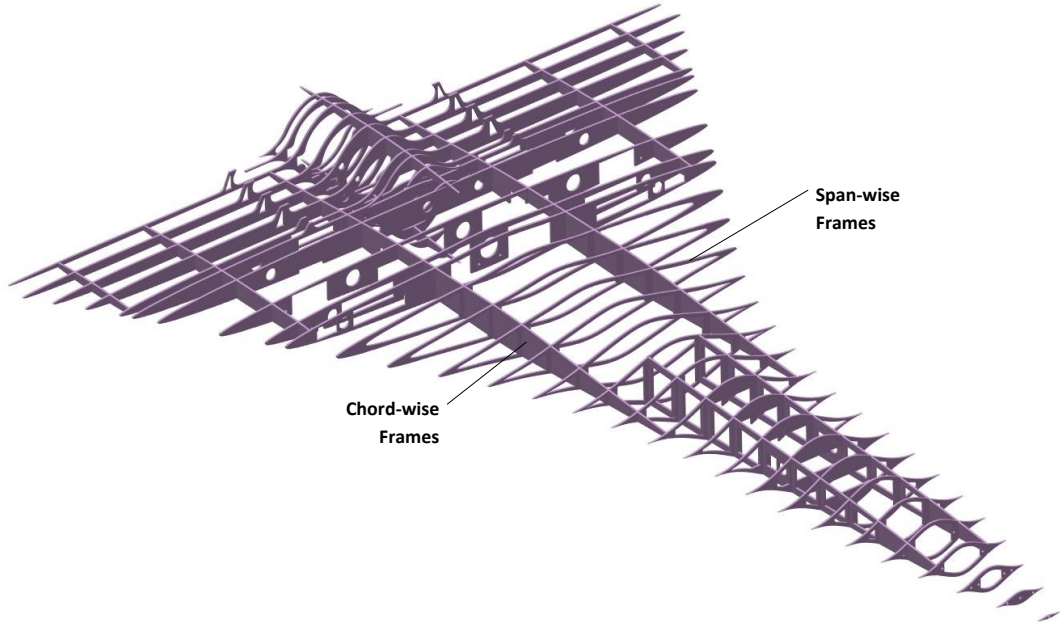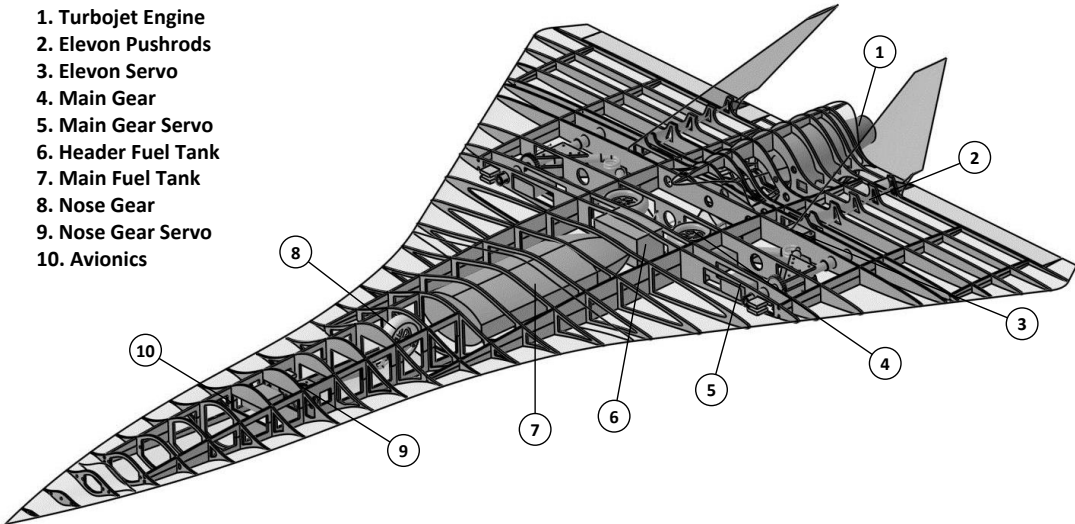| Unit	Weight (gr)	X (mm)	Z	Unit	Weight (gr)	X (mm)	Z
Blended Wing-Body Skin	3519	728	0	Main Gear	1892.48	848.26	0
Inlet Skin	240	156	0	Nose Gear	630.82	1950	0
Elevon	138.4	-46.8	0	Elevon Servos(x2)	60	156	0
Boya	1055.7	728	0	Autopilot	100	775.78	0
Frames	2304.18	750.82	0	Data Modem	70	2210	0
Tail	102.33	156	90	Video Modem	70	2210	0
Rudder Pushrod	10	50	0	Data Modem Antenna	36	2210	0
Main Gear Dood Pushrod	6	0	0	Video Modem Antenna	20	2210	0
Nose Gear Dood Pushrod	3	0	0	GPS Antenna	28	2210	80
Engine	2850	156	0	AGL Sensor	50	2210	-70
Engine Controller	200	624	0	Elevon Servo Cables	20	1300	0
Fuel pump	80	624	0	LED	10	2210	10
Gas Solenoid Valve	50	624	0	Autopilot Cables	30	910	0
Gas Tank	100	780	0	Parachute	1261.65	1560	0
Fuel Shuoff Valve	50	624	0	System Battery	300	2210	0
Engine Battery	300	2210	0	Engine Mount	80	156	0
Fuel	6910.14	832	0	Fuel Pumps	100	520	0
Fuel Tank	547.44	832	0	Payload	2000	2340	0
				TOTAL	25233.1	893.76	0.31

During the optimization process some of the sub-system weights such as autopilot, modems, antennas, cables, engine and components and battery weights are considered as inputs. The positions are reconsidered to provide a sufficient static margin. The static margin is considered as acceptable for values around 5%.

Initially the neutral point of the aircraft is found. The neutral point is defined as;

$$hn = ac_{TOTAL} + \frac{C_{L_{\alpha_H}}}{C_{L_\alpha}}.V_{HT}\left(1 + \left(\frac{d\epsilon}{d\alpha}\right)_{downwash}\right)$$

Where;

ac_{TOTAL} is the total aerodynamic center of the main and front wing which is calculated according to the area distribution of the main and front wing. It is calculated from;

$$ac_{TOTAL} = hn_{wing} - \frac{\frac{S_{LEX}}{S_{TOTAL}} \cdot \left(c_r + c_{r,LEX} - \left(\bar{c} - hn_{wing} \cdot \bar{c} \right) - \left(c_{r,LEX} - \left(\bar{c}_{LEX} - hn_{LEX} \cdot \bar{c}_{LEX} \right) \right) \right)}{\bar{c}}$$

As described in Chapter 2 hn_{wing} and hn_{LEX} are the neutral points of the main wing and front wing, respectively and found from the Figure 3.44 in [9]. The total aerodynamic center is found as $ac_{TOTAL} = \mathbf{0.1689}$ and the neutral point, $hn = \mathbf{0.1683.}$ Detailed calculations are shown in The Appendix section which can be found at the end of the thesis.

The static margin is defined as;

$$Static\ Margin\ (\%) = \frac{hn - \left(c_r + c_{r,LEX} - x_{CG} - l_{LE} \right)}{c_r + c_{r,LEX}} \cdot 100$$

Where;

l_{LE} is the distance from aircraft nose to the leading edge at the mean chord. Above calculation is valid when the dimensions are taken from the back of the aircraft due to the fact that positions of all of the components are referenced from end point of the aircraft instead of the nose point. l_{LE} is found from;

$$l_{LE} = c_r + c_{r,LEX} - \bar{c} - \bar{y} \cdot \tan \left(\Lambda_{TE} \right)$$

It is calculated as $l_{LE} = \mathbf{1.581m}$ and the static margin is found as %$\mathbf{3.52}$ and this value is considered as acceptable for a highly maneuverable aircraft.

The angle between the main landing gear wheel rotation center and the center of gravity of the aircraft is found as $\mathbf{8.62}$ degrees by taking the vertical distance between the gear rotation center and center gravity of aircraft as 300 mm. Figure 4. 14 shows the tail touch-down angle together with the angle between the gear and the center of gravity.
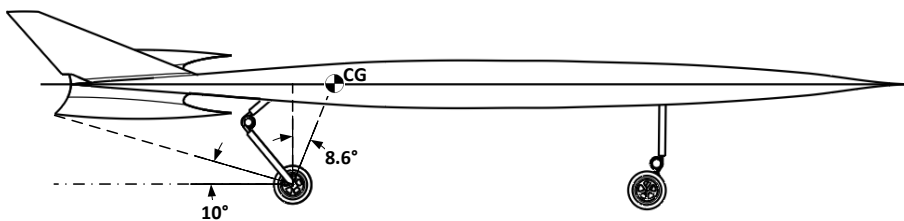

Figure 4. 14 The Angle Between Center of Gravity and Wheel Rotation Center and The Tail Touch-Down Angle.

CHAPTER 5

PRODUCTION AND MAIDEN FLIGHT

1. Production Methodology

Initial production is conducted for a scale version of the final design. The geometry of the aircraft together with the internal structures is scaled down to 1:2. The aircraft structure consists of span-wise and longitudinal frames and a skin which covers internal structure. Frames are produced from Beech plywood due to higher stiffness to weight ratio among other wood types. The skin is formed by covering the frames with 1mm Balsa wood which is properly shaped via a laser cutting process prior to the covering process. The outer layer of the skin is produced by covering the surface with fiberglass and resin to provide more stiffness. Figure 5. 1 shows the production methodology basically.
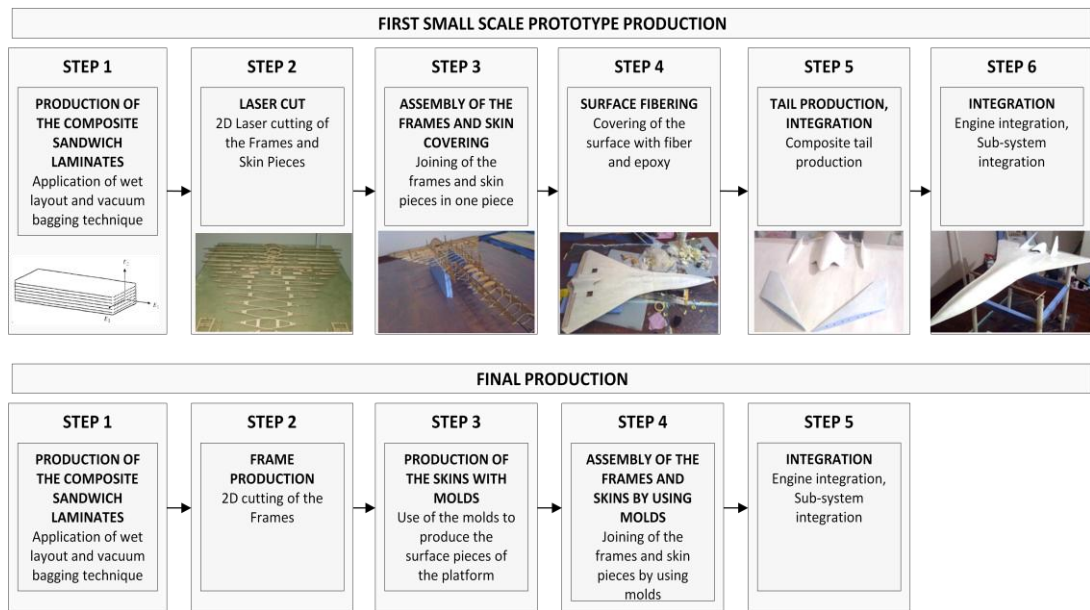

Figure 5. 1 Production Methodology.

The Initial scaled prototype is produced without using molds due to the fact that the design is prone to minor changes before the final production.

1.1 Step 1: Laser Cutting

The first step is the laser cutting of the frames and skin pieces. Skin pieces are formed by unfolding the 3D geometry so that 2D surface pieces are obtained for laser cutting. Figure 5. 2 shows the skin divisions one the 3D geometry. Each piece is unfolded to produce 2D geometry.
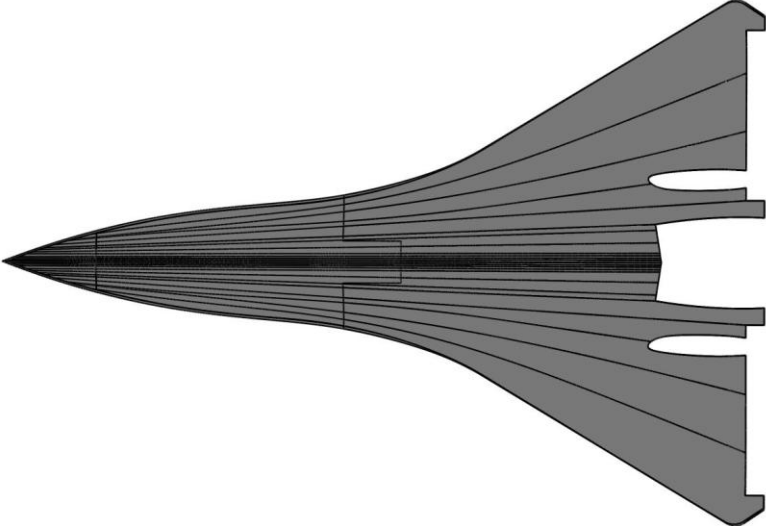

Figure 5. 2 Surface Skin Pieces on 3D Geometry.

Figure 5. Error*! Bookmark not defined.* shows the surface pieces which are produced from 1 mm balsa sheets via laser cutting technique. At the places where high curvature exists, the pieces are kept narrow due to the fact that balsa can be broken due to the high curvature during skin adhesion process.

The internal frames are produced in a similar way. The Beech plywood panels with 3mm thickness are applied laser cutting to produce the internal frame sections. Figure 5. 3 shows the span-wise and chord-wise laser cut frames.

Figure 5. 3 The Laser Cut Internal Frames.

1.2 Step 2: Adhesion of Skin and Internal Structure and Wiring

After producing the necessary components for the construction of the wing-body, the adhesion process is applied. For accurate positioning the chord-wise frames sections which are nearest to the symmetry line are fixed as in Figure 5. 5. Before covering the frames the cables are located inside as in Figure 5. 4.
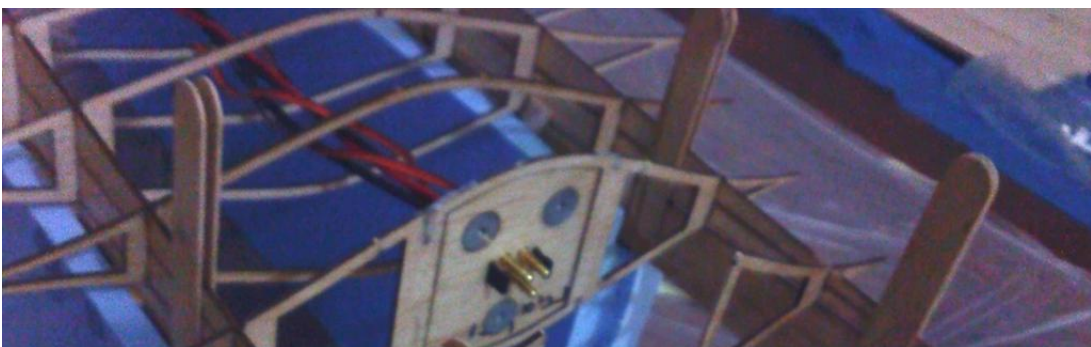
Figure 5. 4 The engine and servo cables located inside of the UAV.
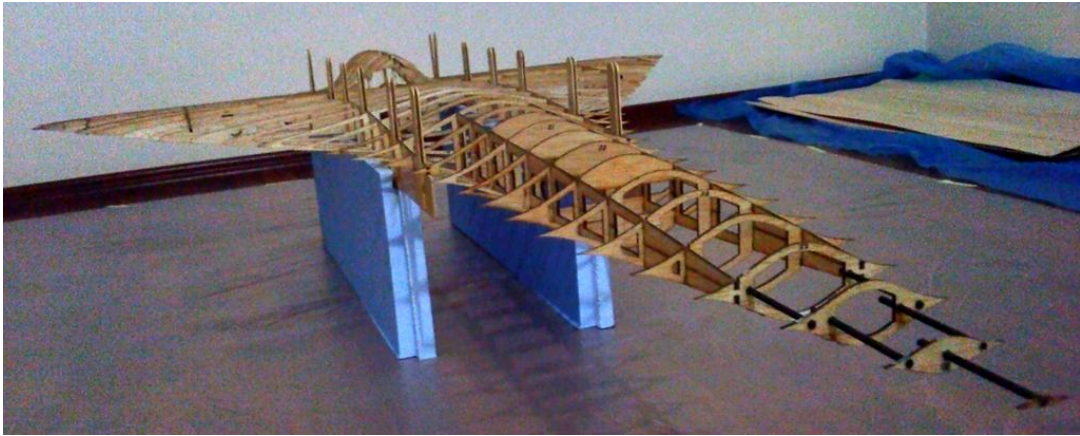
Figure 5. 5 The Internal Frames are Fixed.

1.3 Step 3: Surface Fibering

After the skin and the frames are stuck with each other, the surface is reinforced with 80 gr/m^2 E-glass and epoxy-resin for higher stiffness. Figure 5. 6 shows the surface after the surface covering process. The white color is obtained by mixing the epoxy-resin with white color pigment which is applied to the mixture with a ratio of %5.

Figure 5. 6 The Surface is applied e-glass and epoxy resin.

1.4 Step 4: Tail Production and Integration

The tail is considered as a passive stability device for the UAV as stated in previous chapters. The whole tail is produced from foam with E-glass combination. Initial tail geometry is given to the foam block and the surface is reinforced with 80 gr/m^2 E-glass and epoxy-resin as in the wing-body. Figure 5. 7 and Figure 5. 8 show the tails before and after the sanding and fibering process, respectively.

Figure 5. 7 The tail blocks before sanding process.

Figure 5. 8 The Left and Right Tails after the sanding and fibering process.

1.5 Step 5: Landing Gear and Electronic Equipment Deployment

The main and nose landing gears are located as in Table 4. 8 . Before landing gear deployment the necessary gear doors are opened. The radio control receiver, gear controllers, and batteries are located at the nose section of the UAV.

Figure 5. 9 The Landing Gears are deployed.

2. Maiden Flight

The maiden flight is conducted with the initial scaled prototype. The flight runway is located at Mamak in Ankara. Figure 5. 10 and Figure 5. 11 show some pictures during the flight day.

Figure 5. 10 The initial prototype is ready to fly.

Figure 5. 11 The initial prototype is controlled with remote controller by a pilot.

Figure 5. 12 The initial prototype is on the takeoff run.

Figure 5. 13 While the initial prototype in the sky.

The flight has taken approximately 2.5 min. The takeoff and flight are conducted successfully. Takeoff distance was approximately 70-80 m. The aircraft longitudinal stability was as desired. The high maneuvering capability of the aircraft was clearly observed.

2. Weight Comparison

After the initial prototype production, the estimated weight and the measured weight are compared. Due to the fact that the weight estimation is heavily based on the sample structural inputs and they are obtained from the sample plates which are produced prior to the production of the prototype, the estimated weight is expected to be quite close to the measured one. Table 5. 1shows the comparison of estimated and measured weights.

Table 5. 1 The Weight Comparison

Unit	Estimated Weights (gr)	Measured Weights (gr)
Aircraft (Structural)	1889.89	1835
Battery	700	700
Engine	450	450
Electronics	410	410
Main Gear	287.54	250
Nose Gear	95.84	100
TOTAL	**3833.96**	**3745**

The estimated values in Table 5. 1 are obtained by using the small scale prototype parameters. The small scale prototype is 1:2 scaled version of the final design.

CHAPTER 6

CONCLUSION

In this thesis study design of a high speed target drone which is capable of flying at 0.5 Mach is conducted. Total flight time is set to 30 minutes. The engine is selected as a single turbojet engine which gives 230 N of thrust at sea level. The takeoff is performed on the runway while landing can be performed via parachute. Fuel tanks are located inside of the wing-body. Engine nozzle is located outside of the wing-body to increase the heat signature. Passive tail surfaces are inclined inwards for longitudinal stability. Control surfaces are selected as elevons.

The slender wing-body geometry is assumed to be a combination of the main wing and front wing which is called as LEX (Leading edge extension) in this thesis. The total lift curve slope is calculated by considering the virtual wing in up-wash and virtual horizontal tail in down-wash. The lifting contribution of the virtual wing and horizontal tail is quite lower than the main wing. The projected area of the tail which is considered as the virtual horizontal tail area is inadequate to have a considerable effect on the total lift curve slope. The aspect ratio of the wing is intentionally kept low to benefit from the vortex lift which is effective at high angles of attack. Low aspect ratio delta wing configuration also provides better structural stiffness than a conventional moderate aspect ratio wing.

Design parameters are divided into the constant design parameters which are not changed during the optimization process and the variable design parameters which are changed during the optimization. Variable design parameters are selected as to define the basic wing-body planform geometry. Increasing the number of variable design parameters causes more calculation time because of the iterative calculations. In this thesis 729 design cases are built with six variable design parameters.

The optimization process is conducted by assigning the each design case parameters to the corresponding cells in the Excel file and writing the results to a new file. The key point for optimization process is to find a good starting point since the optimization is conducted around the initial design parameters.

The total weight is heavily dependent on the cruise time input which forces the mission profile to generate the necessary fuel amount for the given input. Sample structural weights are considered as design inputs. In this thesis, the design methodology does not include structural modules to check whether the generated geometry is satisfactory for the pre-determined g loads or not. Instead, sample structural weight inputs which are determined experimentally prior to the design process are used to satisfy the structural stiffness. To determine these inputs sample structures are built and checked whether they are satisfactory for the desired g loads prior to the final design.

Production is started with 3D modeling of the aircraft. The skin is divided into pieces and unfolded for the 2D laser cut process. Wooden panels are used to produce the internal frames. During the assembly of the frames the positioning is important to eliminate shifting of the frames. So, the longitudinal frames are fixed by using a fixture which is produced according to the longitudinal frame geometry.

Maiden flight is performed with the initial design scaled prototype. The scale factor is determined to be 1:2. The high maneuvering capability of the UAV is observed during the flight. The longitudinal stability of the aircraft is observed as satisfactory.

As a future work following remarks are determined;

♦ The scale version of the final design is planned with the integration of the turbojet engine.
♦ The verification of the performance parameters such as maximum speed, cruise time and maneuvering capability is supposed to be conducted.
♦ The deployment of avionics including the autopilot and radar systems may be done.
♦ The cruise time may be increased by removing the parachute option. Alternatively, landing gears may be removed by introducing the catapult lunch and parachute recovery.
♦ Thrust vectoring option may be considered to increase the maneuvering capability.
♦ To increase the lifting performance a thicker airfoil may be selected.
♦ The vertical tail area may be increased for better lateral stability.
♦ Skin can be produced by using molds instead of covering the frames with pre-produced skin pieces.

REFERENCES

[1] Roskam, Jan , *Airplane Flight Dynamics And Automatic Flight Controls*, Roskam Aviation and Engineering Corporation, 1979.

[2] Anderson, John D., *Aircraft Performance and Design*, McGraw-Hill, 1999

[3] Roskam, Jan , Tau Edward Lan, Dr. Chuan, *Airplane Aerodynamics and Performance*, DarCorporation, 1997.

[4] Roskam, Jan, *Methods for Estimating Stability and Control Derivatives of Conventional Subsonic Airplanes*, 1971.

[5] Roskam, Jan, *Airplane Design-Part VI: Preliminary Calculation of Aerodynamic, Thrust and Power Characteristics,* DARcorporation, 2000.

[6] Raymer, Daniel P., *Aircraft Design: A conceptual Approach*, AIAA, 1992.

[7] Abbott, Ira H., *Theory of Wing Sections*, Dover Publications, INC., 1959.

[8] Amt Netherlands, URL: http://www.amtjets.com, [cited May 2013].

[9] Schlichting, Hermann and Truckenbrodt, Erich, *Aerodynamics of the Airplane,* McGraw-Hill, 1979

[10] CEI Firejet, URL: http://www.cei.to/aerialtargetsystems/firejet.aspx, [cited March 2013].

[11] AAA Phoenix, URL: http://www.airaffairs.com.au/phoenix_jet.html, [cited March 2013]

[12] ADCOM Yabhon HMD , URL:http://adcom-systems.com/eng/Targets/YAHBON-HMD, [cited March 2013]

[13] Houghton, E.L. and Carpenter, P.W., *Aerodynamics for Engineering Students*, Butterworth-Heinermann, 2003.

[14] Özyetiş, E., Alemdaroğlu, N. "*Yüksek Hızlı Hedef Uçağı Tasarımı ve Üretimi*", Ulusal Havacılık ve Uzay Konferansı, Eskişehir, Türkiye, 2013.

This page is intentionally left blank.

APPENDIX A

INITIAL DESIGN CALCULATIONS

In this appendix the initial design calculations are performed for demonstration purpose only.

A1.WEIGHT ANALYSIS

In this appendix the initial design weight analysis is demonstrated step by step. All of the formulation is given in Chapter 2.

Total weight is calculated from the equation;

$$W_0 = W_{TOTAL} = W_{empty} + W_{fuel} + W_{payload}$$

Aircraft total weight;

$$W_{empty} = W_{wing\_body} + W_{tail} + W_{sys\_internal}$$

The weight of the wing-body;

$$W_{wing\_body} = W_{blended\_wing} + W_{inlet} + W_{paint}$$

The weight of blended wing-body;

$$W_{blended\_wing} = W_{wing\_skin} + W_{frame}$$

The weight of skin;

$$W_{wing\_skin} = 2.3 \cdot S_{TOTAL} \cdot W_{s\_skin}$$

By using the design inputs the total wing-body area is calculated as;

$$S_{TOTAL} = S = S_{main\_wing} + S_{LEX} = \frac{(c_r + c_t) \cdot b}{2} + \frac{(c_{r,LEX} + c_{t,LEX}) \cdot b_{LEX}}{2}$$
$$= \frac{(1.55 + 0.2) \cdot 1.6}{2} + \frac{(0.96 + 0) \cdot 0.4}{2} = \mathbf{1.592m^2}$$

Then the skin weight;

$$W_{wing\_skin} = 2.3 \cdot (1.592) \cdot (1000) = \mathbf{3661.6gr}$$

The total frame weight is found as;

$$W_{frame} = W_{sp\_frame} + W_{lng\_frame} + W_{in\_frame}$$

The number of span-wise frames parameters is selected as $N_{sp\_f} = 30$. That is 30 span-wise frames are located in the aircraft structure. By using the method described in Chapter 2 following table is constructed. The longitudinal position parameters of the frames and fill ratio parameters are design inputs.

Table A1. 1 Location and Weight Distribution of the Span-wise Frames

$Frame(i)$	$W_{sp\_frame}(i)$	$S_{sp\_frame}(i)$	$x(i)$	$F_{fill}(i)$
Frame 1	43.630674	0.0218153	62.75	1
Frame 2	49.698006	0.024849	112.95	1
Frame 3	56.561069	0.0282805	163.15	1
Frame 4	64.060091	0.03203	225.9	1
Frame 5	70.879943	0.03544	276.1	1
Frame 6	74.488524	0.0372443	301.2	1
Frame 7	81.867809	0.0409339	351.4	1
Frame 8	95.841576	0.0479208	451.8	1
Frame 9	78.996422	0.0526643	539.65	0.75
Frame 10	162.35805	0.0541193	577.3	1.5
Frame 11	167.88252	0.0559608	665.15	1.5
Frame 12	83.388422	0.0555923	753	0.75
Frame 13	79.518491	0.0530123	845.87	0.75
Frame 14	72.887202	0.0485915	938.74	0.75
Frame 15	64.453992	0.0429693	1029.1	0.75
Frame 16	54.652376	0.0364349	1119.46	0.75
Frame 17	43.928802	0.0292859	1209.82	0.75
Frame 18	32.598004	0.021732	1300.18	0.75
Frame 19	20.891119	0.0139274	1390.54	0.75
Frame 20	0	0	1550	0.75
Frame 21	0.8232096	0.0005488	1543.65	0.75
Frame 22	40.33631	0.0268909	1631.5	0.75
Frame 23	35.231592	0.0234877	1719.35	0.75
Frame 24	30.018381	0.0200123	1807.2	0.75
Frame 25	24.717576	0.0164784	1897.56	0.75
Frame 26	19.664689	0.0131098	1987.92	0.75
Frame 27	15.005964	0.010004	2078.28	0.75
Frame 28	10.804856	0.0072032	2168.64	0.75
Frame 29	7.0417906	0.0046945	2259	0.75
Frame 30	3.7042498	0.0024695	2349.36	0.75

Table A1. 1 shows the weight, area, fill ratio and position parameters of the span-wise frames. The position and fill ratio parameters are the inputs for the calculation. The

calculation is performed according the formulas described in Chapter 2. The total weight of span-wise frames;

$$W_{sp\_frame} = \sum_{i=1}^{30} W_{sp\_frame}(i) = \mathbf{1585.93\,gr}$$

The weights of longitudinal frames are calculated for the main wing and the front wing. The number of longitudinal frames in main wing parameter is selected as $N_{mw\_sp\_f} = 3$ while $N_{fw\_sp\_f} = 1$.

$$W_{lng\_frame} = W_{mw\_lng\_frame} + W_{fw\_lng\_frame}$$

Table A1. 2 Location and Weight Distribution of Longitudinal Main Wing Frames.

$Frame(i)$	$W_{mw\_lng\_frame}(i)$	$S_{mw\_lng\_frame}(i)$	$y(i)$	$F_{fill}(i)$
Long. Frame1	18.90436	0.009452	640	1
Long. Frame2	55.61158	0.027806	440	1
Long. Frame3	142.4408	0.07122	152	1
Long. Frame3S	142.4408	0.07122	-152	1
Long. Frame2S	55.61158	0.027806	-440	1
Long. Frame1S	18.90436	0.009452	-640	1

$$W_{mw\_lng\_frame} = 2 \cdot \sum_{i=1}^{3} W_{mw\_lng\_frame}(i) = \mathbf{433.91\,gr}$$

Table A1. 3 Location and Weight Distribution of Longitudinal Front Wing Frames.

$Frame(i)$	$W_{fw\_lng\_frame}(i)$	$S_{fw\_lng\_frame}(i)$	$y(i)$	$F_{fill}(i)$
Long. Frame4	52.98435	0.017661	66	1.5
Long. Frame4S	52.98435	0.017661	-66	1.5

$$W_{fw\_lng\_frame} = 2 \cdot \sum_{i=1}^{1} W_{fw_{lng\,frame}}(i) = \mathbf{105.97\,gr}$$

The total weight longitudinal frames;

$$W_{lng\_frame} = W_{mw\_lng\_frame} + W_{fw\_lng\_frame} = 433.91 + 105.97 = \mathbf{539.88\,gr}$$

The weight of inlet frames are calculated for $N_{in\_f} = 5$

$Frame(i)$	$W_{in\_frame}(i)$	$S_{in\_frame}(i)$	$F_{fill}(i)$
Inlet Frame1	30.410617	0.0152053	0.4
Inlet Frame2	30.410617	0.0152053	0.4
Inlet Frame3	30.410617	0.0152053	0.4
Inlet Frame4	30.410617	0.0152053	0.4
Inlet Frame5	30.410617	0.0152053	0.4

$$W_{in\_frame} = \sum_{i=1}^{5} W_{in\_frame}(i) = \mathbf{152.053} \boldsymbol{gr}$$

The total frame weight;

$$W_{frame} = W_{sp\_frame} + W_{lng\_frame} + W_{in\_frame} = 1585.93 + 539.88 + 152.053$$
$$= \mathbf{2277.863} \boldsymbol{gr}$$

The weight of inlet skin is calculated as;

$$W_{inlet} = 2 \cdot 2\pi \cdot R_{inlet} \cdot l_{inlet} \cdot W_{s\_skin} = 2 \cdot 2\pi \cdot (0.11) \cdot (0.274) \cdot (1000) = \mathbf{378.4} \boldsymbol{gr}$$

The weight of paint;

$$W_{paint} = 2.3 \cdot (S_{TOTAL}) \cdot W_{s\_paint} = 2.3 \cdot (1.592) \cdot (300) = \mathbf{1098.48} \boldsymbol{gr}$$

The weight of the blended wing-body;

$$W_{blended\_wing} = W_{wing\_skin} + W_{frame} = 3661.6 + 2277.863 = \mathbf{5939.463} \boldsymbol{gr}$$

The weight of the wing-body;

$$W_{wing\_body} = W_{blended\_wing} + W_{inlet} + W_{paint} = 5939.463 + 378.4 + 1098.48$$
$$= \mathbf{7416,343} \boldsymbol{gr}$$

The weight of the tail is as follows;

$$W_{tail} = 2 \cdot S_{tail} \cdot W_{s\_tail}$$

The area of the tail is calculated as follows;

The vertical tail height;

$$h_{tail} = \frac{c_{r,tail} - c_{t,tail}}{tan\,(\Lambda_{LE,tail}) - \dfrac{1}{tan\,(\Lambda_{TE,tail})}} = \frac{0.45 - 0.096}{tan\,(66°) - \dfrac{1}{tan\,(50°)}} = \boldsymbol{0.252m}$$

Then the tail area by considering two tails ;

$$S_{tail} = 2 \cdot h_{tail} \cdot \left(\frac{c_{r,tail} + c_{t,tail}}{2}\right) = 2 \cdot 0.252 \cdot \left(\frac{0.45 + 0.096}{2}\right) = \boldsymbol{0.1378m^2}$$

Then the tail weight;

$$W_{tail} = 2 \cdot S_{tail} \cdot W_{s\_tail} = 2 \cdot (0.1378) \cdot (1000) = \boldsymbol{275.59gr}$$

Then the aircraft structural weight is found as;

$$W_{aircraft} = W_{wing\_body} + W_{tail} = 7416.343 + 275.59 = \boldsymbol{7691.933gr}$$

The internal system weight includes the weight of, landing gear and parachute and fuel tank calculation is conducted iteratively since the total weight which is an output of the weight analysis is an input for the mission profile.

The system weight;

$$W_{sys\_internal} = W_{main\_l\_gear} + W_{nose\_l\_gear} + W_{engines} + W_{engine\_comp} + W_{avionics} + W_{batteries} + W_{parachute}$$

Table A1. 5 shows the internal system weight build-up.

Table A1. 5 The internal System Weight Build-up

Unit	Weight (gr)
Engine	**2850**
Engine Controller	200
Fuel Pump	80
Gas Solenoid Valve	50
Gas Tank	100
Fuel Shutoff Valve	50
Fuel Tank	558.204
Engine Mount	80
Fuel Pipes	100
TOTAL Engine Component	**1218.204**
Main Landing Gear	**1941.051**
Nose Landing Gear	**647.017**
Servos	60
Autopilot	100
Data Modem	70
Video Modem	70
GPS Antenna	28
AGL Sensor	50

Servo Cables	20
LED	10
Autopilot Cables	30
TOTAL Avionics	**438**
Engine Battery	300
System Battery	300
TOTAL Battery	**600**
Payload	**2000**

The landing gear and parachute weights;

$$W_{main\_l\_gear} = \left({W_{m.gear}} \Big/ {W_{TOTAL}} \right) \cdot W_{TOTAL}$$

$$W_{nose\_l\_gear} = \left({W_{nose\ gear}} \Big/ {W_{TOTAL}} \right) \cdot W_{TOTAL}$$

$$W_{parachute} = 0.05 \cdot W_{TOTAL}$$

By combining the aircraft, internal system and payload weights;

$$\begin{aligned} W_{TOTAL} &= W_{empty} + W_{payload} + W_{fuel} \\ &= 7691.933 \\ &+ [(0.075) \cdot 25880.679 + (0.025) \cdot 25880.679 + 2850 + 1218.204 \\ &+ 438 + 600 + (0.05 \cdot 25880.679)] + 2000 + 7117.43 = \mathbf{25880.67} \end{aligned}$$

The fuel weight, landing gear weights and parachute weights are calculated according to the mission profile. The calculations of the values are presented in the next sections.

A2.AERODYNAMIC ANALYSIS

In this appendix the initial design aerodynamic analyses are demonstrated step by step. All of the formulation is given in Chapter 2.

A2.1 Initial Design Geometric Calculations

The geometric properties of the wing-body and LEX are presented here.

The main wing area;

$$S_{main\_wing} = \frac{(c_r + c_t) \cdot b}{2} = \frac{(1.55 + 0.2) \cdot 1.6}{2} = 1.4 \text{m}^2$$

The aspect ratio of the main wing;

$$AR_{main\_wing} = \frac{b^2}{S_{main\_wing}} = \frac{(1.6)^2}{1.4} = 1.828$$

Taper ratio;

$$\lambda = \frac{c_t}{c_r} = \frac{0.2}{1.55} = 0.129$$

Sweep angle at quarter chord;

$$\Lambda_{c/4} = \text{atan}\left(\frac{b}{2} \cdot \tan(\Lambda_{LE}) + \frac{c_t - c_r}{2b}\right) = \text{atan}\left(\frac{1.6}{2} \cdot \tan(60°) + \frac{0.2 - 1.55}{2(1.6)}\right) = 52.65°$$

Sweep angle at semi chord;

$$\Lambda_{c/2} = \text{atan}\left(\frac{b}{2} \cdot \tan(\Lambda_{LE}) + \frac{c_t - c_r}{b}\right) = \text{atan}\left(\frac{(1.6)}{2} \cdot \tan(60°) + \frac{0.2 - 1.55}{1.6}\right) = 41.62°$$

Mean aerodynamic chord;

$$\bar{c} = \frac{2}{3} c_r \frac{1 + \lambda + \lambda^2}{1 + \lambda} = \frac{2}{3}(1.55)\frac{1 + 0.129 + (0.129)^2}{1 + 0.129} = 1.0458 \text{m}$$

The position of the mean aerodynamic chord in spanwise direction;

$$\bar{y} = \frac{b}{6}\frac{1 + 2\lambda}{1 + \lambda} = \frac{1.6}{6}\frac{1 + 2(0.129)}{1 + 0.129} = 0.297 \text{m}$$

Similarly for the virtual front wing, LEX;

The LEX area;

$$S_{LEX} = \frac{(c_{r,LEX} + c_{t,LEX}) \cdot b_{LEX}}{2} = \frac{(0.96 + 0) \cdot 0.4}{2} = 0.192 \text{m}^2$$

The aspect ratio of the LEX;

$$AR_{LEX} = \frac{b_{LEX}^2}{S_{LEX}} = \frac{(0.4)^2}{0.192} = 0.8333$$

Taper ratio;

$$\lambda_{LEX} = \frac{c_{t,LEX}}{c_{r,LEX}} = \frac{0}{0.96} = 0$$

Sweep angle at quarter chord;

$$\Lambda_{c/4,LEX} = \text{atan}\left(\frac{b_{LEX}}{2} \cdot \tan(\Lambda_{LE,LEX}) + \frac{c_{t,LEX} - c_{r,LEX}}{2b_{LEX}}\right)$$

$$= \text{atan}\left(\frac{0.4}{2} \cdot \tan(78.23°) + \frac{0 - 0.96}{2(0.4)}\right) = 74.48°$$

Sweep angle at semi chord;

$$\Lambda_{c/2,LEX} = \text{atan}\left(\frac{b_{LEX}}{2} \cdot \tan(\Lambda_{LE,LEX}) + \frac{c_{t,LEX} - c_{r,LEX}}{b_{LEX}}\right)$$

$$= \text{atan}\left(\frac{0.4}{2} \cdot \tan(78.23°) + \frac{0 - 0.96}{0.4}\right) = 67.38°$$

Mean aerodynamic chord;

$$\bar{c}_{LEX} = \frac{2}{3} c_{r,LEX} \frac{1 + \lambda_{LEX} + \lambda_{LEX}^2}{1 + \lambda_{LEX}} = \frac{2}{3}(0.96)\frac{1 + 0 + 0^2}{1 + 0} = 0.64m$$

The position of the mean aerodynamic chord in spanwise direction;

$$\bar{y}_{LEX} = \frac{b_{LEX}}{6} \frac{1 + 2\lambda_{LEX}}{1 + \lambda_{LEX}} = \frac{0.4}{6} \frac{1 + 2(0)}{1 + 0} = 0.06667m$$

The total wing-body area;

$$S_{TOTAL} = S = S_{main\_wing} + S_{LEX} = 1.4 + 0.92 = 1.592m^2$$

The tail geometric properties are calculated as follows;

The vertical tail height;

$$h_{tail} = \frac{c_{r,tail} - c_{t,tail}}{\tan(\Lambda_{LE,tail}) - \frac{1}{\tan(\Lambda_{TE,tail})}} = \frac{0.45 - 0.096}{\tan(66°) - \frac{1}{\tan(50°)}} = 0.252m$$

The tail area;

$$S_{tail} = h_{tail} \cdot \left(\frac{c_{r,tail} + c_{t,tail}}{2}\right) = 0.252 \cdot \left(\frac{0.45 + 0.096}{2}\right) = 0.13779m^2$$

Aspect ratio of the tail;

$$AR_{tail} = \frac{(2h_{tail})^2}{S_{tail}} = \frac{(2 \cdot 0.252)^2}{0.13779} = 1.8489$$

Taper ratio of the tail;

$$\lambda_{tail} = \frac{c_{t,tail}}{c_{r,tail}} = \frac{0.096}{0.45} = 0.213$$

Sweep angle at quarter chord;

$$\Lambda_{c/4,tail} = atan\left(\frac{3}{4} \cdot \frac{c_{r,tail} - c_{t,tail}}{h_{tail}}\right) = atan\left(\frac{3}{4} \cdot \frac{0.45 - 0.096}{0.252}\right) = 64.62^{\circ}$$

Sweep angle at semi chord;

$$\Lambda_{c/2,tail} = atan\left(\frac{1}{2} \cdot \frac{c_{r,tail} - c_{t,tail}}{h_{tail}}\right) = atan\left(\frac{1}{2} \cdot \frac{0.45 - 0.096}{0.252}\right) = 54.56^{\circ}$$

Mean aerodynamic chord of the tail;

$$\bar{c}_{tail} = \frac{2}{3}c_{r,tail}\frac{1 + \lambda_{tail} + \lambda_{tail}^2}{1 + \lambda_{tail}} = \frac{2}{3}(0.45)\frac{1 + 0.213 + 0.213^2}{1 + 0.213} = 0.311m$$

The position of the mean aerodynamic chord in spanwise direction;

$$\bar{y}_{tail} = \frac{0.252}{3}\frac{1 + 2(0.213)}{1 + 0.213} = 0.0989m$$

A2.2 Air Properties

Air properties are formulated according to the air properties inputs.

The densities;

$$\rho_{takeoff} = ((1 - 6.875 \cdot 10^{-6} \cdot 3.2808 \cdot h_{takeoff})^{4.2561}) \cdot \rho_0$$
$$= ((1 - 6.875 \cdot 10^{-6} \cdot 3.2808 \cdot 1000)^{4.2561}) \cdot 1.225 = 1.111647\,kg/m^3$$

$$\rho_{cruise} = ((1 - 6.875 \cdot 10^{-6} \cdot 3.2808 \cdot h_{cruise})^{4.2561}) \cdot \rho_0$$
$$= ((1 - 6.875 \cdot 10^{-6} \cdot 3.2808 \cdot 1700)^{4.2561}) \cdot 1.225 = 1.037207\,kg/m^3$$

$$\rho_{descent} = ((1 - 6.875 \cdot 10^{-6} \cdot 3.2808 \cdot h_{descent})^{4.2561}) \cdot \rho_0$$
$$= ((1 - 6.875 \cdot 10^{-6} \cdot 3.2808 \cdot 1100)^{4.2561}) \cdot 1.225 = 1.10077\,kg/m^3$$

$$\rho_{cruise2} = ((1 - 6.875 \cdot 10^{-6} \cdot 3.2808 \cdot h_{cruise2})^{4.2561}) \cdot \rho_0$$
$$= ((1 - 6.875 \cdot 10^{-6} \cdot 3.2808 \cdot 2300)^{4.2561}) \cdot 1.225 = 0.976491\,kg/m^3$$

$$\rho_{cruise3} = ((1 - 6.875 \cdot 10^{-6} \cdot 3.2808 \cdot h_{cruise3})^{4.2561}) \cdot \rho_0$$
$$= ((1 - 6.875 \cdot 10^{-6} \cdot 3.2808 \cdot 3800)^{4.2561}) \cdot 1.225 = 0.836573\,kg/m^3$$

The temperatures;

$$T_{cruise} = (1 - 6.875 \cdot 10^{-6} \cdot 3.2808 \cdot h_{cruise}) \cdot T_0$$
$$= (1 - 6.875 \cdot 10^{-6} \cdot 3.2808 \cdot 1700) \cdot (288.16) = 277.11K$$

$$T_{cruise2} = (1 - 6.875 \cdot 10^{-6} \cdot 3.2808 \cdot h_{cruise2}) \cdot T_0$$
$$= (1 - 6.875 \cdot 10^{-6} \cdot 3.2808 \cdot 2300) \cdot (288.16) = 273.211K$$

$$T_{cruise3} = (1 - 6.875 \cdot 10^{-6} \cdot 3.2808 \cdot h_{cruise3}) \cdot T_0$$
$$= (1 - 6.875 \cdot 10^{-6} \cdot 3.2808 \cdot 3800) \cdot (288.16) = 263.462K$$

The viscosities;

$$\mu_{cruise} = 1.458 \cdot 10^{-6} \cdot (T_{cruise})^{\frac{3}{2}} \cdot \left(\frac{1}{T_{cruise} + 110.4}\right)$$
$$= 1.458 \cdot 10^{-6} \cdot (277.11)^{\frac{3}{2}} \cdot \left(\frac{1}{277.11 + 110.4}\right) = 1.736E^{-5} \ (Pa \cdot s)$$

$$\mu_{cruise2} = 1.458 \cdot 10^{-6} \cdot (T_{cruise2})^{\frac{3}{2}} \cdot \left(\frac{1}{T_{cruise2} + 110.4}\right)$$
$$= 1.458 \cdot 10^{-6} \cdot (273.211)^{\frac{3}{2}} \cdot \left(\frac{1}{273.211 + 110.4}\right) = 1.716E^{-5} \ (Pa \cdot s)$$

$$\mu_{cruise3} = 1.458 \cdot 10^{-6} \cdot (T_{cruise3})^{\frac{3}{2}} \cdot \left(\frac{1}{T_{cruise3} + 110.4}\right)$$
$$= 1.458 \cdot 10^{-6} \cdot 263.462^{\frac{3}{2}} \cdot \left(\frac{1}{263.462 + 110.4}\right) = 1.668E^{-5} \ (Pa \cdot s)$$

The Reynolds Numbers (mean chord is taken for the main wing);

$$Re_{cruise} = \rho_{cruise} \cdot V_{cruise} \cdot \frac{\overline{c}}{\mu_{cruise}} = 1.037207 \cdot 87 \cdot \frac{1.0458}{1.736E^{-6}} = 5451666$$

$$Re_{cruise2} = \rho_{cruise2} \cdot V_{cruise2} \cdot \frac{\overline{c}}{\mu_{cruise2}} = 0.976491 \cdot 87 \cdot \frac{1.0458}{1.716E^{-6}} = 5190057$$

$$Re_{cruise3} = \rho_{cruise3} \cdot V_{cruise3} \cdot \frac{\overline{c}}{\mu_{cruise3}} = 0.836573 \cdot 87 \cdot \frac{1.0458}{1.668E^{-6}} = 4576130$$

The Mach Numbers;

$$M_{cruise} = \frac{V_{cruise}}{\sqrt{\gamma \cdot R \cdot T_{cruise}}} = \frac{87}{\sqrt{1.4 \cdot 287 \cdot 277.11}} = 0.260728$$

$$M_{cruise2} = \frac{V_{cruise}}{\sqrt{\gamma \cdot R \cdot T_{cruise}}} = \frac{87}{\sqrt{1.4 \cdot 287 \cdot 273.21}} = 0.262582$$

$$M_{cruise3} = \frac{V_{cruise3}}{\sqrt{\gamma \cdot R \cdot T_{cruise3}}} = \frac{87}{\sqrt{1.4 \cdot 287 \cdot 263.46}} = 0.267396$$

A2.3 Lift Curve Slopes

The lift curve slopes are calculated for the so called front wing, main wing and the tail. The total lift curve slope is calculated by assuming tail is in downwash while front wing is in upwash. The formula is shown as;

$$C_{L_\alpha} = C_{L_{\alpha_{WB}}} + C_{L_{\alpha_H}} \cdot \eta_H \cdot \frac{S_H}{S}\left(1 - \left(\frac{d\epsilon}{d\alpha}\right)_{downwash}\right) + C_{L_{\alpha_{LEX}}} \cdot \eta_{LEX} \cdot \frac{S_{LEX}}{S}(1 - \left(\frac{d\epsilon}{d\alpha}\right)_{upwash})$$

The wing-body or blended wing body lift curve slope is calculated as;

$$C_{L_{\alpha_{WB}}} = C_{L_{\alpha_W}} \cdot \left(1 - 0.25\left(\frac{d_{fuselage}}{b}\right)^2 + 0.025\left(\frac{d_{fuselage}}{b}\right)\right)$$

$$= C_{L_{\alpha_W}} \cdot \left(1 - 0.25\left(\frac{0.078986}{1.6}\right)^2 + 0.025\left(\frac{0.078986}{1.6}\right)\right)$$

$$= 2.132076 \ (rad^{-1})$$

The virtual fuselage diameter is calculated from the inputs;

$$d_{fuselage} = \sqrt{4\pi \cdot w_{fuselage} \cdot h_{fuselage}} = \sqrt{4\pi \cdot (0.07) \cdot (0.07)} = 0.078986m$$

The lift curve slope of the wing;

$$C_{L_{\alpha_W}}\Big|_M = \frac{2\pi AR_{main\_wing}}{2 + \sqrt{\frac{(AR_{main\_wing})^2 \beta^2}{\kappa^2} \cdot \left(1 + \frac{\tan^2 \Lambda_{c/2}}{\beta^2}\right) + 4}}$$

$$= \frac{2\pi(1.828)}{2 + \sqrt{\frac{(1.828)^2 0.965413^2}{0.875806^2} \cdot \left(1 + \frac{\tan^2 41.62}{0.965413^2}\right) + 4}} = 2.130972 \ (rad^{-1})$$

Where;

$$\beta = \sqrt{1 - M_{cruise}^2} = \sqrt{1 - 0.260728^2} = 0.965413$$

$$\kappa = \frac{\beta \cdot C_{l_{\alpha,wing}}}{2\pi} = \frac{(0.965413) \cdot 5.7}{2\pi} = 0.875806$$

Mach number;

$$M_{cruise} = \frac{87}{\sqrt{1.4 \cdot 287 \cdot 277.11}} = 0.260728$$

Tail lift curve slope is calculated by introducing the virtual horizontal and vertical tails due to the fact that the inclined tail is similar to the V-tail configuration.

The aspect ratio of the virtual horizontal wing;

$$AR_{tail\_HT} = \frac{(2 \cdot h_{tail} \cdot \cos(90 - \alpha_{i.tail}))^2}{S_{tail\_HT}} = \frac{(2 \cdot 0.252 \cdot \cos(90 - 27))^2}{0.0626} = 0.84031$$

The area of the virtual horizontal tail;

$$S_{tail\_HT} = S_{tail} \cdot \cos(90 - \alpha_{i.tail}) = 0.13779 \cdot \cos(90 - 27) = 0.0626 m^2$$

The sweep angle at the semi chord;

$$\Lambda_{c/2,tail\_HT} = atan\left(\frac{1}{2} \frac{c_{r,tail} - c_{t,tail}}{\frac{b_{HT}}{2}}\right) = atan\left(\frac{1}{2} \frac{0.45 - 0.096}{\frac{0.229}{2}}\right) = 57.059°$$

The span of the virtual horizontal tail;

$$b_{HT} = \sqrt{AR_{tail\_HT} \cdot S_{tail\_HT}} = \sqrt{0.84031 \cdot 0.0626} = 0.229 m$$

Similarly, the aspect ratio of the virtual vertical wing;

$$AR_{tail\_VT} = \frac{(2 \cdot h_{tail} \cdot \sin(90 - \alpha_{i.tail}))^2}{S_{tail\_VT}} = \frac{(2 \cdot 0.252 \cdot \sin(90 - 27))^2}{0.1227} = 0.6469$$

The area of the virtual vertical tail;

$$S_{tail\_VT} = S_{tail} \cdot \sin(90 - \alpha_{i.tail}) = 0.13779 \cdot \sin(90 - 27) = 0.1227 m^2$$

The sweep angle at the semi chord;

$$\Lambda_{c/2,tail\_VT} = atan\left(\frac{1}{2} \frac{c_{r,tail} - c_{t,tail}}{\frac{h_{tail\_VT}}{2}}\right) = atan\left(\frac{1}{2} \frac{0.45 - 0.096}{\frac{0.2248}{2}}\right) = 38.217°$$

The span of the virtual vertical tail;

$$h_{tail\_VT} = \frac{\sqrt{AR_{tail\_VT} \cdot S_{tail\_VT}}}{2} = \frac{\sqrt{0.6469 \cdot 0.1227}}{2} = 0.2248 m$$

The lift curve slope is then;

$$C_{L_{\alpha_H}}\bigg|_M = \frac{2\pi AR_{tail\_HT}}{2 + \sqrt{\frac{\left(AR_{tail\_HT}\right)^2 \beta^2}{\kappa_{tail}^2} \cdot \left(1 + \frac{\tan^2 \Lambda_{c/2,tail\_HT}}{\beta^2}\right) + 4}}$$

$$= \frac{2\pi(0.84031)}{2 + \sqrt{\frac{(0.84031)^2 (0.965413)^2}{0.875806^2} \cdot \left(1 + \frac{\tan^2 (57.059)}{0.965413^2}\right) + 4}}$$

$$= 1.134376 \, (rad^{-1})$$

$$\kappa_{tail} = \frac{\beta \cdot C_{l_{\alpha,tail}}}{2\pi} = \frac{0.965413 \cdot 5.7}{2\pi} = 0.875806$$

The downwash factor is found from,

$$\left(\frac{d\epsilon}{d\alpha}\bigg|_M\right)_{downwash} = \frac{d\epsilon}{d\alpha}\bigg|_{M=0} \cdot \frac{C_{L_{\alpha_W}|_M}}{C_{L_{\alpha_W}|_{M=0}}} = (0.9711334) \cdot \frac{2.130972}{2.144756} = 0.9650918$$

$$\frac{d\epsilon}{d\alpha}\bigg|_{M=0} = 4.44 \left[K_A \cdot K_\lambda \cdot K_H \sqrt{\cos \Lambda_{c/4}}\right]^{1.19}$$

$$= 4.44 \left[(0.283016) \cdot (1.373272) \cdot (0.92109)\sqrt{\cos(52.65°)}\right]^{1.19}$$

$$= 0.9711334$$

$$K_A = \frac{1}{AR_{main\_wing}} - \frac{1}{1 + \left(AR_{main\_wing}\right)^{1.7}} = \frac{1}{1.828} - \frac{1}{1 + (1.828)^{1.7}} = 0.283016$$

$$K_\lambda = \frac{10 - 3\lambda}{7} = \frac{10 - 3(0.129)}{7} = 1.373272$$

$$K_H = \frac{1 - \frac{h_{tail\_VT}}{b}}{\left(\frac{2l_{tail}}{b}\right)^{\frac{1}{3}}} = \frac{1 - \frac{0.2248}{1.6}}{\left(\frac{2(0.65)}{1.6}\right)^{\frac{1}{3}}} = 0.92109$$

The wing lift curve slope for $M = 0$;

$$C_{L_{\alpha_W}}\bigg|_{M=0} = \frac{2\pi AR_{main\_wing}}{2 + \sqrt{\frac{\left(AR_{main\_wing}\right)^2 \beta^2}{\kappa^2} \cdot \left(1 + \frac{\tan^2 \Lambda_{c/2}}{\beta^2}\right) + 4}}$$

$$= \frac{2\pi(1.828)}{2 + \sqrt{\frac{(1.828)^2 1^2}{0.90718^2} \cdot \left(1 + \frac{\tan^2 41.62}{1^2}\right) + 4}} = 2.144756 (rad^{-1})$$

Where;

$$\beta = \sqrt{1 - M_{cruise}{}^2} = \sqrt{1 - 0^2} = 1$$

$$\kappa = \frac{\beta \cdot C_{l\alpha,wing}}{2\pi} = \frac{5.7}{2\pi} = 0.90718$$

The lift curve slope of the LEX is calculated by assuming the front wing is similar to a canard.

$$C_{L_{\alpha_{LEX}}}\Big|_M = \frac{2\pi AR_{LEX}}{2 + \sqrt{\frac{(AR_{LEX})^2\beta^2}{\kappa_{LEX}{}^2} \cdot \left(1 + \frac{\tan^2\Lambda_{c/2,LEX}}{\beta^2}\right) + 4}} =$$

$$= \frac{2\pi(0.8333)}{2 + \sqrt{\frac{(0.8333)^2 0.965413^2}{0.875806^2} \cdot \left(1 + \frac{\tan^2(67.38°)}{0.965413^2}\right) + 4}}$$

$$= 1.012461 \ (rad^{-1})$$

$$\kappa_{LEX} = \frac{\beta \cdot C_{l\alpha,LEX}}{2\pi} = \frac{(0.965413) \cdot 5.7}{2\pi} = 0.875806$$

The up-wash parameter is taken as $\left(\frac{d\epsilon}{d\alpha}\right)_{upwash} = 0.1$ according to the Figure A2. 1 .
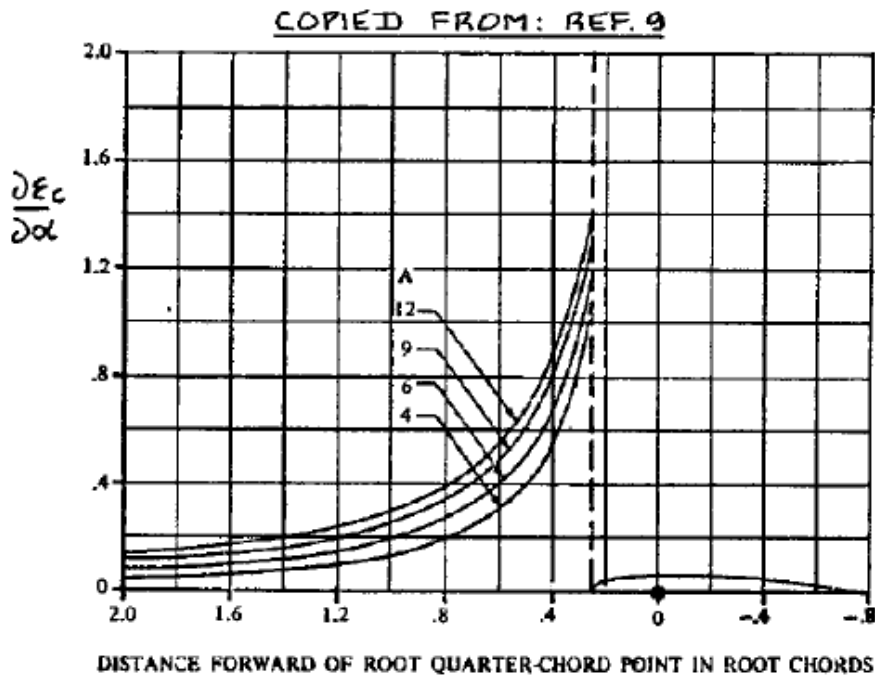

Figure A2. 1 Wing Up-wash Gradient. (Copied From Ref. [5])

A2.4 Maximum lift Coefficient

The maximum lift coefficient is calculated by using the Figure 2.26.

$$C_{L,max} = 0.9 \cdot C_{l,max} = 0.9 \cdot (0.82) = 0.738$$

A2.5 Parasite Drag Coefficient

The aircraft parasite drag coefficient is calculated for the main wing, the virtual fuselage and the tail.

The total parasite drag coefficient;

$$C_{D0_{subsonic}} = \frac{\sum\left(C_{F_c} \cdot FF_c \cdot Q_c \cdot S_{wet_c}\right)}{S_{ref}} + C_{d_{misc}} + C_{d_{L\&P}}$$

For turbulent flow;

$$C_F = \frac{0.455}{(\log_{10}Re)^{2.58}(1 + 0.144M^2)^{0.65}}$$

For wing and tail surfaces;

$$FF = \left[1 + \frac{0.6}{\left(\frac{x}{c}\right)_m}\left(\frac{t}{c}\right) + 100\left(\frac{t}{c}\right)^4\right] \cdot [1.34M^{0.18}(\cos\Lambda_m)^{0.28}]$$

For the fuselage;

$$FF = 1 + \frac{60}{f^3} + \frac{f}{400}$$

$$f = \frac{l}{d}$$

The parasite drag coefficient for the wing;

$$C_{F,wing} = \frac{0.455}{(\log_{10}Re)^{2.58}(1 + 0.144M^2)^{0.65}}$$
$$= \frac{0.455}{(\log_{10}5451666)^{2.58}(1 + 0.144(0.260728)^2)^{0.65}} = 0.0032953$$

$$FF_{wing} = \left[1 + \frac{0.6}{\left(\frac{x}{c}\right)_m}\left(\frac{t}{c}\right) + 100\left(\frac{t}{c}\right)^4\right] \cdot [1.34M^{0.18}(\cos\Lambda_m)^{0.28}]$$
$$= \left[1 + \frac{0.6}{0.459}(0.06) + 100(0.06)^4\right]$$
$$\cdot \left[1.34(0.260728)^{0.18}(\cos(42.08°))^{0.28}\right] = 1.0449131$$

$$S_{wet_{wing}} = 2.1 \cdot S_{TOTAL} = 2.1 \cdot 1.592 = 3.3432 \, \text{m}^2$$

$$C_{D0_{wing}} = \frac{C_{F_{wing}} \cdot FF_{wing} \cdot Q_{wing} \cdot S_{wet_{wing}}}{S_{ref}} = \frac{(0.0032953) \cdot (1.0449131) \cdot 1 \cdot 3.3432}{1.592}$$
$$= 0.007230953$$

The interference factor for the wing, Q_{wing} is taken as 1.

The parasite drag coefficient for the tail;

$$C_{F,tail} = \frac{0.455}{(\log_{10} Re)^{2.58}(1 + 0.144 M^2)^{0.65}}$$
$$= \frac{0.455}{(\log_{10} 1618245)^{2.58}(1 + 0.144(0.260728)^2)^{0.65}} = 0.0040668$$

$$FF_{tail} = \left[1 + \frac{0.6}{\left(\frac{x}{c}\right)_m}\left(\frac{t}{c}\right) + 100\left(\frac{t}{c}\right)^4\right] \cdot [1.34 M^{0.18}(\cos\Lambda_m)^{0.28}]$$
$$= \left[1 + \frac{0.6}{0.459}(0.06) + 100(0.06)^4\right]$$
$$\cdot [1.34(0.260728)^{0.18}(\cos(57.9°))^{0.28}] = 0.9515912$$

$$S_{wet_{tail}} = 2.1 \cdot S_{tail} = 2.1 \cdot 0.13779 = 0.2893767 \, \text{m}^2$$

$$C_{D0_{tail}} = \frac{C_{F_{tail}} \cdot FF_{tail} \cdot Q_{tail} \cdot S_{wet_{tail}}}{S_{ref}} = \frac{(0.0040668) \cdot (0.9515912) \cdot 1 \cdot 0.2893767}{1.592}$$
$$= 0.000703442$$

The Reynolds Number for the tail;

$$Re_{tail} = \rho_{cruise} \cdot V_{cruise} \cdot \frac{\bar{c}}{\mu_{cruise}} = 1.037207 \cdot 87 \cdot \frac{0.311}{1.736E^{-6}} = 1618245$$

The parasite drag coefficient for the virtual fuselage;

$$C_{F,fuselage} = \frac{0.455}{(\log_{10} Re)^{2.58}(1 + 0.144 M^2)^{0.65}}$$
$$= \frac{0.455}{(\log_{10} 13049834)^{2.58}(1 + 0.144(0.260728)^2)^{0.65}} = 0.0028612$$

$$FF_{fuselage} = 1 + \frac{60}{f^3} + \frac{f}{400} = 1 + \frac{60}{16.67^3} + \frac{16.67}{400} = 1.0546267$$

$$f = \frac{l}{d} = \frac{2.51}{0.1506} = 16.67$$

The virtual fuselage diameter is calculated as;

$$d = \left(\frac{t}{c}\right) \cdot \left(c_r + c_{r,LEX}\right) = 0.06 \cdot 2.51 = 0.1506m$$

$$S_{wet_{fuselage}} = 2.1 \cdot d \cdot l = 2.1 \cdot 0.1506 \cdot 2.51 = 0.7938126m^2$$

$$C_{D0_{fuselage}} = \frac{C_{F_{fuselage}} \cdot FF_{fuselage} \cdot Q_{fuselage} \cdot S_{wet_{fuselage}}}{S_{ref}}$$
$$= \frac{(0.0028612) \cdot (1.0546267) \cdot 1 \cdot 0.7938126}{1.592} = 0.001504626$$

The Reynolds Number for the fuselage;

$$Re_{fuselage} = \rho_{cruise} \cdot V_{cruise} \cdot \frac{\bar{c}}{\mu_{cruise}} = 1.037207 \cdot 87 \cdot \frac{2.51}{1.736E^{-6}} = 13049834$$

The mean aerodynamic chord is taken as; $\bar{c} = c_r + c_{r,LEX}$ due to the fact that the virtual fuselage length is actually the sum of the main wing root chord and the LEX root chord.

The total parasite drag coefficient;

$$C_{D0,TOTAL} = C_{D0,wing} + C_{D0,tail} + C_{D0,fuselage} = C_{D0,wing} + C_{D0,tail} + C_{D0,fuselage}$$
$$= 0.007230953 + 0.000703442 + 0.001504626 = 0.009439022$$

The lift to drag ratio at cruise conditions are found as;

$$\left(\frac{C_L}{C_D}\right)_{cruise} = \frac{C_{L,cruise}}{C_{D0_{TOTAL}} + kC_{L,cruise}^2}$$

The cruise lift and drag coefficients are found from below equations;

$$C_{L,cruise} = \frac{2 \cdot W_{TOTAL}/S}{\rho_{cruise} \cdot V_{cruise}^2} = \frac{2 \cdot 9.81 \cdot 26.112/1.592}{1.037207 \cdot 87^2} = 0.04099$$

$$k = \frac{1}{\pi \cdot e \cdot AR_{main\_wing}} = \frac{1}{\pi \cdot 0.772929 \cdot 1.828} = 0.2253297$$

The span efficiency factor for $\Lambda_{LE} > 30 \ deg.$;

$$e = 4.61 \cdot \left(1 - 0.045\left(AR_{main\_wing}\right)^{0.68}\right) \cdot (\cos{(\Lambda_{LE})})^{0.15} - 3.1$$
$$= 4.61 \cdot (1 - 0.045(1.828)^{0.68}) \cdot \left(\cos{(60°)}\right)^{0.15} - 3.1 = 0.772929$$

109

The drag coefficient;

$$C_{D,cruise} = C_{D0,TOTAL} + k \cdot \left(C_{L,cruise}\right)^2 = 0.009439022 + 0.2253297 \cdot (0.04099)^2$$
$$= 0.0098176$$

A3. PERFORMANCE CALCULATIONS

In this section performance calculations are shown step by step.

A3.1 Stall Velocity

The wing loading of the aircraft;

$$\frac{W}{S} = \frac{9.81 \cdot 26.112}{1.592} = 160.908 \, \text{N/m}^2$$

Stall velocity is calculated at the cruise altitude as follows;

A3.2 Turn Performance

Corner velocity is found as $V^* = 42.24\text{m/s}$ in previous section.

Maximum turn rate is calculated as;

$$\omega_{max} = \frac{g\sqrt{n_{\omega_{max}}{}^2 - 1}}{V^*} = \frac{9.81\sqrt{4.245^2 - 1}}{42.24} = 54.88 \text{ deg/s}$$

Minimum turn radius;

$$R_{min} = \frac{(V^*)^2}{g\sqrt{n_{max}{}^2 - 1}} = \frac{(42.24)^2}{9.81\sqrt{4.245^2 - 1}} = 44.102\text{m}$$

Maximum bank angle;

$$\emptyset_{max} = \text{acos}\left(\frac{1}{n_{max}}\right) = \text{acos}\left(\frac{1}{4.245}\right) = 83.03°$$

A4.MISSION PROFILE CALCUALTIONS

In this section the mission profile calculations are demonstrated in detail.

A4.1 Takeoff Ground Roll: Segment 0-1

Figure A4. 1 shows the Ground roll distance, S_g , the initial velocity, $V_{i,01}$ and the final velocity, $V_{f,01}$.
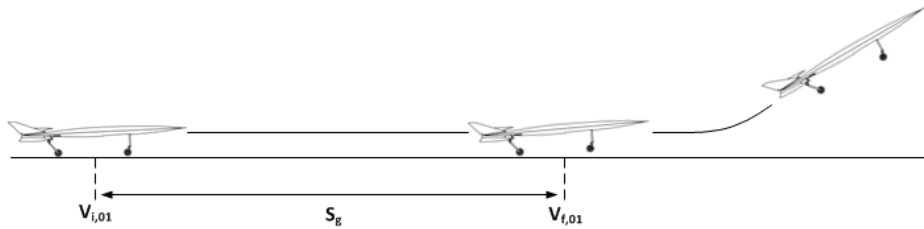

Figure A4. 1 Takeoff Ground Roll

By taking the initial velocity zero and the takeoff rotation time $N = 1$, the takeoff distance is calculated as;

$$S_g = \frac{1}{2gK_A} \ln\left(\frac{K_T + K_A \cdot V_{f,01}^2}{K_T + K_A \cdot V_{i,01}^2}\right) + N \cdot V_{f,01}$$

$$= \frac{1}{2(9.81)(-3.26E^{-5})} \ln\left(\frac{0.784754 + (-3.26E^{-5}) \cdot 25.747^2}{0.784754 + (-3.26E^{-5}) \cdot 0^2}\right) + 1$$

$$\cdot (25.747) = 69.408m$$

Where;

$$K_A = \frac{\rho}{2(W/S)} \cdot \left[\mu_r C_{L0} - C_{D0} - k \cdot C_{L0}^2\right]$$

$$= \frac{1.111647}{2(160.908)} \cdot [0.03 \cdot 0 - 0.009439022 - 0.2253297 \cdot 0^2] = -3.26E^{-5}$$

$$K_T = \left(\frac{T_A}{W}\right)_{takeoff} - \mu_r = 0.814754 - 0.03 = 0.784754$$

$$T_{A,takeoff} = T_{A,0} \cdot \left(\frac{\rho_{takeoff}}{\rho_0}\right) = 230 \cdot \left(\frac{1.111647}{1.225}\right) = 208.71337 \text{ N}$$

$$\left(\frac{T_A}{W}\right)_{takeoff} = \frac{208.71337}{26.112 \cdot 9.81} = 0.814754$$

The final velocity on the takeoff leg is calculated as;

$$V_{f,01} = 1.3 \cdot V_{stall} = 1.3 \cdot 20.505 = 25.749m/s$$

The time, t_{01}, to accelerate to $V_{f,01}$ from $V_{i,01}$;

$$t_{01} = \frac{2S_g}{V_{f,01}} = \frac{2(69.421)}{25.749} = 5.392s$$

Total weight after the takeoff;

$$W_1 = W_0 - \left(c_{t,ground\_roll}\right) \cdot T_{A,takeoff} \cdot t_{01}$$
$$= 256.20098 - (0.00049719) \cdot 208.71337 \cdot 5.392 = 255.64144 \, N$$

The thrust specific fuel consumption during takeoff ground roll is calculated as follows;

$$c_{t,ground\_roll} = \frac{WF_{ground\_roll}}{\left(\frac{T_{ground\_roll}}{g}\right)} = \frac{0.01057801}{\left(\frac{208.71337}{9.81}\right)} = 0.00049719 \, (1/s)$$

From the engine model;

$$RPM = 0.0010673 \cdot (230)^7 - 0.099774 \cdot (230)^6 + 3.7964 \cdot (230)^5 - 75.755 \cdot (230)^4$$
$$+ 855.69 \cdot (230)^3 - 5597.3 \cdot (230)^2 + 23412 \cdot (230) + 18776$$
$$= 107816.5$$

The equivalent thrust for the ground roll;

$$T_0 = T_{A,takeoff} \cdot \left(\frac{\rho_0}{\rho_{takeoff}}\right) = 208.71337 \cdot \left(\frac{1.225}{1.111647}\right) = 230N$$

The fuel flow is calculated as;

$$WF = -3.5E^{-28} \cdot (107816.5)^6 + 1.33E^{-22} \cdot (107816.5)^5 - 1.96E^{-17} \cdot (107816.5)^4$$
$$+ 1.43E^{-12} \cdot (107816.5)^3 - 5.48E^{-8} \cdot (107816.5)^2 + 0.0010834$$
$$\cdot (107816.5) - 7.147 = 10.57801 \left(\frac{gr}{s}\right) = 0.01057801 \left(\frac{kg}{s}\right)$$

A4.2 Transition: Segment 1-2

Figure A4. 2 shows the transition section. S_a represents the distance to clear an obstacle with a height of h_{obs}.
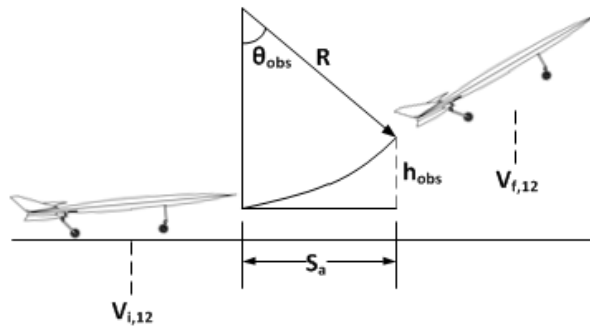

Figure A4. 2 The Transition

112

The transition distance is calculated form;

$$S_a = R \cdot \sin(\theta_{obs}) = 88.1754 \cdot \sin(19.3875) = 29.2703 m$$

The climb radius;

$$R = \frac{\left(\dfrac{V_{i,12} + V_{f,12}}{2}\right)^2}{g \cdot (n-1)} = \frac{\left(\dfrac{25.747 + 27.7281}{2}\right)^2}{9.81 \cdot (1.826489 - 1)} = 88.1754 m$$

Where;

$$n = \frac{\dfrac{1}{2} \rho \cdot S \cdot C_{L_{max}} \cdot \left(\dfrac{V_{i,12} + V_{f,12}}{2}\right)^2}{W} = \frac{\dfrac{1}{2} 1.111647 \cdot 1.592 \cdot 0.738 \cdot \left(\dfrac{25.747 + 27.7281}{2}\right)^2}{205.60736}$$
$$= 1.826489$$

$V_{i,12}$ is the initial speed at the start of the section and $V_{f,12}$ is the final speed at the end of the section.

$$V_{i,12} = V_{f,01} = 25.747 m/s$$

$$V_{f,12} = 1.4 \cdot V_{stall} = 1.4 \cdot 20.505 = 27.73001 m/s$$

The climb angle is calculated by taking the obstacle height as 5m as defined in t he input parameters;

$$\theta_{obs} = Acos\left(1 - \frac{h_{obs}}{R}\right) = Acos\left(1 - \frac{5}{88.1754}\right) = 19.3875°$$

The time, t_{01}, to accelerate to $V_{f,12}$ from $V_{i,12}$;

$$t_{12} = \frac{2S_a}{V_{f,12} + V_{i,12}} = \frac{2(29.2703)}{27.7281 + 25.747} = 1.0947 s$$

Total weight after the transition;

$$W_2 = W_1 - \left(c_{t,transition}\right) \cdot T_{A,transition} \cdot t_{12}$$
$$= 255.641 - (0.00049719) \cdot 208.71337 \cdot 1.0947 = 255.527 N$$

The thrust specific fuel consumption during transitionl is calculated as follows;

$$c_{t,transition} = \frac{WF_{transition}}{\left(\dfrac{T_{transiton}}{g}\right)} = \frac{0.01057801}{\left(\dfrac{208.71337}{9.81}\right)} = 0.00049719 \ (1/s)$$

From the engine model;

113

$$RPM = 0.0010673 \cdot (230)^7 - 0.099774 \cdot (230)^6 + 3.7964 \cdot (230)^5 - 75.755 \cdot (230)^4$$
$$+ 855.69 \cdot (230)^3 - 5597.3 \cdot (230)^2 + 23412 \cdot (230) + 18776$$
$$= 107816.5$$

The equivalent thrust for the ground roll;

$$T_0 = T_{A,transition} \cdot \left(\frac{\rho_0}{\rho_{transition}}\right) = 208.71337 \cdot \left(\frac{1.225}{1.111647}\right) = 230N$$

The fuel flow is calculated as;

$$WF = -3.5E^{-28} \cdot (107816.5)^6 + 1.33E^{-22} \cdot (107816.5)^5 - 1.96E^{-17} \cdot (107816.5)^4$$
$$+ 1.43E^{-12} \cdot (107816.5)^3 - 5.48E^{-8} \cdot (107816.5)^2 + 0.0010834$$
$$\cdot (107816.5) - 7.147 = 10.57801 \left(\frac{gr}{s}\right) = 0.01057801 \left(\frac{kg}{s}\right)$$

The transition segment is assumed to be performed at full throttle so the available thrust is the same as the one at the takeoff segment.

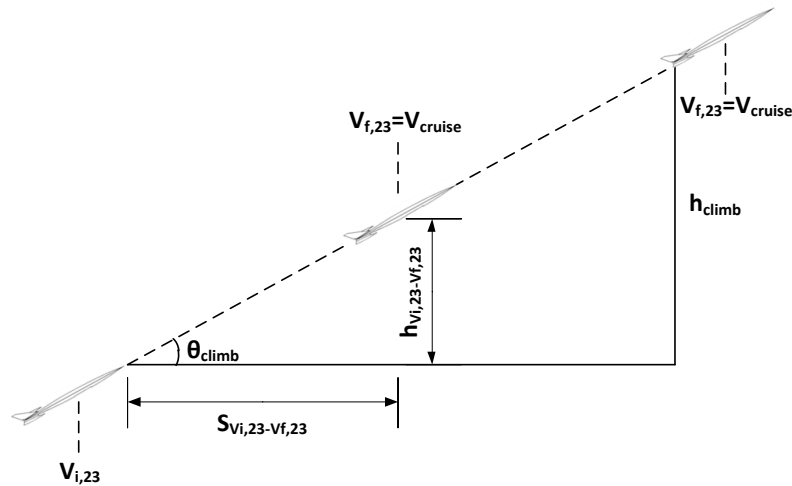**A4.3 Climb: Segment 2-3**

Figure A4. 3 shows the climb segment details.

Figure A4. 3 Climb Segment

The initial speed at the start of the climb segment;

$$V_{i,23} = V_{f,12} = V_{f,12} = 27.73001 m/s$$

The final speed at the end of the climb segment is taken as the cruise speed which is an input;

$$V_{f,23} = V_{cruise} = 87 \text{ m/s}$$

114

$$\theta_{climb} = asin\left(\frac{(R/C)_f}{V_{cruise}}\right) = asin\left(\frac{45.835}{87}\right) = 31.79°$$

The rate of climb at end of the climb segment;

$$(R/C)_f = \frac{V_{cruise} \cdot \left(T_{A,cruise} - \frac{1}{2}\rho_{cruise}V_{cruise}^2 S(C_{D0,TOTAL} + kC_{L,cruise}^2)\right)}{W_3}$$

$$= \frac{87 \cdot \left(194.7372 - \frac{1}{2}(1.037207) \cdot 87^2 \cdot 1.592 \cdot (0.009439022 + 0.225329 \cdot 0.04101^2)\right)}{253.173}$$

$$= 45.835 m/s$$

$$T_{A,cruise} = T_{A,0} \cdot \left(\frac{\rho_{cruise}}{\rho_0}\right) = 230 \cdot \left(\frac{1.037207}{1.225}\right) = 194.7372 \text{ N}$$

The climb time to cruise speed during climb;

$$t_{Vi,23-Vf,23} = \frac{V_{f,23} - V_{i,23}}{g\left(\left(\frac{T_A}{W}\right)_{climb} - sin(\theta_{climb})\right)} = \frac{87 - 27.73001}{9.81(0.7926 - sin(31.79))} = 13.112s$$

$$\left(\frac{T_A}{W}\right)_{climb} = \frac{T_{A,climb}}{W_{climb}} = \frac{201.632}{254.382} = 0.7926$$

$$T_{A,climb} = T_{A,0} \cdot \left(\frac{\frac{\rho_{cruise} + \rho_{takeoff}}{2}}{\rho_0}\right) = 230 \cdot \left(\frac{\frac{1.037207 + 1.111647}{2}}{1.225}\right) = 201.632 \text{ N}$$

$$W_{climb} = \frac{W_3 + W_2}{2} = \frac{253.175 + 255.589}{2} = 254.382 N$$

The height achieved during $t_{Vi,23-Vf,23}$,

$$h_{Vi,23-Vf,23} = \left[V_{i,23} \cdot (t_{Vi,23-Vf,23}) + \frac{1}{2}\left(g \cdot \left(\left(\frac{T_A}{W}\right)_{climb} - sin(\theta_{climb})\right)\right) \cdot (t_{Vi,23-Vf,23})^2\right]$$
$$\cdot sin(\theta_{climb})$$
$$= \left[27.73001 \cdot (13.112) + \frac{1}{2}\left(9.81 \cdot (0.7926 - sin(31.79))\right) \cdot (13.112)^2\right]$$
$$\cdot sin(31.79) = 309.68m$$

The time elapsed during constant speed climb;

$$t_{climb} = \frac{h_{cruise} - \left(h_{Vi,23-Vf,23}\right) - h_{obs}}{\left(\frac{(R/C)_{Vi,23-Vf,23} + (R/C)_f}{2}\right)} = \frac{1700 - 309.68 - 5}{\left(\frac{30.22 + 45.83}{2}\right)} = 10.132s$$

Where;

$(R/C)_{Vi,23-Vf,23}$ is the rate of climb at the acceleration segment during the climb and $(R/C)_{cruise}$ is the rate of climb at cruise altitude.

$$(R/C)_{Vi,23-Vf,23} = \sin(\theta_{climb}) \cdot \left(\frac{V_{i,23} + V_{f,23}}{2}\right) = \sin(31.39) \cdot \left(\frac{27.723 + 87}{2}\right) = 30.22 m/s$$

The total time during the climb segment;

$$t_{climb,TOTAL} = t_{23} = 13.112 + 10.132 = 23.244s$$

Total weight after the climb segment;

$$W_3 = W_2 - \left(c_{t,climb}\right) \cdot \left(\frac{T_{A,takeoff} + T_{A,cruise}}{2}\right) \cdot t_{23}$$
$$= 255.589 - (0.0004972) \cdot (201.725) \cdot 23.244 = 253.175N$$

The thrust specific fuel consumption during climb;

$$c_{t,climb} = \frac{WF_{climb}}{\left(\frac{T_{climb}}{g}\right)} = \frac{0.01057801}{\left(\frac{201.725}{9.81}\right)} = 0.00049719 \ (1/s)$$

$$T_{climb} = \frac{T_{A,takeoff} + T_{A,cruise}}{2} = \frac{208.713 + 194.737}{2} = 201.725N$$

From the engine model;

$$RPM = 0.0010673 \cdot (230)^7 - 0.099774 \cdot (230.1)^6 + 3.7964 \cdot (230)^5 - 75.755 \cdot (230)^4$$
$$+ 855.69 \cdot (230)^3 - 5597.3 \cdot (230)^2 + 23412 \cdot (230) + 18776$$
$$= 107816.5$$

The equivalent thrust for the climb;

$$T_0 = T_{A,climb} \cdot \left(\frac{\rho_0}{\frac{\rho_{cruise} + \rho_{takeoff}}{2}}\right) = 201.725 \cdot \left(\frac{1.225}{1.073934}\right) = 230N$$

The fuel flow is calculated as;

$$WF = -3.5E^{-28} \cdot (107816.5)^6 + 1.33E^{-22} \cdot (107816.5)^5 - 1.96E^{-17} \cdot (107816.5)^4$$
$$+ 1.43E^{-12} \cdot (107816.5)^3 - 5.48E^{-8} \cdot (107816.5)^2 + 0.0010834$$
$$\cdot (107816.5) - 7.147 = 10.586 \left(\frac{gr}{s}\right) = 0.010586 \left(\frac{kg}{s}\right)$$

A4.4 Cruise: Segment 3-4

The total weight after the cruise is;

$$W_4 = \frac{W_3}{e^{\left(\frac{t_{cruise} \cdot c_{t,cruise}}{(C_L/C_D)_{cruise}}\right)}} = \frac{253.175}{e^{\left(\frac{30 \cdot 60 \cdot 0.0006557}{4.176}\right)}} = \mathbf{190.854}\boldsymbol{N}$$

The thrust specific fuel consumption during cruise;

$$c_{t,cruise} = \frac{WF_{cruise}}{\left(\frac{T_{cruise}}{g}\right)} = \frac{0.00410085}{\left(\frac{61.353}{9.81}\right)} = 0.0006557 \ (1/s)$$

The thrust value during the cruise is actually the required thrust values during the cruise.

From the engine model;

$$\begin{aligned}
RPM &= 0.0010673 \cdot (7.386)^7 - 0.099774 \cdot (7.386)^6 + 3.7964 \cdot (7.386)^5 - 75.755 \\
&\quad \cdot (7.386)^4 + 855.69 \cdot (7.386)^3 - 5597.3 \cdot (7.386)^2 + 23412 \cdot (7.386) \\
&\quad + 18776 = 74211.7
\end{aligned}$$

The equivalent thrust for the cruise;

$$T_0 = T_{R,cruise} \cdot \left(\frac{\rho_0}{\rho_{cruise}}\right) = 61.353 \cdot \left(\frac{1.225}{1.037207}\right) = 72.4616N = 7.386kg$$

$$\begin{aligned}
T_{R,cruise} &= \frac{1}{2}\rho_{cruise}V_{cruise}^2 S\left(C_{D0,TOTAL} + kC_{L,cruise}{}^2\right) \\
&= \frac{1}{2}(1.037207) \cdot 87^2 \cdot 1.592 \cdot (0.009439022 + 0.225329 \cdot 0.04101^2) \\
&= 61.353N
\end{aligned}$$

The fuel flow is calculated as;

$$\begin{aligned}
WF &= -3.5E^{-28} \cdot (74211.7)^6 + 1.33E^{-22} \cdot (74211.7)^5 - 1.96E^{-17} \cdot (74211.7)^4 \\
&\quad + 1.43E^{-12} \cdot (74211.7)^3 - 5.48E^{-8} \cdot (74211.7)^2 + 0.0010834 \\
&\quad \cdot (74211.7) - 7.147 = 4.10085 \left(\frac{gr}{s}\right) = 0.00410085 \left(\frac{kg}{s}\right)
\end{aligned}$$

The lift to drag ratio during the cruise;

$$\left(\frac{C_L}{C_D}\right)_{cruise} = \frac{0.041007}{0.0098179} = 4.176$$

The range achieved during the cruise is;

$$R_{range} = \frac{2}{c_{t,cruise}} \cdot \left(\sqrt{\frac{2}{\rho \cdot S}} \right) \cdot \frac{\sqrt{C_L}}{C_D} \cdot \left(\sqrt{W_3} - W_4 \right)$$

$$= \frac{2}{0.0006557} \cdot \left(\sqrt{\frac{2}{1.037207 \cdot 1.592}} \right) \cdot \frac{\sqrt{0.041007}}{0.0098179}$$

$$\cdot \left(\sqrt{253.175} - 190.854 \right) = 145158.04\text{m} = 145.158\text{km}$$

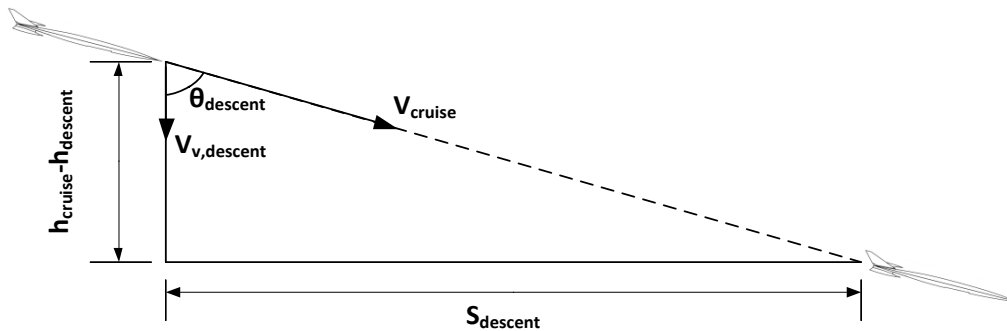## A4.5 Descent: Segment 4-5

Figure A4. 4 shows the descent flight leg.

Figure A4. 4 The Descent Segment

The descent time during the altitude loss of $h_{cruise} - h_{descent}$;

$$t_{45} = \frac{h_{cruise} - h_{descent}}{V_{v,descent}} = \frac{1700 - 1100}{20} = 30\text{s}$$

Where;

$V_{v,descent}$ is the vertical component of the constant descent velocity and selected as 20 m/s as an input.

The descent angle;

$$\theta_{descent} = \text{Asin} \left(\frac{V_{v,descent}}{V_{descent}} \right) = \text{Asin} \left(\frac{20}{87} \right) = 13.608°$$

Where;

$$V_{descent} = V_{cruise}$$

118

The horizontal distance covered during the descent;

$$S_{descent} = \frac{h_{cruise} - h_{descent}}{\tan(\theta_{descent})} = \frac{1700 - 1100}{\tan(13.608)} = 2478.4m$$

The total weight after the descent segment;

$$W_5 = W_4 - (c_{t,descent}) \cdot (T_{R,descent}) \cdot t_{45} = 190.854 - (0.0017274) \cdot (14.384) \cdot 30$$
$$= 190.106N$$

Where;

$c_{t,descent}$ is the thrust specific fuel consumption during descent segment and $T_{R,descent}$ is the necessary thrust to achieve the constant speed descent; it is calculated as follows;

$$T_{R,descent} = \frac{1}{2} \cdot \left(\frac{\rho_{cruise} + \rho_{descent}}{2}\right) \cdot S \cdot (V_{descent})^2 \cdot \left(C_{D0,TOTAL} + k \cdot (C_{L,descent})^2\right) - W_4$$
$$\cdot \sin(\theta_{descent})$$
$$= \frac{1}{2} \cdot \left(\frac{1.037207 + 1.10077}{2}\right) \cdot 1.592 \cdot (87)^2$$
$$\cdot (0.009439 + 0.22532 \cdot (0.03017)^2) - 190.854 \cdot \sin(13.608)$$
$$= 14.384N$$

The lift coefficient during the descent;

$$C_{L,descent} = \frac{2 \cdot W_4 \cdot \cos(\theta_{descent})}{\left(\frac{\rho_{cruise} + \rho_{descent}}{2}\right) \cdot S \cdot (V_{descent})^2} = \frac{2 \cdot 190.854 \cdot \cos(13.608)}{\left(\frac{1.037207 + 1.10077}{2}\right) \cdot 1.592 \cdot (87)^2}$$
$$= 0.03017$$

During descent the lift coefficient changes due to the change of weight and flight angle.

The thrust specific fuel consumption during descent;

$$c_{t,descent} = \frac{WF_{descent}}{\left(\frac{T_{descent}}{g}\right)} = \frac{0.0025329}{\left(\frac{16.488}{9.81}\right)} = 0.0017274 \ (1/s)$$

From the engine model;

$$RPM = 0.0010673 \cdot (1.6808)^7 - 0.099774 \cdot (1.6808)^6 + 3.7964 \cdot (1.6808)^5 - 75.755$$
$$\cdot (1.6808)^4 + 855.69 \cdot (1.6808)^3 - 5597.3 \cdot (1.6808)^2 + 23412$$
$$\cdot (1.6808) + 18776 = 45821.6$$

The equivalent thrust for the cruise;

$$T_0 = T_{R,descent} \cdot \left(\frac{\rho_0}{\rho_{descent}}\right) = 14.384 \cdot \left(\frac{1.225}{1.10077}\right) = 16.488N = 1.6808kg$$

The fuel flow is calculated as;

$$WF = -3.5E^{-28} \cdot (45821.6)^6 + 1.33E^{-22} \cdot (45821.6)^5 - 1.96E^{-17} \cdot (45821.6)^4$$
$$+ 1.43E^{-12} \cdot (45821.6)^3 - 5.48E^{-8} \cdot (45821.6)^2 + 0.0010834$$
$$\cdot (45821.6) - 7.147 = 2.5329 \left(\frac{gr}{s}\right) = 0.0025329 \left(\frac{kg}{s}\right)$$

A4.6 Loiter: Segment 5-6

During the loiter segment, the aircraft is considered to achieve a constant speed loiter. The speed is considered as the same as the cruise speed. The loiter time, t_{56} is the input.

The total weight after the loiter segment;

$$W_6 = \frac{W_5}{e^{\left(\frac{t_{loiter} \cdot c_{t,loiter}}{(C_L/C_D)_{loiter}}\right)}} = \frac{190.106}{e^{\left(\frac{120 \cdot 0.0006257}{3.0024}\right)}} = 186.969 N$$

The loiter time is an input and taken as;

$$t_{loiter} = t_{56} = 2 \cdot 60 = 120 s$$

$c_{t,loiter}$ is the thrust specific fuel consumption during the loiter.

The thrust value during the loiter;

$$T_{R,loiter} = \frac{1}{2} \cdot (\rho_{descent}) \cdot S \cdot (V_{loiter})^2 \cdot \left(C_{D0,TOTAL} + k \cdot (C_{L,loiter})^2\right)$$
$$= \frac{1}{2} \cdot (1.10077) \cdot 1.592 \cdot (87)^2 \cdot (0.009439 + 0.22532 \cdot (0.02866)^2)$$
$$= 63.828 N$$

The lift coefficient during the loiter;

$$C_{L,loiter} = \frac{2 \cdot W_5}{(\rho_{descent}) \cdot S \cdot (V_{loiter})^2} = \frac{2 \cdot 190.106}{(1.10077) \cdot 1.592 \cdot (87)^2} = 0.0289$$

The thrust specific fuel consumption during loiter;

$$c_{t,loiter} = \frac{WF_{loiter}}{\left(\frac{T_{loiter}}{g}\right)} = \frac{0.0040715}{\left(\frac{63.828}{9.81}\right)} = 0.0006257 \ (1/s)$$

From the engine model;

$$\begin{aligned} \text{RPM} = {}& 0.0010673 \cdot (7.2407)^7 - 0.099774 \cdot (7.2407)^6 + 3.7964 \cdot (7.2407)^5 - 75.755 \\ & \cdot (7.2407)^4 + 855.69 \cdot (7.2407)^3 - 5597.3 \cdot (7.2407)^2 + 23412 \\ & \cdot (7.2407) + 18776 = 73740.3 \end{aligned}$$

The equivalent thrust for the cruise;

$$T_0 = T_{R,loiter} \cdot \left(\frac{\rho_0}{\rho_{descent}}\right) = 63.828 \cdot \left(\frac{1.225}{1.10077}\right) = 71.031\text{N} = 7.24072\text{kg}$$

The fuel flow is calculated as;

$$\begin{aligned} \text{WF} = {}& -3.5\text{E}^{-28} \cdot (73740.3)^6 + 1.33\text{E}^{-22} \cdot (73740.3)^5 - 1.96\text{E}^{-17} \cdot (73740.3)^4 \\ & + 1.43\text{E}^{-12} \cdot (73740.3)^3 - 5.48\text{E}^{-8} \cdot (73740.3)^2 + 0.0010834 \\ & \cdot (73740.3) - 7.147 = 4.07154 \left(\frac{\text{gr}}{\text{s}}\right) = 0.0040715 \left(\frac{\text{kg}}{\text{s}}\right) \end{aligned}$$

The lift to drag ratio during the loiter;

$$\left(\frac{C_L}{C_D}\right)_{loiter} = \frac{C_{L,loiter}}{C_{D0,TOTAL} + k \cdot \left(C_{L,loiter}\right)^2} = \frac{0.0289}{0.009439 + 0.22532 \cdot (0.0289)^2} = 3.0024$$

A4.7 Approach: Segment 6-7

Figure A4. 5 shows the approach and flare segment. The aircraft starts to approach with a speed of $V_{approach}$. The vertical component of the velocity is the descent rate for the approach, $V_{v,approach}$.

The flare path is considered as circular. The velocity at the start of the flare segment is V_{flare} and the velocity at the end is V_{TD}.
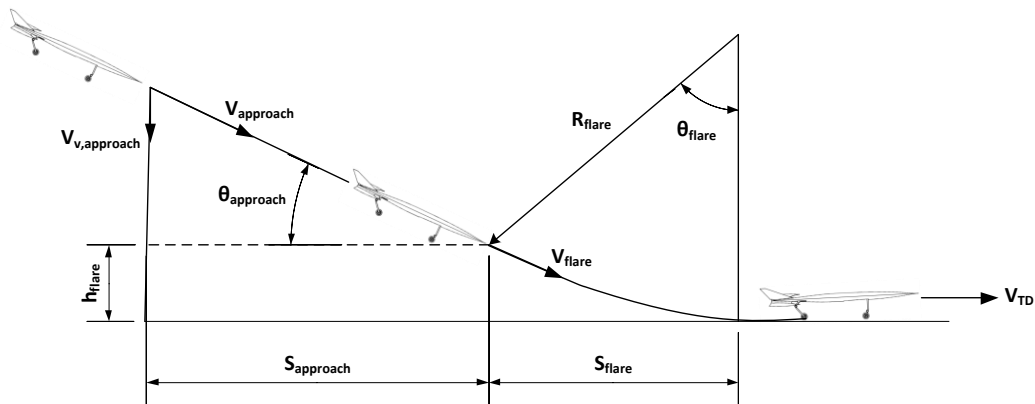

Figure A4. 5 The Approach and Flare Geometry

The approach velocity is found from;

$$V_{approach} = 1.4 \cdot V_{stall,approach} = 1.4 \cdot 16.923 = 23.695 m/s$$

The stall velocity at the approach state;

$$V_{stall,approach} = \sqrt{\frac{2 \cdot W_6}{(\rho_{takeoff}) \cdot S \cdot C_{L,max}}} = \sqrt{\frac{2 \cdot 187.03}{(1.111647) \cdot 1.592 \cdot 0.738}} = 16.923 m/s$$

The flare velocity is found from;

$$V_{flare} = 0.95 \cdot V_{approach} = 0.95 \cdot 23.695 = 22.51 m/s$$

The approach angle is calculated by taking the descent rate as 1 m/s which is an input;

$$\theta_{appraoch} = Asin\left(\frac{V_{v,approach}}{\frac{V_{approach} + V_{flare}}{2}}\right) = Asin\left(\frac{1}{\frac{23.695 + 22.51}{2}}\right) = 2.48°$$

The Flare radius is calculated from;

$$R_{flare} = \frac{V_{flare}^2}{g(C_{L,approach}/\Delta C_L)} = \frac{22.51^2}{9.81\left(\frac{0.3976}{0.02}\right)} = 1028.7 m$$

Where;

ΔC_L is the lift coefficient change during flare and found as;

$$\Delta C_L = C_{L,TD} - C_{L,flare} = 0.4388 - 0.4188 = 0.02$$

Where;

$C_{L,flare}$ is the lift coefficient at the start of the flare segment and $C_{L,TD}$ is the lift coefficient at the end of the flare segment.

$$C_{L,flare} = \frac{2 \cdot W_6 \cdot \cos(\theta_{appraoch})}{\left(\frac{\rho_{landing} + \rho_{descent}}{2}\right) \cdot S \cdot (V_{flare})^2} = \frac{2 \cdot 187.03 \cdot \cos(2.48)}{\left(\frac{1.111647 + 1.10077}{2}\right) \cdot 1.592 \cdot (22.51)^2}$$
$$= 0.4188$$

$$C_{L,TD} = \frac{2 \cdot W_6}{\left(\frac{\rho_{landing} + \rho_{descent}}{2}\right) \cdot S \cdot (V_{TD})^2} = \frac{2 \cdot 187.03}{\left(\frac{1.111647 + 1.10077}{2}\right) \cdot 1.592 \cdot (22.003)^2}$$
$$= 0.4388$$

$$V_{TD} = 1.3 \cdot V_{stall,approach} = 1.3 \cdot 16.925 = 22.003 m/s$$

The vertical distance covered during the flare,

$$h_{flare} = R_{flare} \cdot \left(1 - \cos(\theta_{appraoch})\right) = 1028.7 \cdot \left(1 - \cos(2.48)\right) = 0.964 m$$

The horizontal distance covered during the flare;

$$S_{flare} = \frac{R_{flare}}{\sin(\theta_{appraoch})} = \frac{1028.7}{\sin(2.48)} = 44.53 m$$

The horizontal distance covered during approach;

$$S_{approach} = \frac{h_{descent} - h_{landing} - h_{flare}}{\tan(\theta_{appraoch})} = \frac{1100 - 1000 - 0.964}{\tan(2.48)} = 2285.9 m$$

The time elapsed during the approach;

$$t_{approach} = \frac{h_{descent} - h_{landing} - h_{flare}}{V_{v,approach}} = \frac{1100 - 1000 - 0.964}{1} = 99.035 s$$

The time elapsed during the flare;

$$t_{flare} = \frac{2 \cdot R_{flare} \cdot \theta_{appraoch}}{V_{flare} + V_{TD}} = \frac{2 \cdot 1028.7 \cdot 2.48 \cdot (\pi/180)}{22.51 + 22.003} = 2.001 s$$

The total weight after the approach segment;

$$\begin{aligned}
W_7 &= W_6 - \left(c_{t,approach}\right) \cdot \left(T_{R,approach}\right) \cdot t_{approach} - \left(c_{t,flare}\right) \cdot \left(T_{R,flare}\right) \cdot t_{flare} \\
&= 187.07 - (0.001799) \cdot (13.086) \cdot 99.035 - (0.00144) \cdot (18.99) \\
&\quad \cdot 2.001 = 184.69 N
\end{aligned}$$

The thrust required during the approach;

$$\begin{aligned}
T_{R,approach} &= \frac{1}{2} \cdot \left(\frac{\rho_{landing} + \rho_{descent}}{2}\right) \cdot S \cdot \left(\frac{V_{approach} + V_{flare}}{2}\right)^2 \\
&\quad \cdot \left(C_{D0,TOTAL} + k\left(C_{L,approach}\right)^2\right) - W_6 \cdot \sin(\theta_{appraoch}) \\
&= \frac{1}{2} \cdot \left(\frac{1.111647 + 1.10077}{2}\right) \cdot 1.592 \cdot \left(\frac{23.695 + 22.51}{2}\right)^2 \\
&\quad \cdot (0.009439 + 0.22532(0.3976)^2) - 187.07 \cdot \sin(2.48) = 13.086 N
\end{aligned}$$

The lift coefficient during the approach;

$$C_{L,approach} = \frac{2 \cdot W_6 \cdot \cos(\theta_{appraoch})}{\left(\frac{\rho_{landing} + \rho_{descent}}{2}\right) \cdot S \cdot \left(\frac{V_{approach} + V_{flare}}{2}\right)^2}$$

$$= \frac{2 \cdot 187.077 \cdot \cos(2.48)}{\left(\frac{1.111647 + 1.10077}{2}\right) \cdot 1.592 \cdot \left(\frac{23.695 + 22.51}{2}\right)^2} = 0.3976$$

The thrust specific fuel consumption during approach;

$$c_{t,approach} = \frac{WF_{approach}}{\left(\frac{T_{approach}}{g}\right)} = \frac{0.0024002}{\left(\frac{13.086}{9.81}\right)} = 0.001799 \ (1/s)$$

From the engine model;

$$\begin{aligned}
RPM &= 0.0010673 \cdot (1.47)^7 - 0.099774 \cdot (1.47)^6 + 3.7964 \cdot (1.47)^5 - 75.755 \cdot (1.47)^4 \\
&\quad + 855.69 \cdot (1.47)^3 - 5597.3 \cdot (1.47)^2 + 23412 \cdot (1.47) + 18776 \\
&= 43485.9
\end{aligned}$$

The equivalent thrust for the approach;

$$T_0 = T_{R,approach} \cdot \left(\frac{\rho_0}{\rho_{approach}}\right) = 13.086 \cdot \left(\frac{1.225}{1.111647}\right) = 14.42N = 1.47kg$$

The fuel flow is calculated as;

$$\begin{aligned}
WF &= -3.5E^{-28} \cdot (43485.9)^6 + 1.33E^{-22} \cdot (43485.9)^5 - 1.96E^{-17} \cdot (43485.9)^4 \\
&\quad + 1.43E^{-12} \cdot (43485.9)^3 - 5.48E^{-8} \cdot (43485.9)^2 + 0.0010834 \\
&\quad \cdot (43485.9) - 7.147 = 2.4002 \left(\frac{gr}{s}\right) = 0.0024002 \left(\frac{kg}{s}\right)
\end{aligned}$$

The thrust required during the flare;

$$\begin{aligned}
T_{R,flare} &= \frac{1}{2} \cdot \left(\frac{\rho_{landing} + \rho_{descent}}{2}\right) \cdot S \cdot \left(\frac{V_{TD} + V_{flare}}{2}\right)^2 \cdot \left(C_{D0,TOTAL} + k(C_{L,TD})^2\right) - W_6 \\
&\quad \cdot \sin(\theta_{appraoch}) \\
&= \frac{1}{2} \cdot \left(\frac{1.111647 + 1.10077}{2}\right) \cdot 1.592 \cdot \left(\frac{22.003 + 22.51}{2}\right)^2 \\
&\quad \cdot (0.009439 + 0.22532(0.4388)^2) - 187.07 \cdot \sin(2.48) = 18.99N
\end{aligned}$$

The thrust specific fuel consumption during flare;

$$c_{t,flare} = \frac{WF_{flare}}{\left(\frac{T_{flare}}{g}\right)} = \frac{0.0027884}{\left(\frac{18.99}{9.81}\right)} = 0.00144 \ (1/s)$$

From the engine model;

$$RPM = 0.0010673 \cdot (2.133)^7 - 0.099774 \cdot (2.133)^6 + 3.7964 \cdot (2.133)^5 - 75.755$$
$$\cdot (2.133)^4 + 855.69 \cdot (2.133)^3 - 5597.3 \cdot (2.133)^2 + 23412 \cdot (2.133)$$
$$+ 18776 = 50149.1$$

The equivalent thrust for the flare;

$$T_0 = T_{R,flare} \cdot \left(\frac{\rho_0}{\rho_{approach}}\right) = 18.99 \cdot \left(\frac{1.225}{1.111647}\right) = 20.92N = 2.133kg$$

The fuel flow is calculated as;

$$WF = -3.5E^{-28} \cdot (50149.1)^6 + 1.33E^{-22} \cdot (50149.1)^5 - 1.96E^{-17} \cdot (50149.1)^4$$
$$+ 1.43E^{-12} \cdot (50149.1)^3 - 5.48E^{-8} \cdot (50149.1)^2 + 0.0010834$$
$$\cdot (50149.1) - 7.147 = 2.7884 \left(\frac{gr}{s}\right) = 0.0027884 \left(\frac{kg}{s}\right)$$

The necessary fuel for the cruise segment;

$$W_{fuel} = W_0 - W_7 = 258.045 - 184.69 = 73.355N$$

In terms of liters;

$$V_{fuel} = \frac{(W_0 - W_7)}{g \cdot d_{fuel}} = \frac{(258.045 - 184.69)}{9.81 \cdot 0.75} = 9.97 \text{ litres}$$

d_{fuel} is the density of the fuel and taken as 0.75 kg/L.

A4.8 Landing Ground Roll: Segment 7-8

Figure A4. 6 shows the landing segment. The landing starts with the velocity V_{TD} and continues with the same velocity a few seconds meanwhile the nose gear is off the ground. This part is called the free roll. After the free roll, the aircraft stops in the distance, S_L. During this period, the brakes are applied.
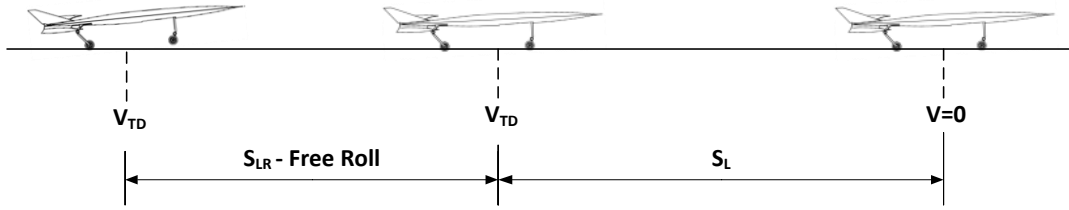
Figure A4. 6 The Landing Segment

The free roll distance is calculated from;

$$S_{LR} = N_L \cdot V_{TD} = 1 \cdot 22.003 = 22.003 \text{m}$$

N_L is the landing rotation time and taken as 1.

The total landing distance;

$$
\begin{aligned}
S_{L,TOTAL} &= S_{LR} + \frac{1}{2gJ_A} \cdot \ln\left(1 + \frac{J_A}{J_T}\right) \cdot (V_{TD})^2 \\
&= 22.003 + \frac{1}{2 \cdot 9.81 \cdot (-0.000372)} \cdot \ln\left(1 + \frac{-0.000372}{0.3}\right) \cdot (22.003)^2 \\
&= 147.76 \text{m}
\end{aligned}
$$

Where;

$$
\begin{aligned}
J_A &= \frac{\rho_{landing}}{2\left(\frac{W}{S}\right)} \cdot \left(C_{D0,landing} + k(C_{L,landing})^2\right) - (\mu_{r,landing}) \cdot C_{L,landing} \\
&= \frac{1.111647}{2\left(\frac{184.69}{1.592}\right)} \cdot (0.0097078 + 0.22532(0.4311)^2) - (0.3) \cdot 0.4311 \\
&= -0.000372
\end{aligned}
$$

$$J_T = \frac{T_{rev}}{W} + \mu_{r,landing} = \frac{0}{184.69} + 0.3 = 0.3$$

$C_{D0,landing}$ is the parasite drag coefficient during landing. T_{rev} is the thrust reverse value and taken as 0. The lift coefficient during landing;

$$C_{L,landing} = \frac{2W_7}{\rho_{landing} \cdot S \cdot (V_{TD})^2} = \frac{2 \cdot 184.69}{1.111647 \cdot 1.592 \cdot (22.003)^2} = 0.4311$$

The parasite drag coefficient during the landing is calculated as $C_{D0,landing} = 0.0097078$ by using the methods described in section 6 for the landing conditions.

The landing ground roll time;

$$t_{land\_grd\_roll} = \frac{2 \cdot S_{L,TOTAL}}{V_{TD}} = \frac{2147.76}{22.003} = 13.43s$$

The total mission time;

$$
\begin{aligned}
t_{mission} &= t_{01} + t_{12} + t_{23} + t_{34} + t_{45} + t_{56} + t_{67} + t_{78} \\
&= 5.4301 + 1.094 + 23.39 + 30 \cdot 60 + 30 + 2 \cdot 60 + 99.035 + 2.001 \\
&+ 13.43 = 2094.36s = 34.9min
\end{aligned}
$$

t_{34} and t_{56} are inputs which are the cruise time and loiter time, respectively. t_{67} is the sum of approach and flare times.